17/06/2022
Master Thesis of the Sustainable Development Master, at Utrecht University.

REGREENING VERSUS LOCAL CLIMATE CHANGE

HOW VEGETATION ACTIVITY ALTERATIONS RELATE TO LOCAL HYDRO-METEOROLOGY IN THE MEDITERRANEAN BASIN.

Eva Asmus 6976840 (e.m.asmus@students.uu.nl)
Supervisor: Arie Staal (a.staal@uu.nl)

Word count: 10397

SUMMARY

In the Mediterranean, heatwaves and drought intensity and occurrence are projected to increase. As some studies and theories suggest a cooling and wetting effect of vegetation activity, this study aimed to gain a better understanding of how vegetation relates to the local climate of the Mediterranean Basin. The research was conducted by means of a remote-sensing data analysis. The change from 1982-2020 of the NOAA ANVHRR NDVI was correlated with changes of hydro-meteorological variables of the ERA5-Land dataset or the same period. Results shows positive relationships between both precipitation and temperature with vegetation activity, and hint at a potential mitigating effect of droughts by regreening. However, the complexity of the interplay between the variables impedes drawing hard conclusions, and further research is suggested.

Key concepts: Mediterranean, drought, heatwave, vegetation, regreening.

Front page picture made by author in July 2019 at Kalamos, Greece.

TABLE OF CONTENTS

1. INTRODUCTION

1.1. MEDITERRANEAN AREAS UNDER PRESSURE

Global climate change is affecting areas all around the world and undeniably, the Mediterranean are no exception. In fact, global climate models indicate that the Mediterranean Basin is the most responsive region to climate change, a so-called 'hot-spot' (Giorgi, 2006). Additionally, temperature is projected to warm 20% more than the global average (Lionello & Scarascia, 2018). The effects of this are already visible, as there has been an increase in hot extremes and drought (IPCC, 2021). For example, from 1960-2006, the mean heat wave intensity, their length and their number have increased by a factor of 7.6 ± 1.3, 7.5 ± 1.3 and 6.2 ± 1.1, respectively (Kuglitsch et al., 2010). Furthermore, future projections to the end of the 21st century estimate that heat wave severity will strongly increase, with heat wave amplitudes increased by 6-10 °C and a combined total increase of tropical nights and hot days of 2-3 months (Zittis et al., 2015). The extreme events of European heat waves in 2003 and 2007 will be less and less exceptional ((Lionello & Scarascia, 2018). Additionally, globally the largest increases in the drought area and duration are projected to appear in the Mediterranean. Under a warming of 3°C, the longest duration of consecutive yearly returning droughts is expected to exceed 10 years, whilst the drought area could change from 28% to 49% (Samaniego el al., 2018). Likewise, researchers have found that drought severity has increased in the last five decades in Southern Europe (Vicente-Serrano et al., 2014).

Resulting from the abovementioned climatic changes in the Mediterranean, undesirable consequences have increased and will augment further. For example, past wildfires are found to be mainly driven by heatwaves and droughts, (San-Miguel-Avanz et al., 2013; Turco et al., 2019) and the burnt area is projected to increase for different scenarios by at least more than 100% around 2075 (Sousa et al., 2015; Turco et al., 2018). Moreover, deaths have not only resulted from these wildfires (San-Miguel-Avanz et al., 2013), but equally from past heatwaves. However, the latter has been much more fatal, causing more than 35000 deaths in 2003 in Europe (Bhatachara, 2003). In the future, heatwave deaths are expected to rise 60-fold from the 1981-2010 reference period to 2100 (Forzieri et al., 2017). Additionally, some diseases might become more prevalent with increasing temperatures, as has already been the case with West Nile fever (Tran et al., 2014). The virus is also projected to spread by 2025 and even further by 2050 (Semenza et al., 2016). Furthermore, ecosystem services such as regulating for erosion, drinking and freshwater provision, and hydropower production are expected to decrease (Bangash et al., 2013; Terrado et al., 2014; Tsanis et al., 2011). In addition, agriculture is threatened by the climatic changes, with yields of dominant crops already having been affected and projected to decrease even further (Moore et al., 2015; Ray et al, 2019). Thus, considering these issues induced by climate changes that potentially

transform Madrid's and Marseille's climate to be more like the current climate of respectively Marrakech and Algiers (Bastin et al., 2019), more insights into potential mitigation strategies for droughts and heatwaves are desirable.

1.2. REGREENING AS A POTENTIAL ADAPTATION STRATEGY

Such insights can be provided by studying the underlying feedbacks of climate change. One of such feedbacks involves the way in which vegetation and climate interact. Under the influence of climatic changes, such as glaciations and rapid cooling and warming effects, land vegetation cover has gradually changed in many areas. Even the current driest region of the world, the Sahara, was once largely covered with tropical vegetation, and had a tropical seasonal climate (Hély & Lézine, 2014; Larrasoaña et al., 2013). However, nowadays, climate change sometimes negatively feedbacks on vegetation. For example, in the Mediterranean a strong control of drought on for its typical vegetation was observed (Gouveia et al., 2017).

Reversely, vegetation changes can influence to the climate. For example, previous research suggests that the intensification of extreme droughts and heatwaves could be mitigated by land cover changes (e.g., Bonan, 2008; Miralles et al., 2019). However, a lot about such vegetation-climate interactions remains unknown (Miralles et al, 2019; Seneviratne et al., 2010). It has been suggested that droughts and heatwaves aggravate and propagate through land-atmosphere feedbacks (Miralles et al., 2019). The underlying feedback here is that land deterioration and vegetation cover decrease positively feedback with rainfall decrease and temperature rises by mechanisms like evapotranspiration limitation and runoff enhancement. For the already hot and dry Mediterranean, more insights into such mechanisms are necessary for finding adequate adaptation strategies, especially since here land use changes such as land abandonment and agricultural intensification have been observed (Serra et al., 2008). However, the effects on the hydrological cycle of land use change in temperate regions such as the Mediterranean are commonly underexamined (te Wierik et al., 2021).

Therefore, this study aimed to answer the following question: 'How has vegetation activity interacted with the local climate within areas in the Mediterranean Basin?'. It was hypothesized that decreases in vegetation have led to a warmer and drier climate, whilst increases have led to the opposite. To understand which mechanisms underly these vegetation-climate interactions, the change of several hydro-meteorological variables in relation to vegetation acitivy alterations were investigated. The selection of the studied variables was based on the literature review provided in the theoretical framework section. For the data analysis, satellite remote-sensing data from the years 1982-1985 and 2017-2020 was used, as described in the methods section. Next, the results are

presented, followed by an interpretation and research limitations and implications in the discussion. Finally, the conclusion states the main findings and answers the research question.

2. THEORETHICAL FRAMEWORK

This section provides a theoretical foundation of the research, eventually leading to the hypothesis formulation. First, the widely accepted land-atmospheric feedbacks are addressed. Next, the state-of-the-art science on vegetation-climate interactions is reviewed. Additionally, the Normalized Vegetation Index (NDVI) as a vegetation indicator is discussed. Lastly, the area investigated in this research, the Mediterranean Basin, is presented. First a brief elaboration on the vegetation and climate characteristics of the area is provided, followed by a conceptual model and hypothesis based on the literature.

2.1. LAND-ATMOSPHERIC FEEDBACKS

For the analysis of climate change feedbacks with vegetation, first it is important to understand the underlying mechanisms of droughts and heatwaves. Commonly, they are indicated by respectively precipitation shortages and extreme temperature rises. Thus, studying the hydrological and energy (heat) cycle should provide a better understanding of vegetation-climate interactions. Figure 1 shows a simple overview of these. What follows is a discussion of each, and how they interact with each other.

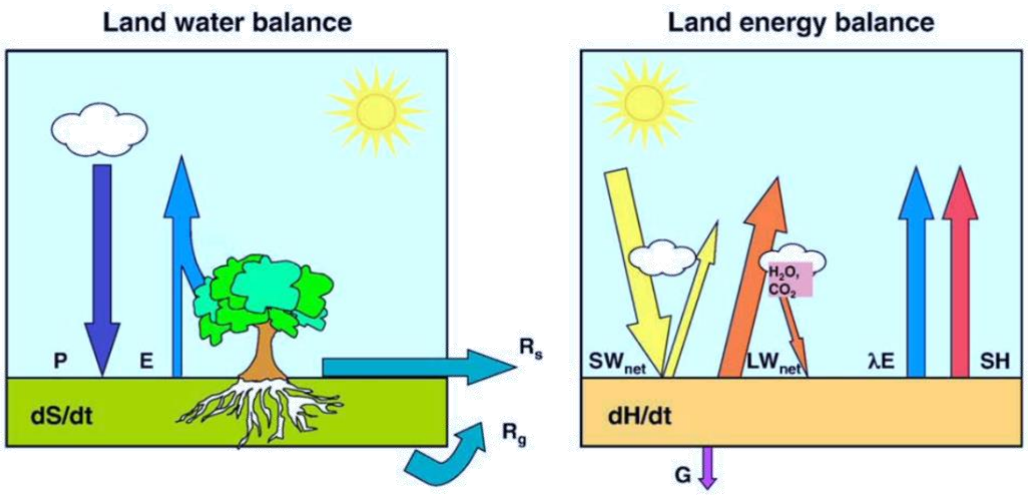

Figure 1. Schematic of the land water balance (left) and land energy balance (right) for a given surface soil layer (Source: Seneviratne et al., 2010). See the text below for explanation of the terms.

For the land water balance, total precipitation P, evapotranspiration E, and runoff R are important (figure 1). Firstly, precipitation increases the soil moisture, surface water, snow, and/or ground water. Second, evapotranspiration can be further divided into evaporation and transpiration. The first ascribes mainly to the process of bare soil water evaporation into water vapor, but evaporated water can also stem from intercepted water by leaves. Transpiration consists of water stemming from plants, which evaporates through the stomata. Evapotranspiration in total returns about 60%

of the whole land precipitation back to the atmosphere (Oki & Kanae, 2006). It is not clear how much of evapotranspiration is accounted for by transpiration (Coenders-Gerrits et al, 2014) and how much by bare soil evaporation and canopy interception, mostly due to uncertainty of plant canopy interception (Wei et al., 2017). Often, the latter process of evaporation is underestimated in models, as well as interception due to wet surface evaporation (Savenije, 2004). Additionally, it is often assumed that transpiration accounts for the largest part of evapotranspiration (e.g. Lawrence et al., 2007; Wei et al., 2017). Furthermore, runoff can be divided further into surface runoff Rs and drainage Rg (figure 1). dS/dt (figure 1) stands for the change of water content within the soil, which includes soil moisture, surface water, snow, and ground water changes. It can be calculated by subtracting the total evaporation and runoff from the precipitation.

Next, for the land energy balance, the net shortwave radiation SWnet and net longwave radiation LWnet need to be considered (figure 1). The sun mainly emits shortwave radiation, of which a part is directly reflected by clouds or the soil surface. The ratio of reflection of the soil surface out of the total solar radiation, the albedo, can be decreased by an increase in soil moisture (Guan et al., 2009; Sugathan et al., 2014) and differs per land cover type (Rahman et al., 1993). For example, compared to bare soil or cropland, dark vegetation cover such as forests has a low albedo (Bonan, 2008). Absorption of shortwave radiation by the atmosphere or soil generates heat, which is emitted as longwave radiation. Part of this longwave radiation is reemitted back to the Earth's surface and atmosphere by greenhouse gasses such as CO2 and H2O. Additionally, the heat that is released from the soil to the atmosphere can be described by the sensible heat flux SH and the latent heat flux λE (figure 1). The first heat flux indicates the energy released from the soil that changes the temperature of the atmosphere, whilst the latter does not change the temperature. It indicates the energy released from the soil for the phase change of water, and thus indicates the energy used for evapotranspiration. This way, the land water balance and land energy balance are coupled. In total, more than half of the solar radiation absorbed by the Earth's surface is used for evapotranspiration (Stephens et al., 2012; Trenberth et al., 2009), and the energy required for evaporating a certain water mass is more than 600 times higher than the energy necessary to increase its temperature by 1 degree Celsius, and even 2400 times higher for a corresponding air mass (Seneviratne et al., 2010). Thus, a change in evapotranspiration goes together with an altered land energy balance, which can potentially affect the sensible heat flux or the amount of heat stored in the soil, affecting the temperature. Furthermore, dH/dt (figure 1) stands for change of energy within the soil (including vegetation), which includes the water phase changes and temperature change for evaporation, runoff, and drainage. It can be calculated by subtracting the latent heat flux, sensible heat flux, and ground heat flux from the net radiation (shortwave and longwave).

Another important variable to consider is soil moisture, as it plays a key role in both the energy and water land balances by its storage function, and by being a source for evapotranspiration. In dry regions, it is the main controlling factor for evapotranspiration, although variations are small due to limited water availability (Seneviratne et al., 2010). It is commonly defined as the water held in the unsaturated soil area (e.g. Hillel, 1998). The field capacity describes the maximum of water that can be held by the soil before gravitational drainage, and the wilting point describes the minimum of water that is held strongly by the soil matrix and therefore not accessible to plants. Thus, the water volume in the soil that is available to plants is the field capacity minus the wilting point. They differ for soil properties such as soil texture (Anders & Rockel, 2008) and for vegetation types, especially concerning their roots (Schenk & Jackson, 2002). In dry areas such as the Mediterranean, where soil moisture is limited, the water in the soil is less available to plants due to stronger soil suction, potentially reducing evapotranspiration (Seneviratne, 2010). Additionally, soil water limitations influence vegetation dynamics and patterns (e.g. Prentice et al., 1992; Rietkerk et al., 2004). Furthermore, changes in soil moisture impact biochemical cycles such as the carbon and nitrogen cycle by influencing plant transpiration and photosynthesis. For example, when soil moisture is too low plant CO2 uptake can be decreased (Angert et al., 2005), potentially enhancing the greenhouse gas effect.

2.2. VEGETATION INFLUENCING DROUGHTS AND HEATWAVES

Climate-vegetation interactions are very complex, and a lot of uncertainty still exists around them (Miralles et al, 2019; Seneviratne et al., 2010). However, for the magnitude of hydro-meteorological extremes like droughts and heatwaves, large-scale responses of ecosystems to the high atmospheric demand, (surface and atmospheric) water stress and heat are thought to be critical (Miralles et al., 2018). There exists no ubiquitous definition of droughts or heatwaves, but they are commonly assigned to events that exceed a given threshold for respectively precipitation deficits or temperature extremes. For example, Stefanon et al., (2012) classified heatwaves according to their temporal and spatial extension of passing a certain temperature threshold in summer. They found that past heatwaves in the Mediterranean area had a duration about one week. On the other hand, droughts typically are assigned a duration of months to years (e.g. Miralles et al., 2018). However, both extremes often concur. For Mediterranean areas, there is a probability of 70% that periods of precipitation deficits are succeeded by an above average number of hot days (Mueller & Seneviratne, 2012). In figure 2, a simplification of the relevant feedbacks during such events is depicted, which are elaborated on in what follows.

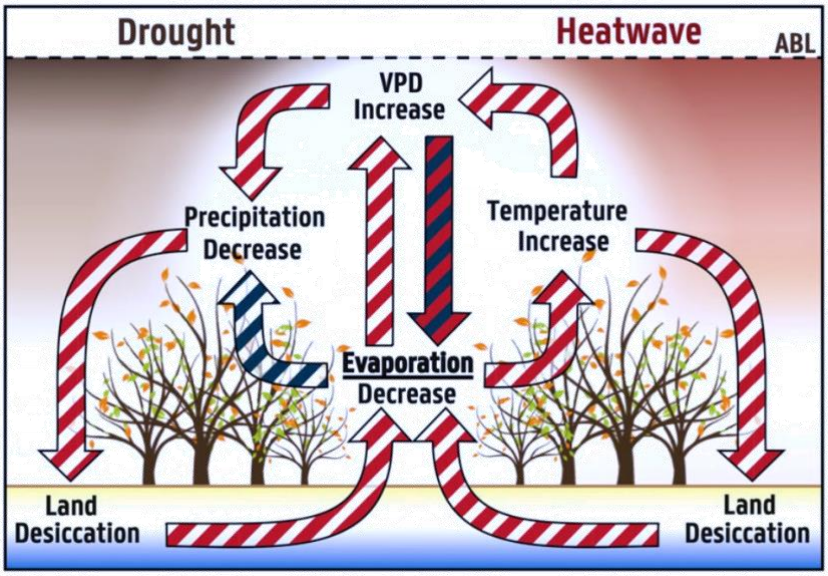

Figure 2. Simplified diagram of land feedbacks as local intensifiers on droughts and heatwaves. A red colour indicates a positive relation, while a blue colour means a negative correlation. (Source: Miralles et al., 2018).

As already mentioned in the previous section, low soil moisture conditions, or land desiccation, deteriorate the water availability for evapotranspiration. In turn, this can result in temperature rises due to the increase of the sensible heat flux resulting from the latent heat flux decrease. This has been confirmed for southeastern Europe, as land desiccation correlates there with summer hot extremes (Hirschi et al., 2010). However, this relationship does not have to be direct. Often, the soil acts as a water reservoir, storing water for not only days but also longer seasonal periods. This way, it acts as a kind of climate memory. For example, if Mediterranean winters are dry, European summers are hot, due to the lower soil water storage levels available for evapotranspiration (Quesada et al., 2012; Vautard et al., 2007). On the other hand, it has been observed that due to the initiation of convection and meso-scale circulation, rain falls preferentially over soils that are drier than the surrounding area (Taylor et al., 2012). However, over time rain occurs more often in wet soil conditions and it is not more likely that rain falls during droughts (Guillod et al., 2015). Furthermore, the effect of winter low soil moisture levels in the Mediterranean on temperature are large scale, as they extended to regions all over Europe (Zampieri et al., 2009). Moreover, land desiccation and temperature increase form a positive feedback loop, increasing the likeliness for heatwave occurrence. As evaporation declines, more solar radiation is employed for the sensible heat flux, which accumulates in the atmosphere and therefore may induce or intensify heatwaves (Miralles et al., 2014).

Next, figure 2 indicates that evaporation or evapotranspiration decreases can lead to precipitation increases. However, the relationship between precipitation and evapotranspiration is

the most subject to uncertainty and the most difficult to ascertain since there are many processes involved (Seneviratne, 2010). As evapotranspiration cannot be directly observed from satellite data but is often modelled by using data from related observable variables (Miralles et al., 2014), its observed interactions with other variables are dependent on the model assumptions. Within modelling studies, often a positive relationship between the two is established (Seneviratne, 2010). For example, evaporation has been found to affect precipitation more strongly when the moisture recycling is local compared to more remote regions (Wei & Dirmeyer, 2012). Specifically for areas around the Mediterranean Basin, the Mediterranean Sea is an important moisture source (Drumond et al., 2011). Additionally, reforestation has been suggested to increase local precipitation in Europe (Meier et al., 2021).

On the other hand, there is a better understanding on how evapotranspiration influences precipitation by studying its coupling to the intermediary feedback of vapor pressure deficit (VPD). This variable describes the difference between the amount of moisture in the air and the amount the air can hold when saturated. When the air is completely saturated, water condenses and clouds are formed. This way, the likelihood for precipitation is increased. When a decrease of evapotranspiration leads to lower atmospheric moisture, the VPD increases. Additionally, VPD is intensified by temperature rise, since warmer air can hold more water, postponing saturation. In turn, VPD enhances evaporation since more moisture is required to saturate the atmosphere (Anderson, 1936). However, the relation between VPD and evaporation can also be negative. Under conditions of water stress, stomatal conductance is lowered, which in turn decreases plant transpiration (e.g. Ad & Rambal, 1995). This causes a positive feedback loop, as lowered transpiration leads to less atmosphere humidity and thus a higher VPD, which further decreases precipitation and hereby a decrease in water availability to plants. Another important positive feedback loop in depicted in figure 2 is that precipitation decreases due to VPD increases further desiccate the soil, leading to a larger deficit in vapor pressure by enhancement of evaporation decrease.

Finally, the type of vegetation influences their effect on transpiration and on soil moisture by infiltration. Savenije (2004) makes a distinction between fast and delayed transpiration. The first is within a time scale of less than a month, from plants with shallow roots such as annual crops and grass. On the other hand, the latter is from plants with deep roots such as trees, shrubs, and perennial crops. Transpiration here has a time scale of more than a month. Additionally, in contrast to grasslands, European forests have been found to mitigate the impact of extreme or long-term heat events (Teuling et al., 2010). Although initially grasslands suppressed heating by increased evaporation as a response to temperature and solar radiation increases, eventually this accelerates

soil moisture depletion and heating. Forests, on the other hand, had a more conservative water use which initially contributed to increased temperatures, but on the long-term evaporation was preserved. Likewise, during the 2003 heatwave in France surface temperature anomalies were greater for crops and pastures than for forests (Zaitchik et al., 2006). Additionally, it was suggested that in the same heatwave event in Europe a decrease in leaf area index amplified the heatwave (Lorenz et al., 2013). Moreover, Mediterranean forests have a small buffering effect against precipitation variability within the area (O'Connor et al., 2021).

2.3. NDVI AS A VEGETATION INDICATOR

To measure the vegetation activity, the Normalized Difference Vegetation Index (NDVI) is often used, which can be measured with the use of instruments on board of satellites. It is a dimensionless index which describes the difference between visible (VIS) and near-infrared reflectance (NIR) of land cover (NDVI = (NIR — VIS)/(NIR + VIS)). As the NIR and VIS are themselves ratios of reflected over incoming radiation and take on values between 0.0 and 1.0, the NDVI values range between -1.0 and + 1.0. Typically, values below 0.1 correspond to bodies of water and bare ground, while higher values are indicators of high photosynthetic activity of different vegetation covers (Meneses-Tovar, 2011). Of these, the lowest NDVI values are found for deserts, followed by rangeland and scrub land (Meneses-Tovar, 2011). This is because the NDVI measures the chlorophyl abundance and energy absorption of plants (Myneni et al., 1995), which peaks around 700 μm (Gitelson et al., 1996; Gitelson & Merzylak, 1998), making it useful to monitor the photosynthetically active biomass of plant canopies (Tucker, 1979). Therefore, it is widely used to study various vegetation properties such as the density of green leaves (Weier & Herring, 2000), chlorophyll concentration in leaves (e.g., Pastor-Guzman et al. 2015), biomass (e.g., Zhu & Liu 2015), tree growth (e.g., Vicente-Serrano et al. 2016), plant drought stress (e.g., Chavez et al. 2016), crop yield (e.g., Franch et al., 2017) and forest cover loss (e.g., Dutrieux et al. 2015).

As for hydro-meteorological factors, globally the NDVI has been reported to positively correlate with evapotranspiration and precipitation (Bounoua et al., 2000), and negatively with VPD (Yuan et al., 2019). Additionally, in the Weihe River Basin in China strong positive correlations were found between NDVI and precipitation, temperature, evaporation, and soil moisture (Zhang et al., 2018). Furthermore, in Europe NDVI correlated positively with temperature and precipitation, of which NDVI anomalies also positively correlated with North Atlantic Oscillation (NAO) and El Niño Southern Oscillation (ENSO) signals (Los et al., 2001).

2.4. THE CASE OF THE MEDITERRANEAN BASIN

ECOSYSTEM CHARACTERISTICS

Figure 3. Picture of Sclerophyllous vegetation (Vulcanello, Italy). Taken by B. Kosztra.

The study area of this research, the Mediterranean Basin, is the largest out of the five Mediterranean regions in the world. Their ecosystems are commonly defined according to their climate. However, the definition of the area is not consistent amongst studies. Blumler (2005) distinguishes between roughly 3 types of classifications, namely either with a climate of areas around the Mediterranean Sea, or with a winter-wet and summer-dry climate, or with a climate that favours broad-leaved, evergreen, sclerophyllous shrubs and trees (e.g. see figure 3). Such vegetation is dominant and unique for the area (Esler et al., 2018), as their thick leathery leaves are well adapted to the dry summer periods. The temperate climate, with mild winters due to the moderating of high temperature fluctuations by the Mediterranean Sea, supports their growth (Dallman, 1998). However, as dry periods are increasing in length and drought stress on these plants increases, it is likely that other, annual plants are taking over (Blumer, 2005).

Furthermore, in general Mediterranean landscapes often consist of eroded mountains, with heterogeneous low-nutrient soils, and pulse-driven river systems (Esler et al., 2018). In the Mediterranean Basin, land degradation due to soil erosion is common in the area (González-Hidalgo et al., 2007). Additionally, wildfires occur frequently, and more increasingly due to global climate change (Turco et al., 2014). Moreover, being the highest outside of the tropics, the biodiversity is unusually high, particularly in vascular plant diversity, with high levels on endemism (Esler et al.,_2018). However, the projected drought increases are threatening this biodiversity (Albano et al., 2021). Furthermore, is expected that droughts and heatwaves will affect terrestrial mammal's species richness in the Mediterranean, severely threatening their survival, particularly of endemic species (Maiorano et al., 2011).

RESEARCH HYPOTHESIS

Considering the abovementioned positive feedbacks of vegetation with hydro-meteorological variables, it is expected that regreened Mediterranean areas have lowered temperatures and increased precipitation, whilst for de-greened areas the opposite is expected. Figure 4 depicts the expected relationships of vegetation with these hydro-meteorological variables, and how they could relate to droughts and heatwaves. Vegetation most directly influences precipitation and temperature through two mechanisms, namely runoff due to the root capability of increasing infiltration, and transpiration due to photosynthetic activity. Next, a decrease in runoff leads to soil moisture increase, which in turn improves water availability for evapotranspiration. As evapotranspiration increases, VPD decreases, which both increase the chance of air saturation and thereby precipitation. Additionally, evapotranspiration increases go together with latent heat flux increases, which presumably decreases the sensible heat flux and hereby temperature.

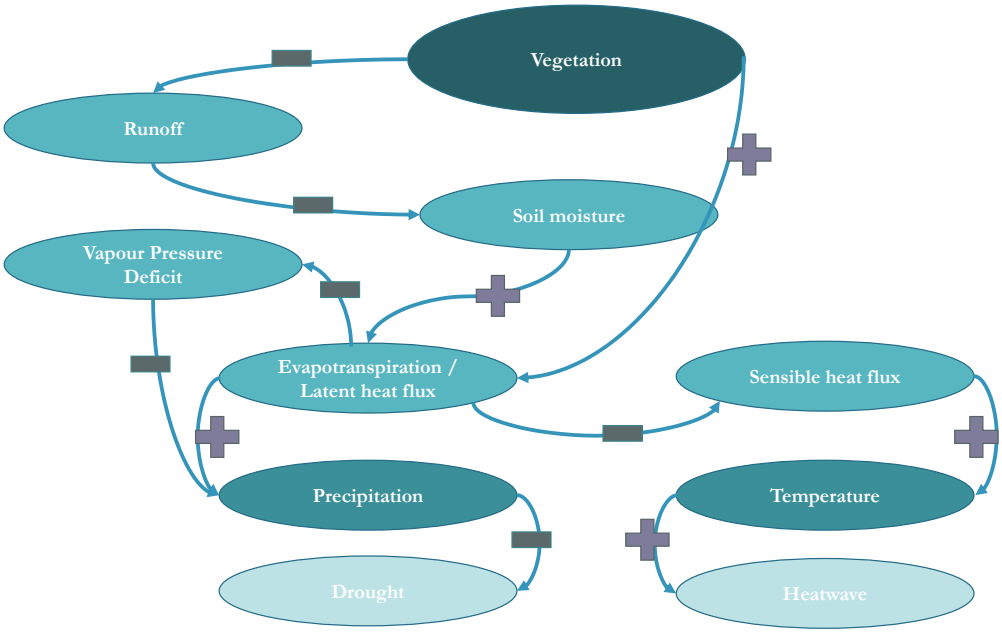

Figure 4. Conceptual model of the assumed pathway from vegetation to droughts and heatwaves. Positive and negative relationships are indicated respectively (+) and (-)-signs.

To validate this conceptual model, the following sub-questions were formulated:

1. How do changes in vegetation correlate with changes in hydro-meteorological variables in the Mediterranean Basin?
2. How has the vegetation of strongly de-greened and regreened areas within the Mediterranean Basin interacted with hydro-meteorological variables in the Mediterranean Basin?

3. METHODS

To investigate how vegetation relates the local climate within areas in the Mediterranean Basin, and heatwaves in the Mediterranean Basin, a remote sensing-based data analysis was performed in MATLAB (Version R2022a). To measure vegetation, NDVI was used as an indicator, and for the other variables the ERA5-Land monthly averaged dataset was used. To detect vegetation changes in the study area, the average values of the variables from 2017-2020 were compared to 1982-1985. Thus, the studied period of the vegetation changes and variables is 38 years, between 1982 and 2020. Below is explained how the Mediterranean areas were selected from the data, followed by how for each grid cell the change in NDVI was calculated. Next, a (hydro-meteorological) variable analysis and correlation with NDVI changes is elaborated upon. Additionally, it is discussed how strongly regreened and de-greened areas were selected from the study area and further examined. Finally, an investigation of how global climate change might have affected the area is discussed. (See Appendix III for the code that was developed for the analysis).

3.1. STUDY AREA

First of all, for making sure only areas with a Mediterranean climate are selected, a mask was developed. The monthly ERA5-Land variables 'total precipitation' and '2m temperature' were the used data sources (Muñoz Sabater, 2019) for this. The ERA5-Land dataset is a reanalysis product, meaning that model data is combined with observations from all over the world (including measurements of the FLUXNET project) into a globally complete and coherent dataset, applying the laws of physics. The variables are downloaded in netCDF files from the Climate Data Store (CDS) of the Copernicus Climate Change Service (C3S), operated by the ECMWF on behalf of the EU. The data has a resolution of resolution 0.1x0.1 degrees (native resolution is 9 km), and is projected on a regular longitude/latitude grid.

For this research, the Mediterranean Basin area is classified by its seasonal characteristics, selecting areas which consist of warm dry summers and cool, moist winters, with a pronounced summer dry period (Esler et al., 2018). This was done by taking the mean monthly values of precipitation and temperature for the years 1982-2020 and applying the Köppen-Geiger climate classification requirements for Csa and Csb regions, and excluding the other climatic regions (Peel et al., 2007). Next, as the focus is on areas in the Mediterranean Basin, and as the typical Mediterranean biome of evergreen shrub vegetation only extends slightly east of the Mediterranean Sea (Blumler, 2005), whilst the Mediterranean climate according to the used classification system extends much further east, a cutoff was made around this biome border (figure A, Appendix I). This way, the map also better matches with those of many other studies on the Mediterranean Basin, as in cartography often an approximate intersection of the Mediterranean climate and

vegetation is made (Blumer, 2012). The computed mask is illustrated in figure 5.

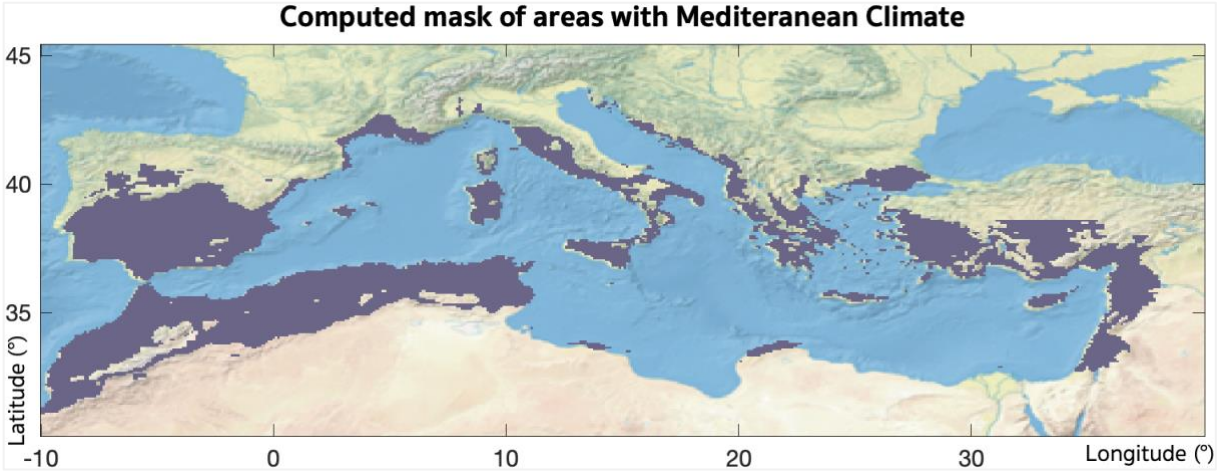

Figure 5. Purple regions indicate areas with a Mediterranean climate according to the Köppen-Geiger climate classification (N=14516).

Furthermore, to overcome interferences of the results by agricultural practices, such as high fluctuations in vegetation cover and irrigation, regions where crops are grown were masked out. This was done by using the data of global land cover maps for the years 1982 and 2020. For 1982 the Global Land Surface Satellite of Global Land Cover (GLASS-GLC) (Liu et al., 2020) map was selected as it was one of the few maps available for this year and it has a high overall accuracy of 85%. The GeoTiff file for 1982, with a 5 km resolution and WGS 84 projection**,** was downloaded and a mask was computed of the 'cropland' classification For 2020 a Land cover classification map of the European Space Agency (ESA) Climate Change Initiative (CCI) Land Cover project (Lamarche et al., 2017) was selected. The netCDF file for the year 2020 was downloaded from the Copernicus Climate Data Store, which had a resolution of 300m. The classifications 'cropland rainfed', 'cropland rainfed herbaceous cover', 'cropland rainfed tree or shrub cover', 'cropland irrigated' and 'mosaic cropland' were used to compute a mask Furthermore, both the 1982 and 2020 cropland masks were averaged to a 0.1 x 0.1 resolution, which led to each grid cell giving a percentage value of the amount of cropland in the cell (figure B, Appendix I). The masks were combined in a mask which deselected all cells that had a percentage of 15% or higher of cropland for one or both years. This percentage was chosen to be optimal upon a visual comparison of different cropland percentages (figure C, Appendix I). Figure 5 depicts the selected cropland mask.

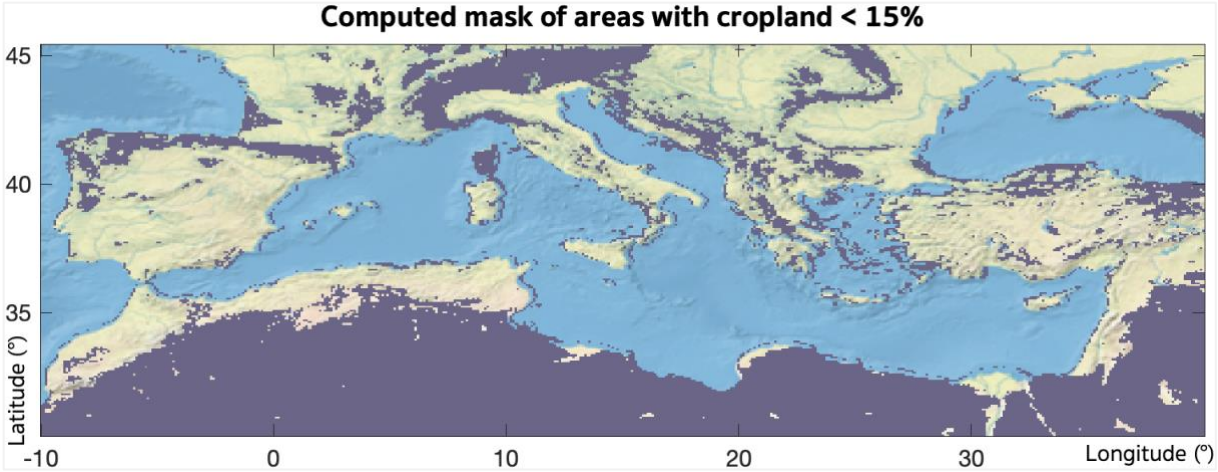

Figure 6. Purple regions indicate the selected grid cells where cropland is below 15% (N= 32534).

3.2. NDVI CHANGE

Next, the NDVI differences between the end period 2017-2020 and start period 1982-1985 were calculated. As it is the only NDVI product which has been operating during the whole course of this period, the Advanced Very High-Resolution Radiometer (AVHRR) NDVI Version 5 dataset of the National Oceanic and Atmospheric Administration (NOAA) was selected for this (Franch et al., 2017; Vermote, 2019). It is one of the Land Surface products of NASA Goddard Space Flight Center and the University of Maryland and contains daily NDVI values on a global grid with a resolution of 0.05 x 0.05 degrees. The values are calculated with a visible light wavelength of 640 μm and near-infrared wavelength of 830 μm (CDR Program, 2018). Although the AVHRR sensors might be less developed, it has a good quality compared to more modern sensors (Brown et al., 2006). The data is corrected for important measurement problems such as Rayleigh scattering, geolocation accuracy, and aerosol, gaseous or water vapor interferences (CDR Program, 2018). NDVI values for vegetation typically range from 0.1 to 0.6 for this dataset (Tarpley, Schneider & Money, 1984). It is available at the Climate Data Record of the NOAA, where netCDF files of each day within the studied periods are downloaded (with a few days in total missing).

However, clouds and cloud shadow interferences are still present amongst the NDVI values, as well as pixels that were measured at nighttime (high solar zenith angle) or that were under the influence of sunglint. As these all reduce the obtained NDVI value, maximum-value compositing (MVC) is a good method to obtain more exact NDVI values (Holben, 1986). It selects the highest pixel value from multi-temporal data, which additionally makes sure that pixel values with the lowest aerosol concentration, lowest water vapor, nearest nadir viewing, and highest Sun illumination are selected (Holben, 1986). Since on a single day, about half of the Earth's surface is obscured by clouds, to get good pixel values a long temporal scale is desired. Therefore, for each

grid cell selected by the previously discussed masks, the mean of the five highest maximum values throughout each year was calculated (further explanation in Appendix II, figure D-F). This also increases the chances that the NDVI value in the peak of the season for each area is selected, thereby overcoming the chance that the growing season might be different for some areas in the Mediterranean Basin.

Next, to calculate the difference in NDVI over 1982-2020, a mean value was calculated for the years 1982-1985 and for 2017-2020 for each grid cell. The four years were averaged to overcome annual fluctuations and incorrect measurements due to interferences. Additionally, the whole grid was averaged from the initial 0.05° to a 0.1° scale, to match with the resolution of the ERA5-Land dataset. Finally, NDVI differences for each coordinate were calculated by subtracting the NDVI value of the start period 1982-1985 from the value of the end period 2017-2020.

3.3. NDVI CORRELATION WITH HYDRO-METEOROLOGICAL VARIABLES

The data for the hydro-meteorological variables came from the ERA5-Land dataset (Muñoz Sabater, 2019). Table X illustrates which variables were selected from the dataset to indicate the variables of the conceptual model in figure 4. Since for evapotranspiration 6 variables were available, all were included in the study, to gain as much insight as possible in how evapotranspiration interacts with vegetation. Additionally, for runoff three variables were available. 'Runoff' represents the total runoff, which is further divided between subsurface and surface runoff. Soil moisture is indicated by 4 variables, each addressing the water present in different soil layers. Layer 1 is 0-7 cm, layer 2 is 7-28 cm, layer 3 is 28-100 cm and layer 4 is 100-289 cm. Furthermore, VPP was calculated as described by Allen et al. (1998), by using variables that indicate the air temperature and the temperature of the dewpoint.

Research variable	***ERA-5 Land dataset variable***
Temperature	2m temperature
Precipitation	Total precipitation
Sensible heat flux	Surface sensible heat flux
Latent heat flux	Surface latent heat flux
Vapor pressure deficit	2m temperature 2m dewpoint temperature
Evapotranspiration	Total evaporation Evaporation from vegetation transpiration Evaporation from the top of the canopy Evaporation from bare soil Evaporation from open water surfaces excluding oceans Snow evaporation

Runoff	Runoff Surface runoff Sub-surface runoff
Soil moisture	Volumetric soil water layer 1 Volumetric soil water layer 2 Volumetric soil water layer 3 Volumetric soil water layer 4

Table 1. For each variable of the conceptual model the ERA5-Land dataset variables that were used to indicate these variables are presented.

For each variable the monthly averages of the years 1982-1985 and 2017-2020 were calculated. Next, the difference between the values of the start period were subtracted from the values of the end period. The months were grouped according to the seasons, and mean variable difference values for each season were calculated. As droughts and heatwaves mainly occur in summer, it is relevant to see how variables are affected during this period by overall vegetation alterations. The seasons were spring (MAM), summer (JJA), fall (SON), and winter (DJF). Additionally, NDVI difference values were correlated with the mean variable difference values over the entire year. Due to the complexity of variable interactions, the relationship between the variables and NDVI was expected to be monotonous but not necessarily linear. Therefore, to calculate the correlation strength, rho values of the Spearman rank correlation were calculated, which are not so much influenced by outliers. For these correlations, NDVI was always the independent variable.

3.4 REGREENING VERSUS DE-GREENING

For more in depth understanding of vegetation-climate interactions, the effects of strong regreening or de-greening on the hydro-meteorological variables were investigated. For this, grid cells that had the highest 10% NDVI increase or decrease were selected, to indicate respectively regreened or de-greened areas. The percentage of 10% was chosen because lower percentages gave no significant correlations due to the low number of grid cells being selected. Correlations of these two groups with the mean hydro-meteorological variable differences over the entire year were analyzed with linear regressions, and the Pearson correlation coefficient was calculated. This method was selected instead of the Spearman rank correlation because it presents the relationship between the variables more directly. For all correlations NDVI was set as the independent variable.

3.5 CLIMATE CHANGE INVESTIGATION

Finally, a small analysis was performed which investigated how the climate has changed in the study area, and how the hydro-meteorological variables might have interplayed here. 10% of grid cells where the NDVI difference was lowest were selected from the study area. For these cells, the mean values of the begin and end period for each variable were calculated. A paired T-test between the two periods was performed to validate if these changes were significant.

4. RESULTS

4.1 STUDY AREA

When both the Mediterranean climate and >15% cropland masks for the region were applied, 2091 grid cells remained. Thus, a total area of 169.371 hectares was studied. As can be read from figure 7, grid cells in the region of the Atlas Mountain range are dominant in the study area selection, with a little more than half of the grid cells located there.

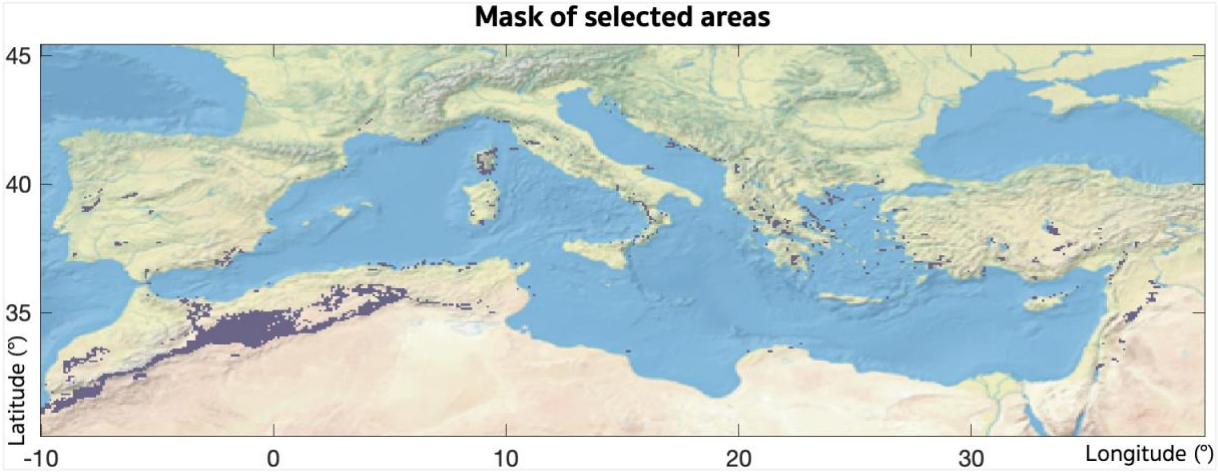

Figure 7. Purple regions indicate the selected grid cells with a Mediterranean climate and cropland below 15% (N= 2091, area of Atlas Mountain range N≈1219).

Figure 8 depicts the distribution of the values of each variable in boxplots, and additionally provides mean values of all grid cells. Paired T-tests were performed to investigate if the difference in mean values between start and end period are significant. This was only true for temperature, bare soil evaporation and VPD ($0.001<p<0.05$), which all increased over time. For transpiration and all three runoff indicators, more than half of the values is near zero. Additionally, for many variables a lot of outliers are presented, indicating that values vary greatly between the study areas.

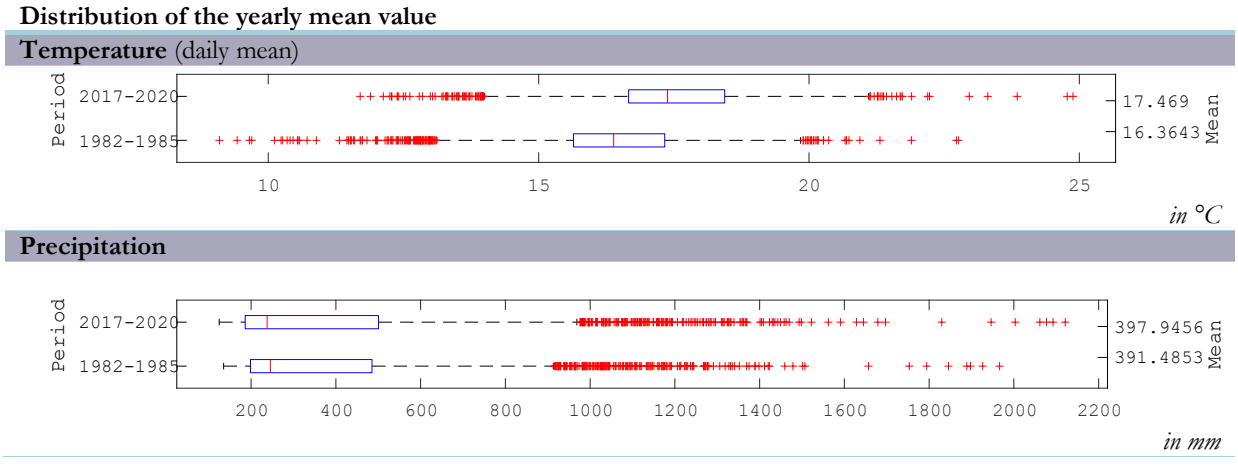

Sensible heat flux (daily mean)

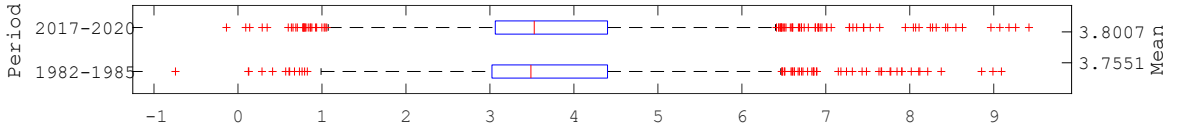

in Joule/m2

Latent heat flux (daily mean)

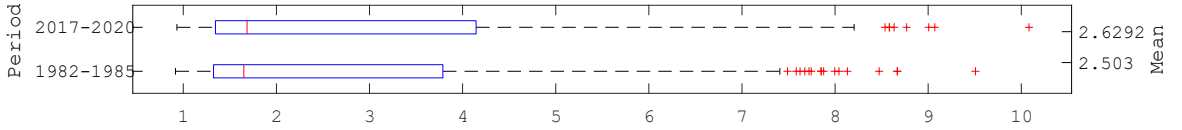

in Joule/m2

Vapor pressure deficit (daily mean)

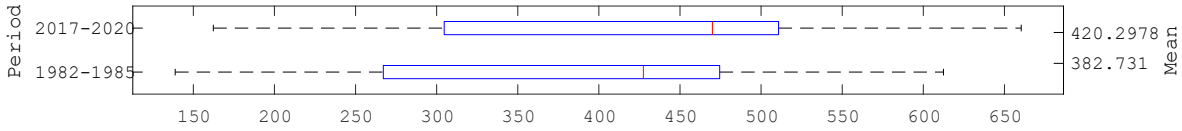

in kPa

Total evaporation

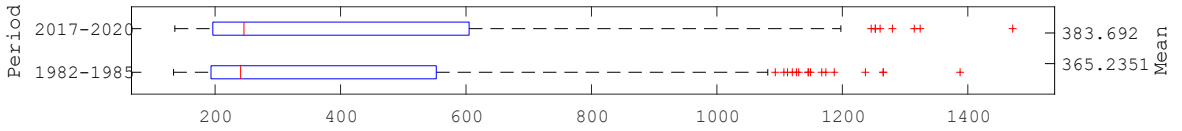

in mm of water equivalent

Transpiration

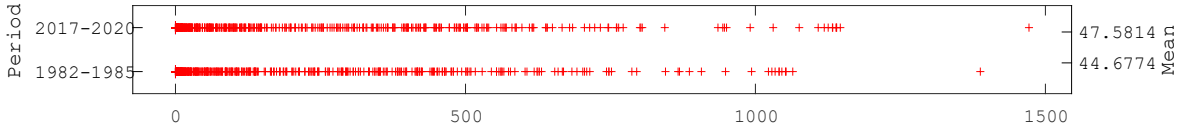

in mm of water equivalent

Canopy evaporation

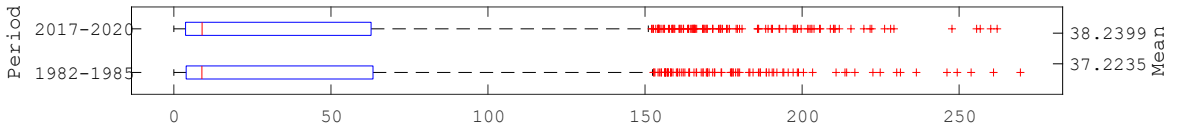

in mm of water equivalent

Bare soil evaporation

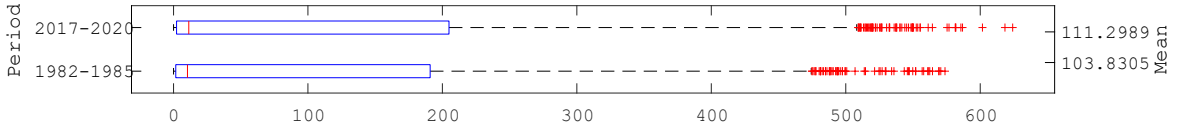

in mm of water equivalent

Snow evaporation

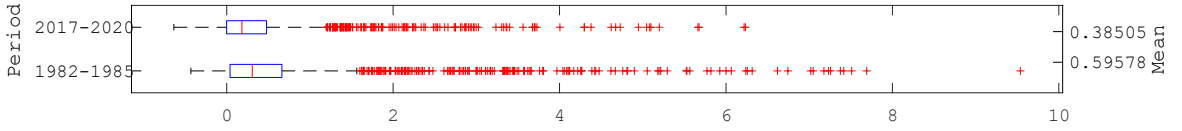

in mm of water equivalent

Open water evaporation

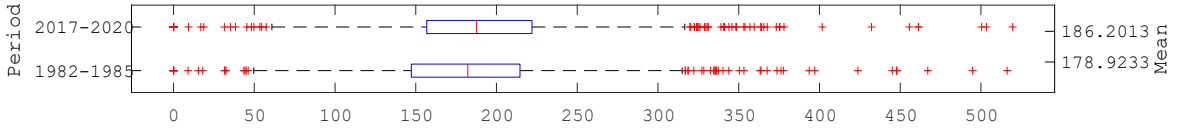

in mm of water equivalent

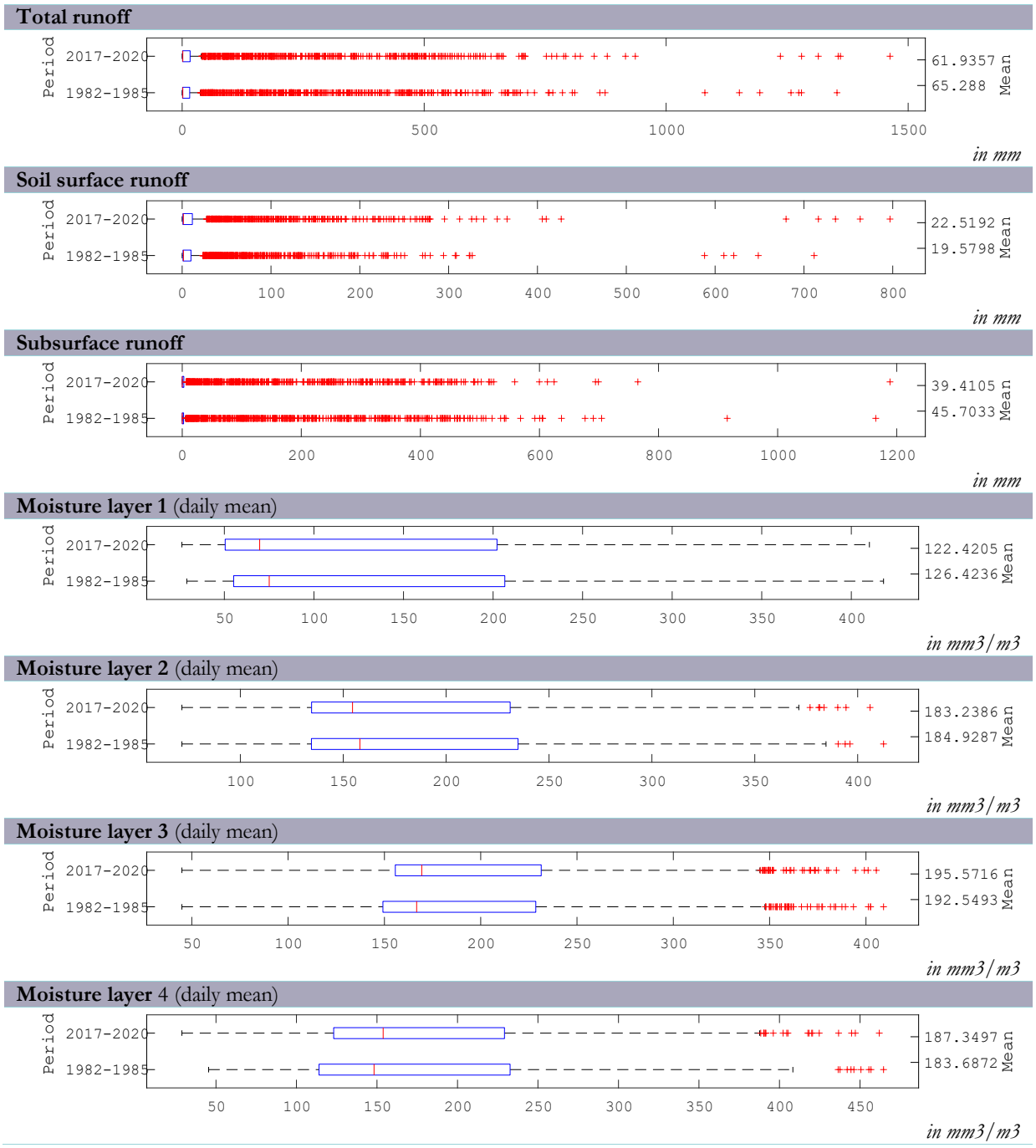

Figure 8. Boxplots of the yearly mean values for the hydro-meteorological variables, obtained from the ERA5-Land dataset. As indicated, for some variables the daily mean values are provided, whilst for the other variables values are accumulated to show a yearly mean value.

Furthermore, figure 9 depicts when on average the study areas are driest and hottest. In line with drought and heatwave behavior, during summer months precipitation is lowest and temperature highest, peaking from June-August. (See Appendix II, figure D for seasonal variations of the other variables).

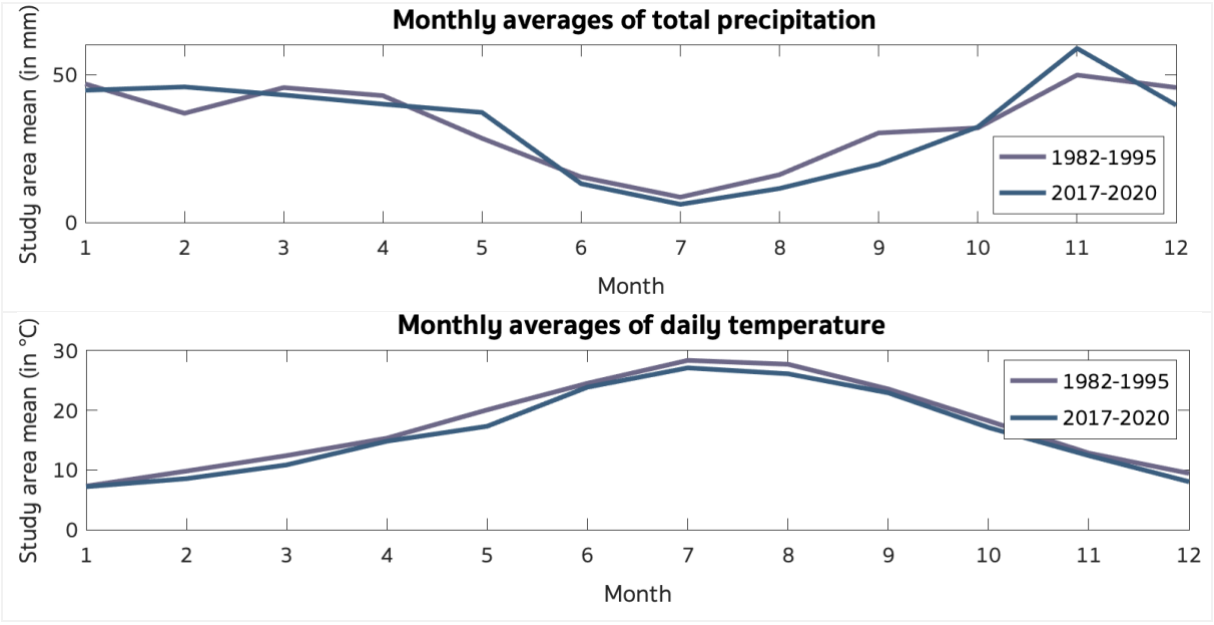

Figure 9. Plots of accumulated precipitation and daily temperature behavior throughout the start and end period. The monthly averages were calculated by taking the mean of all grid cells for each month.

4.2. NDVI CHANGE

Figure 10 depicts the distribution of NDVI values for both periods. It is clear from this figure that for some grid cells NDVI has increased up to 0.8. On the other hand, for some grid cells NDVI has decreased to below 0.2. Most of the grid cells express values around 0.2, while the rest express values mostly between 0.3 and 0.7. Thus, as most values below 0.1 express bare soil, almost all grid cells had some vegetation. Additionally, some areas had quite dense vegetation since they expressed NDVI values of 0.6-0.8.

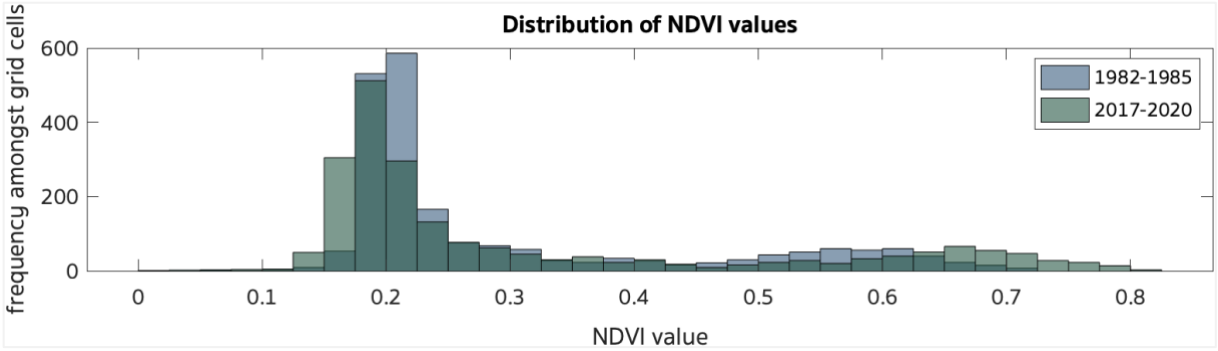

Figure 10. Overlapping histograms of NDVI values of the study area, for the start and end period.

For the entire area, the mean NDVI has increased on average from 0.2941 to 0.3089, which has been proven significant by means of a paired T-test ($p<0.001$). Figure 11 illustrates where in the study area which NDVI values were observed in the end period (for absolute NDVI values in the start period see Appendix II, figure H). Mostly in coastal areas in the northern part of the basin the

values are high, whilst most of the values near 0.2 can be observed in the region of the Atlas Mountains.

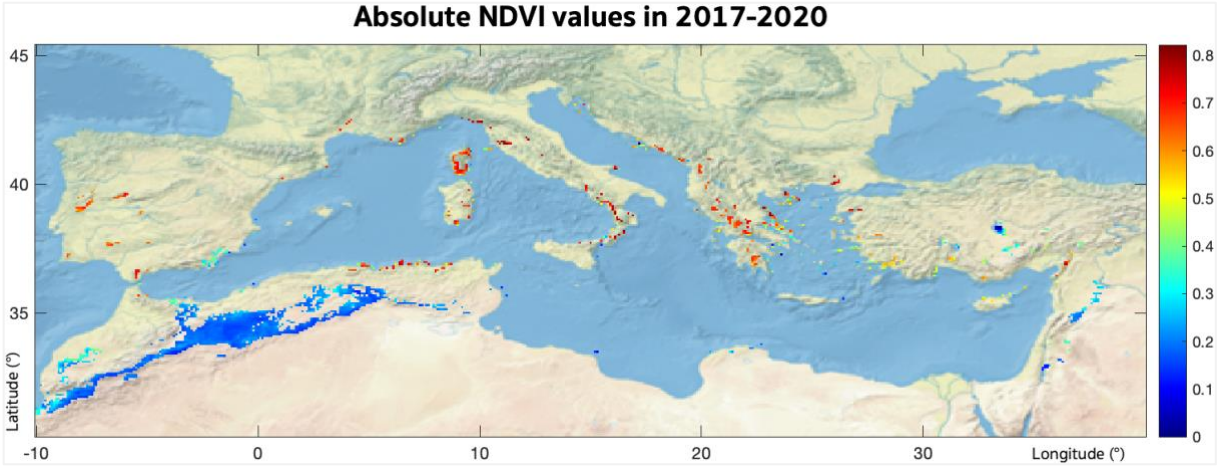

Figure 11. Absolute mean NDVI values in 2017-2020 for the selected cells.

Overall, for the selected areas NDVI changes between 1982-1985 and 2017-2020 differed, as depicted in figure 12. Roughly speaking, in the southern western part of the Mediterranean Basin NDVI has decreased, whilst mostly in region above the Mediterranean Sea the NDVI has increased. Thus, it seems like areas where NDVI was already high, in the north, experienced regreening, whilst areas where NDVI was quite low, in the southwest, underwent de-greening.

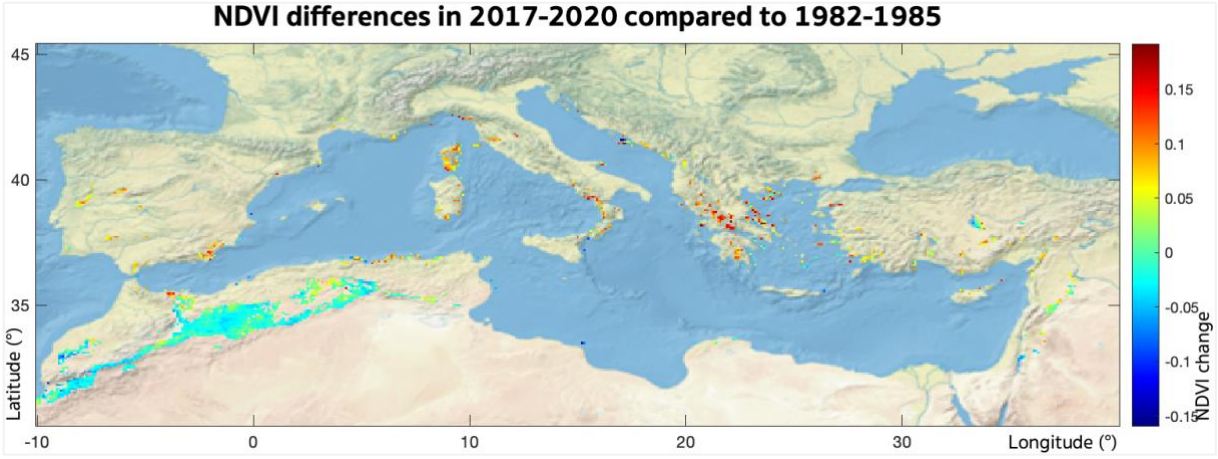

Figure 12. NDVI differences for the selected grid cells.

Furthermore, figure 13 depicts the seasonal behaviour of NDVI throughout the year. It shows that within the region the growing season starts around February and ends around May. Highest vegetation activity is around May-June. Throughout the year on average the NDVI differs with a value of about 0.05.

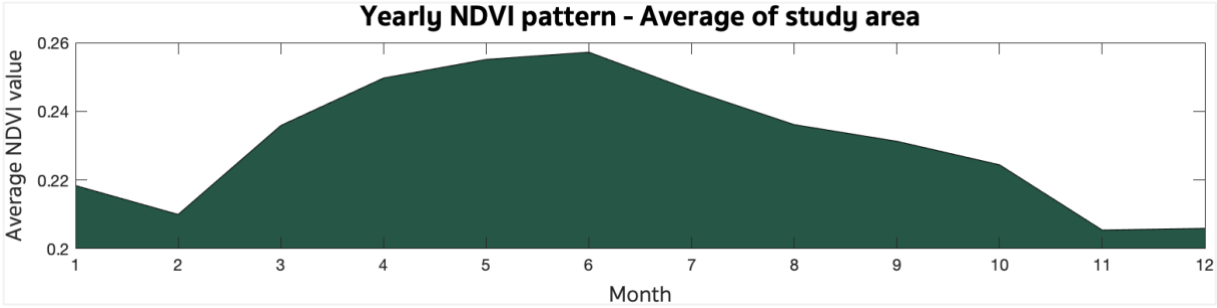

Figure 13. The mean NDVI pattern expressed in the study area, as an average of 1982-1985 plus 2017-2018. Years 2019 and 2020 were excluded from the calculation of this figure, due to bad satellite measurements for October-December of these years (see Appendix I, figures D-F).

4.3. NDVI CORRELATION WITH HYDRO-METEOROLOGICAL VARIABLES

Table 2 shows the results of the Spearman correlation between the NDVI difference and the hydro-meteorological variables (see Appendix II, figure I for visualization of the correlations). These results are further elaborated on in separate sections for the variables.

	Spearman's rho				
Variable	*Total*	*Spring*	*Summer*	*Fall*	*Winter*
Precipitation	0.4074*	*0.018103*	0.11235**	0.3648**	0.33972**
Temperature	0.3145**	-0.21553**	0.43678**	0.10628**	0.20172**
Sensible heat flux	*-0.0411*	0.12246**	0.12332**	-0.11434**	-0.24202**
Latent heat flux	0.4770**	0.36641**	0.17258**	0.34026**	0.47237**
Vapor pressure deficit	-0.2583 **	-0.49025**	*-0.01465*	-0.19668**	-0.53541**
Evapotranspiration:					
Total evaporation	0.4773**	0.36668**	0.17257**	0.34039**	0.47325**
Vegetation transpiration	0.4315*	0.45265**	0.36694**	0.43464**	-0.084017**
Canopy evaporation	0.3030*	0.09827**	0.23462**	0.33754**	0.22573**
Bare soil evaporation	0.4473**	0.46011**	0.20511**	0.27681**	0.54455**
Open water evaporation	0.3092**	0.21874**	*0.016068*	*0.030949*	0.23439**
Snow evaporation	-0.2825**	-0.30314**	*0.014226*	0.11693**	-0.20958**
Runoff:					
Total runoff	*-0.0425*	-0.1121**	-0.26344**	0.16767**	0.18887**
Soil surface runoff	0.3364**	*0.036568*	0.12877**	0.29606**	0.34191**
Sub-surface runoff	-0.2162**	-0.222**	-0.39725**	-0.052074*	-0.026927
Soil moisture:					
Layer 1: 0-7 cm	0.1527**	-0.30138**	*0.041288*	0.29531**	0.22942**
Layer 2: 7-28 cm	*0.0.118*	-0.32992**	0.073438**	0.24089**	0.11621**
Layer 3: 28-100 cm	-0.3301**	-0.40314**	-0.30591**	-0.17441**	-0.18171**
Layer 4: 100-289 cm	-0.4253**	-0.40206**	-0.43651**	-0.424**	-0.3843**

Table 2. Summary of the Spearman rank correlations (*p<0.05, **p<0.001) of the variables with the NDVI differences. From dark to light green the highlighting indicates significant values that had a rounded of value of respectively 0.5, 0.4 and 0.3.

PRECIPITATION

Table 2 shows that, like expected, NDVI correlates quite well with precipitation when using yearly mean precipitation values. Additionally, in fall and winter the correlation is quite strong. Figure 14 illustrates that precipitation mostly increased in the northern part of the basin, where NDVI also mainly increased. On the other hand, for the Atlas Mountain region, where NDVI mainly decreased precipitation mostly stayed the same or even decreased.

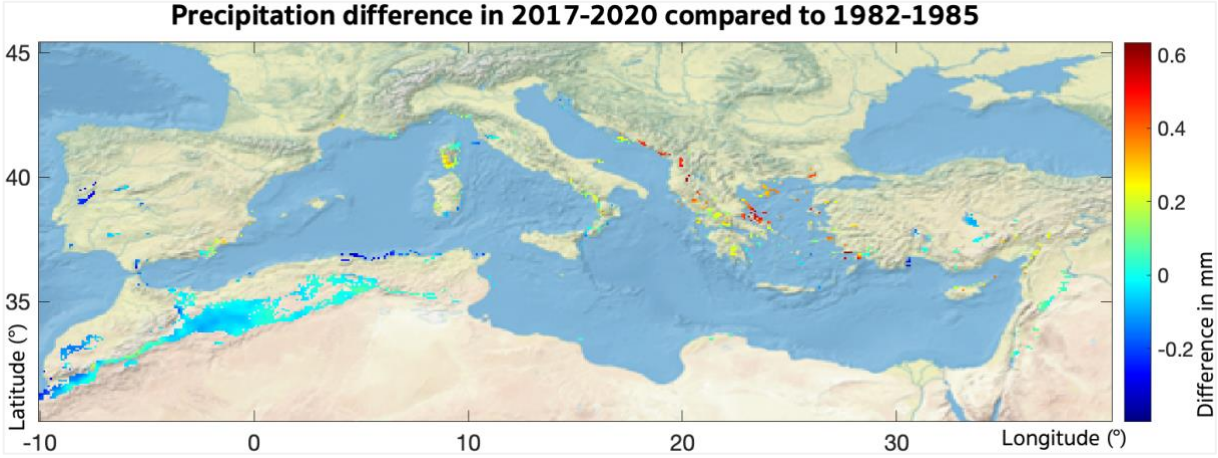

Figure 14. The difference in precipitation between the start and end period. The difference is calculated with values indicating a daily value, averaged over the entire period.

TEMPERATURE

As can be read from table 2, NDVI also correlates quite well with temperature. However, this correlation is not as expected in the conceptual model (figure 4) since it is positive. As discussed in the previous section, in general temperature changed significantly between the two periods, increasing on average with more than 1 degree (figure 8). However, the correlation with NDVI shows that this temperature rise was stronger for the more vegetated areas. This was especially true for summer temperatures, during the months when heatwaves and droughts most often occur. Figure 15 also shows that over the entire study area, the temperature has not decreased.

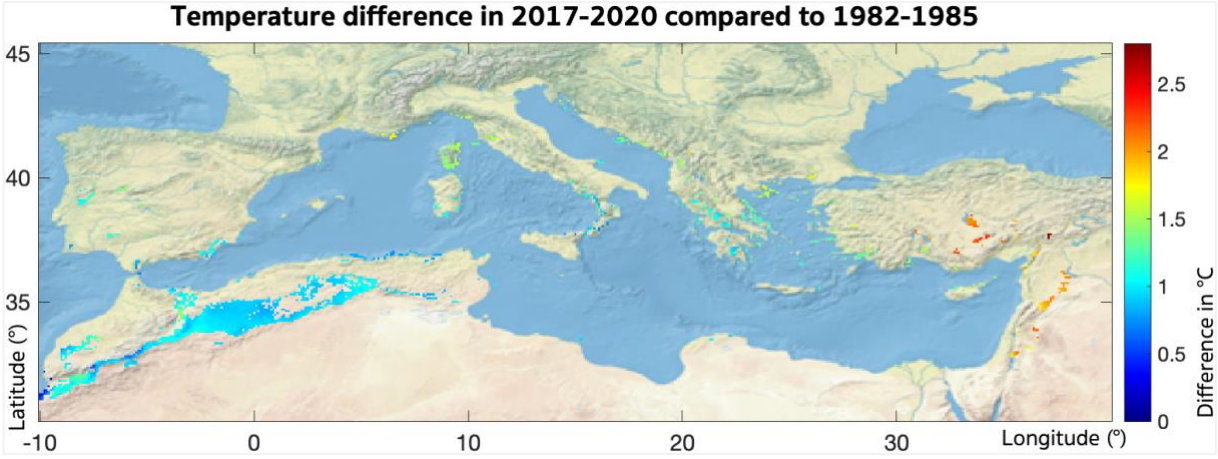

Figure 15. The difference in temperature between the start and end period. The difference is calculated with values indicating a daily value, averaged over the entire period.

HEAT FLUXES

The sensible heat flux showed quite low correlation values (see table 2), which is peculiar since temperature, a variable closely related, did show a significantly moderate correlation. Figure 16 also shows that the sensible heat flux change is varies quite a lot over the area, which can also be concluded from figure 8. On the other hand, latent heat flux shows an overall strong positive correlation with NDVI, the highest amongst all variables. For the seasons, the highest correlation is found in winter, whilst other moderate correlations are found in spring and fall. Figure 16 clearly depicts that most of the regreened areas also underwent high latent heat flux changes, whilst the de-greened areas in the southwest overall have low changes.

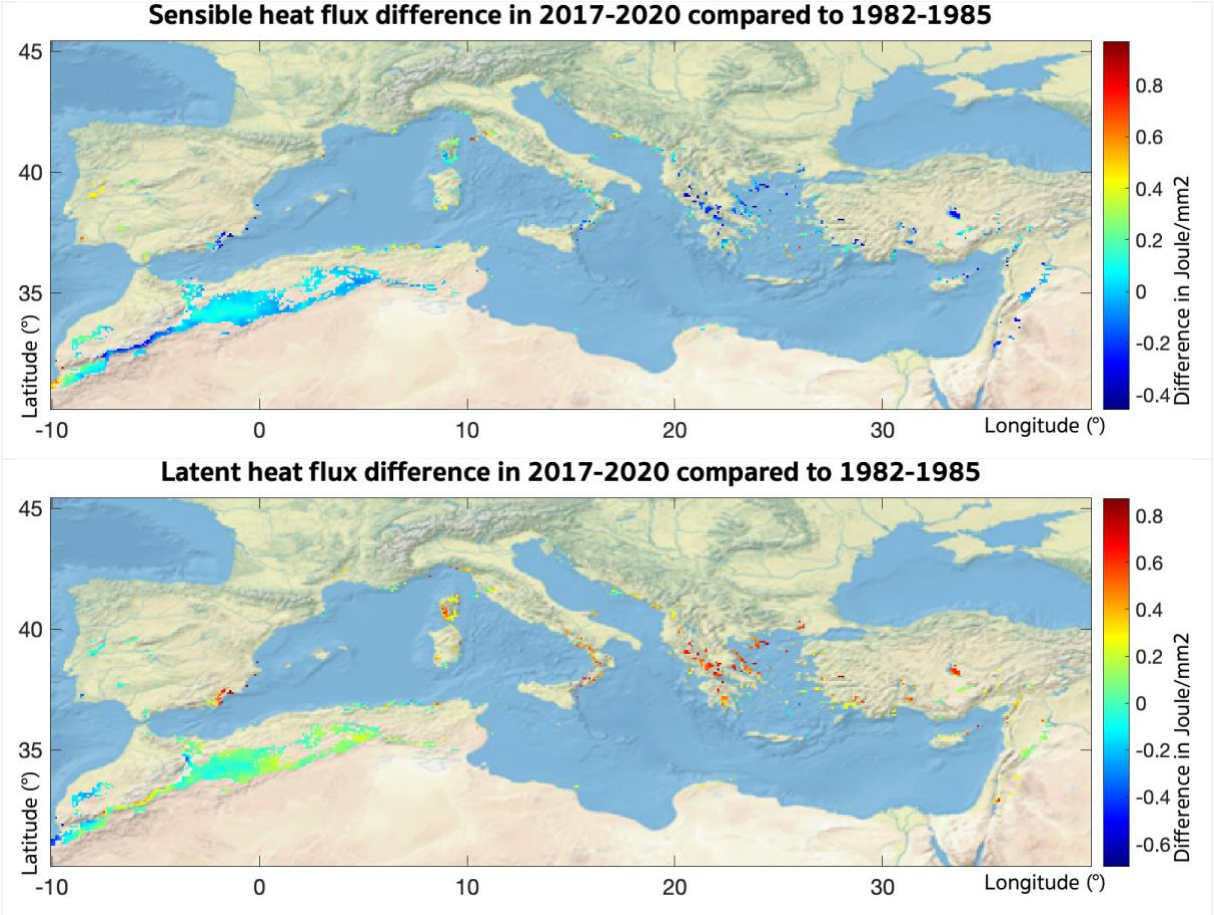

Figure 16. The difference of sensible heat flux (up) and latent heat flux (down) between the start and end period. The difference is calculated with values indicating a daily value, averaged over the entire period.

VAPOR PRESSURE DEFICIT

Overall, the VPD has a moderate negative correlation with NDVI, but especially for spring and winter negative correlations are high (table 2). Again, in the regreened areas this effect is most present (figure 17). Additionally, it is clear from figure 17 that for all grid cells VPD did not decrease.

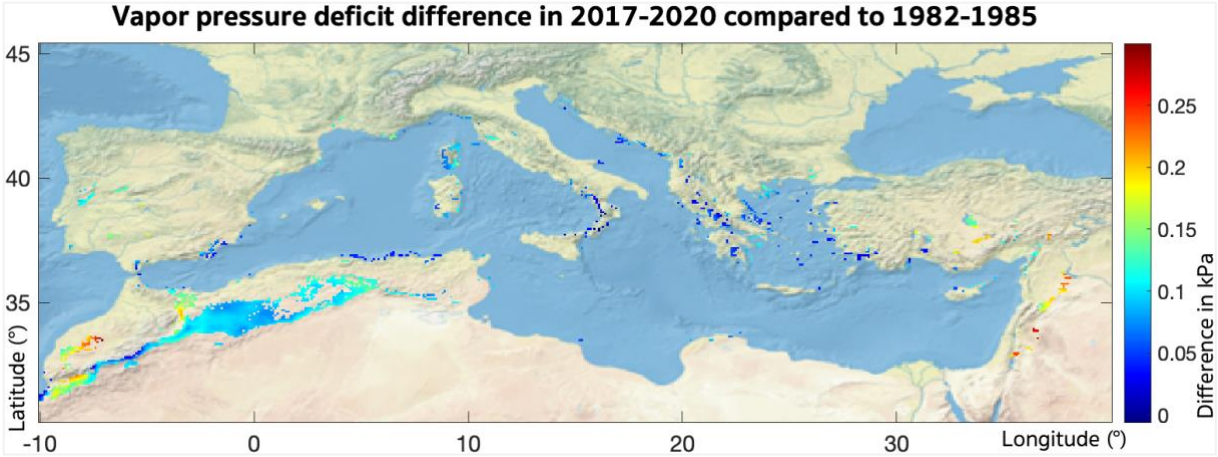

Figure 17. The difference of vapor pressure deficit between the start and end period. The difference is calculated with values indicating a daily value, averaged over the entire period.

EVAPOTRANSPIRATION

Total evaporation has the highest correlation with NDVI of all variables. The relationship is positive, as conceptualized, and especially strong during spring and winter (table 2). Looking at which of the evapotranspiration variables contribute mostly to this, it seems like transpiration plays a large role, correlating strongly in spring, summer, and fall. However, bare soil evaporation correlates even stronger with NDVI. This can be due to increased soil moisture levels in response to infiltration increases. Furthermore, canopy evaporation has a small positive correlation with NDVI, which is consistent with the fact that a vegetation cover extension leads to an increased canopy. Additionally, the moderate correlations of open water and snow evaporation are likely related to the fact that NDVI correlates with temperature increases. This in turn decreases snow cover and increases evaporation from open water. Figure 18 shows that most evaporation increases were found in the regreened areas in the north.

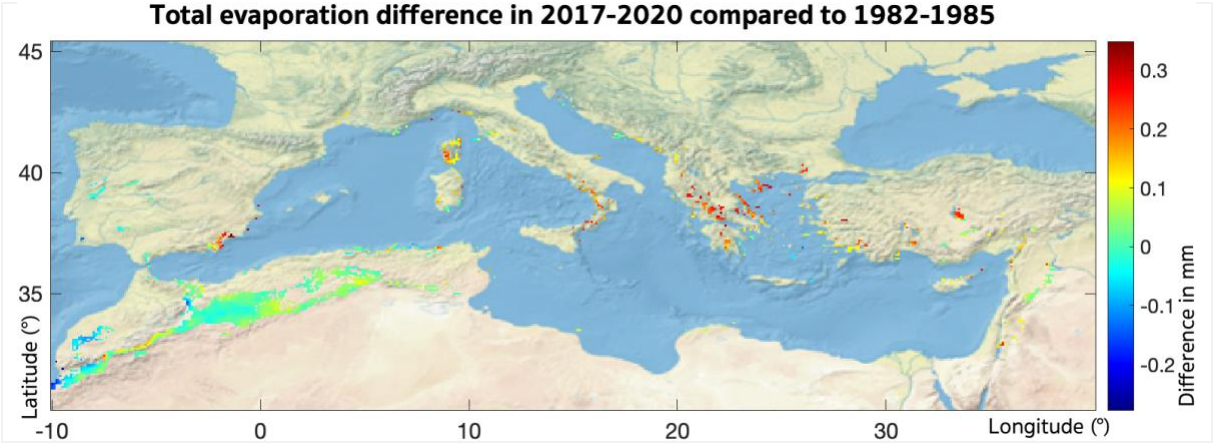

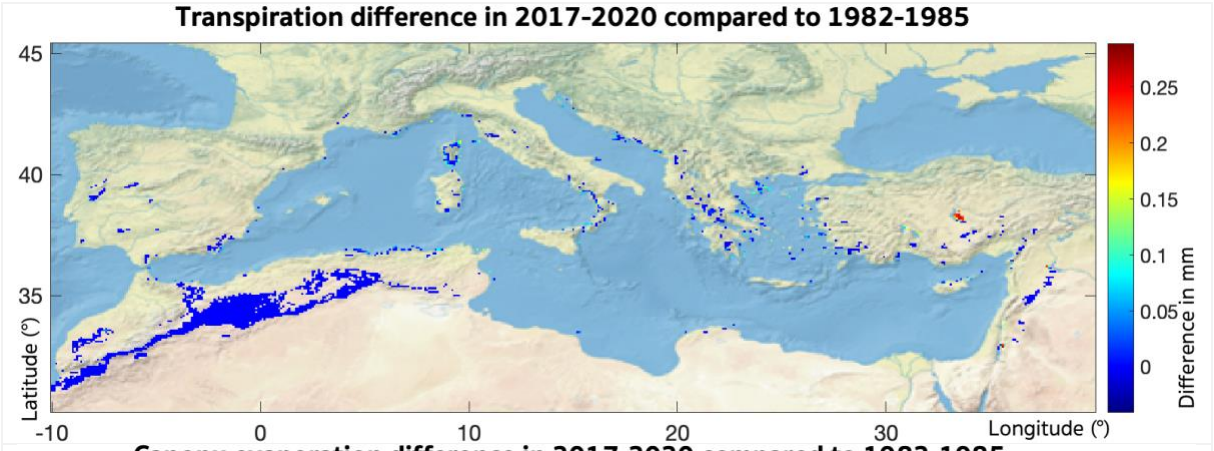
Transpiration difference in 2017-2020 compared to 1982-1985
45
40
35
Latitude (°)
-10
0
10
20
30
Longitude (°)
0.25
0.2
0.15
0.1
0.05
0
Difference in mm

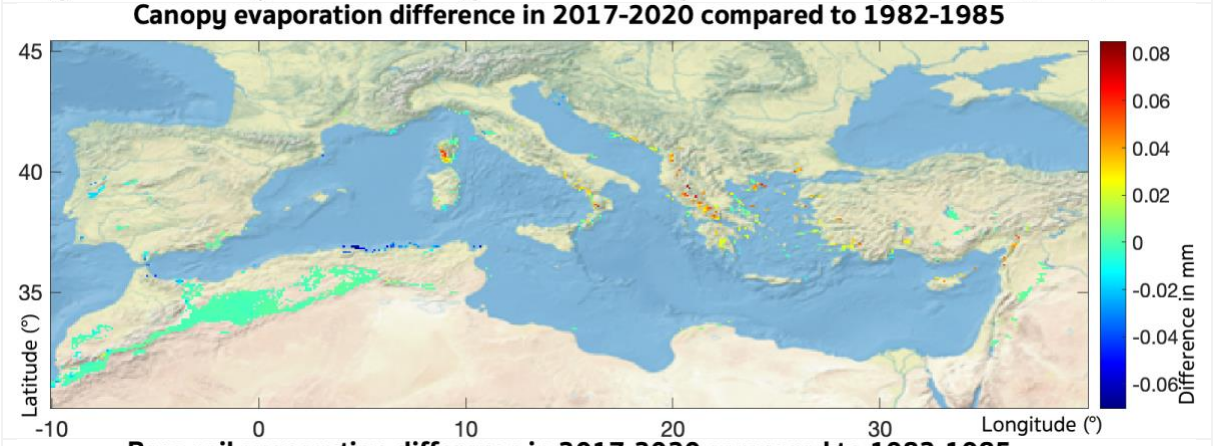
Canopy evaporation difference in 2017-2020 compared to 1982-1985
45
40
35
Latitude (°)
-10
0
10
20
30
Longitude (°)
0.08
0.06
0.04
0.02
0
-0.02
-0.04
-0.06
Difference in mm

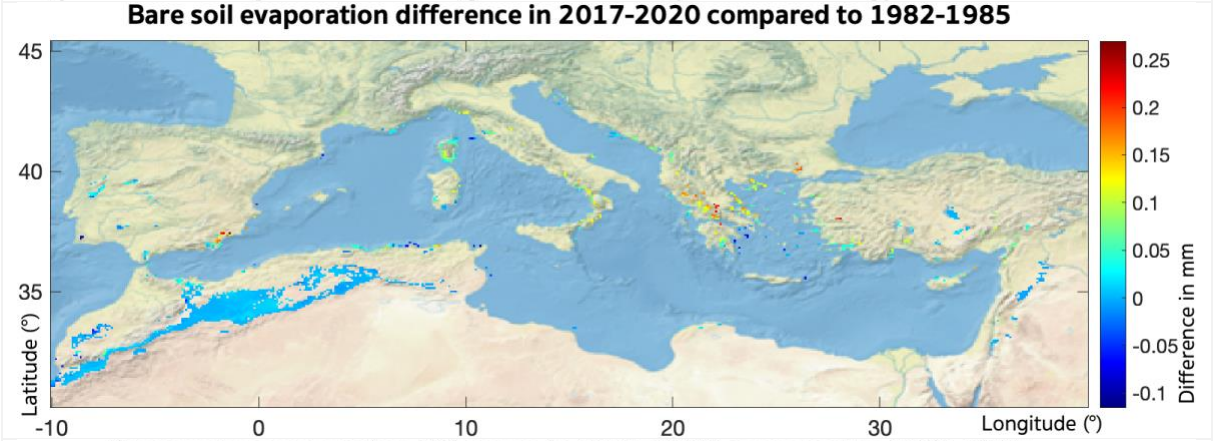
Bare soil evaporation difference in 2017-2020 compared to 1982-1985
45
40
35
Latitude (°)
-10
0
10
20
30
Longitude (°)
0.25
0.2
0.15
0.1
0.05
0
-0.05
-0.1
Difference in mm

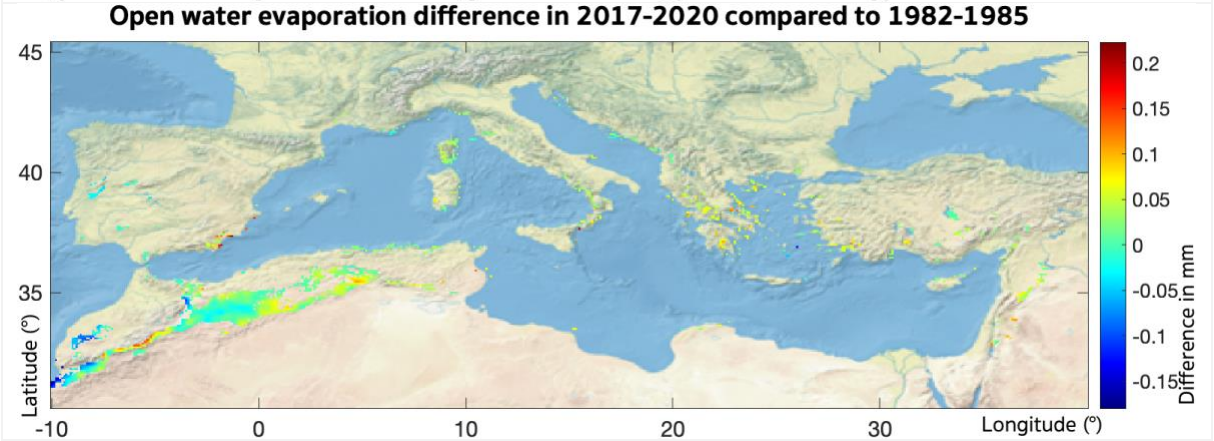
Open water evaporation difference in 2017-2020 compared to 1982-1985
45
40
35
Latitude (°)
-10
0
10
20
30
Longitude (°)
0.2
0.15
0.1
0.05
0
-0.05
-0.1
-0.15
Difference in mm

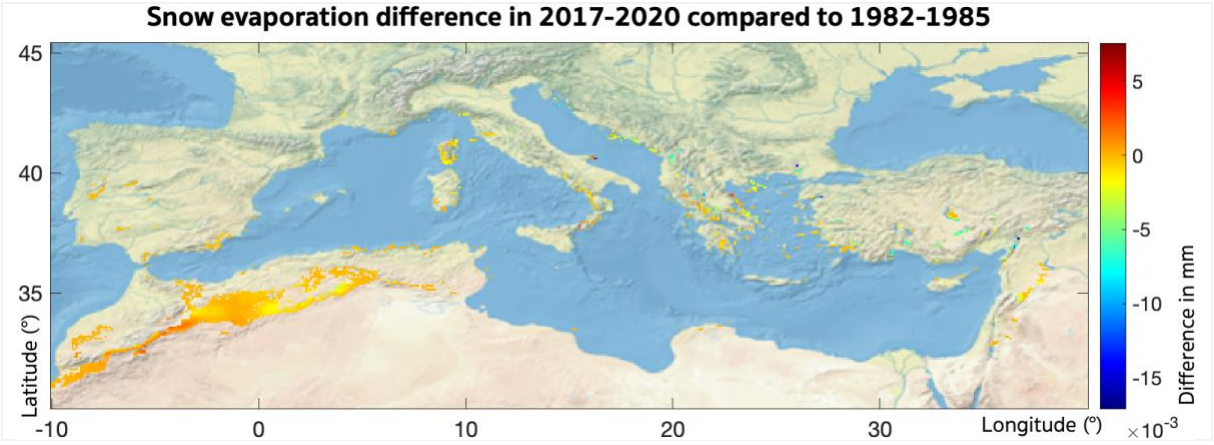

Figure 18. The difference of the different evapotranspiration variables between the start and end period. The difference is calculated with values indicating a daily value, averaged over the entire period.

RUNOFF

For runoff, not many strong correlations were present (table 2). The strongest correlation is found in fall, where a negative correlation of NDVI with sub-surface runoff is present. On the other hand, on a yearly basis soil surface runoff positively correlates with NDVI, of which the effect is strongest in fall and winter. Figure 19 shows again the different changes that occurred in the northern coastal areas of the Mediterranean Basin compared to the southwestern area.

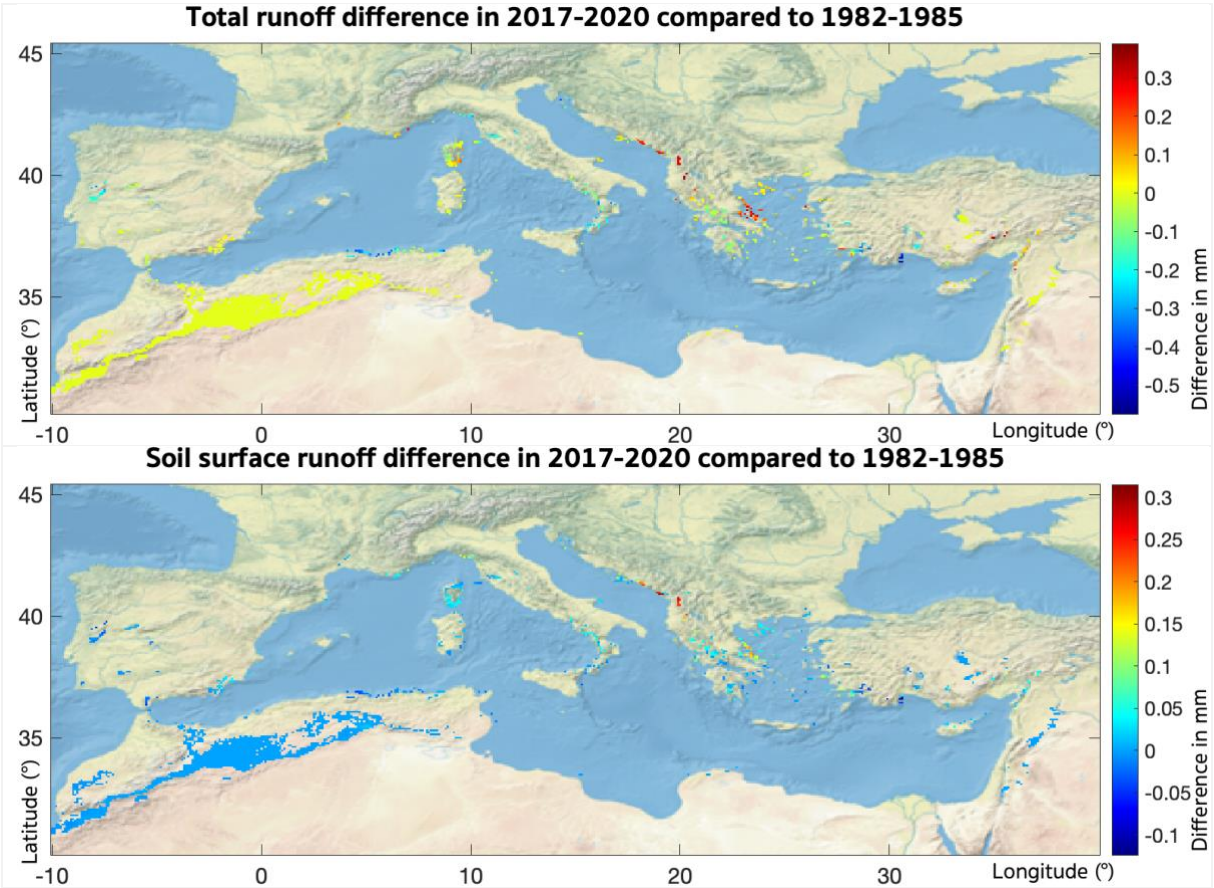

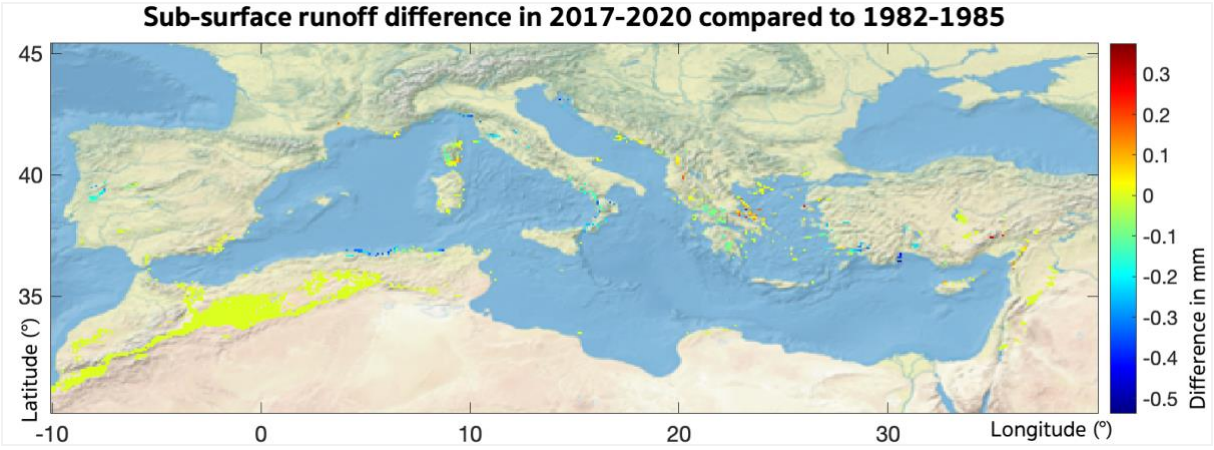

Figure 19. The difference of the different runoff variables between the start and end period. The difference is calculated with values indicating a daily value, averaged over the entire period.

SOIL MOISTURE

Finally, for soil moisture variables quite different correlations are found depending on the soil layer. The strongest correlation is found in the deepest layer, where for all seasons NDVI has a strong negative correlation. Additionally, a moderate overall negative correlation is found for layer 3, which is most strong in spring and summer. On the other hand, layer 1 show moderate positive correlations for fall and winter, but a moderate negative correlation in spring. Layer 2 only shows a substantially large correlation in spring. The area maps only clearly depict the often observed opposite changes for the northern and southwestern region for soil layer 4 (figure 20). For this layer, in the northern regreened areas soil moisture has mostly decreased, whilst around the Atlas Mountains soil moisture slightly increased.

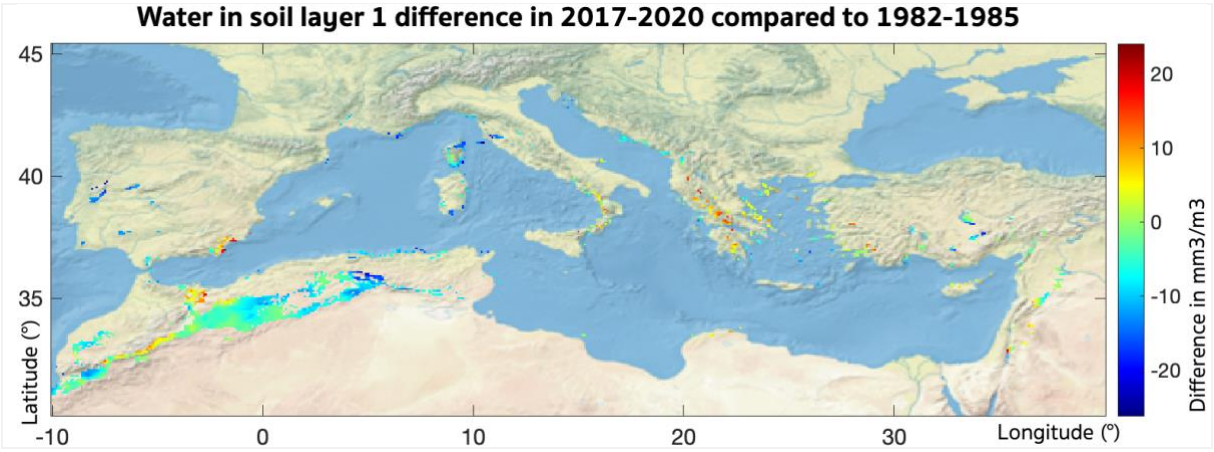

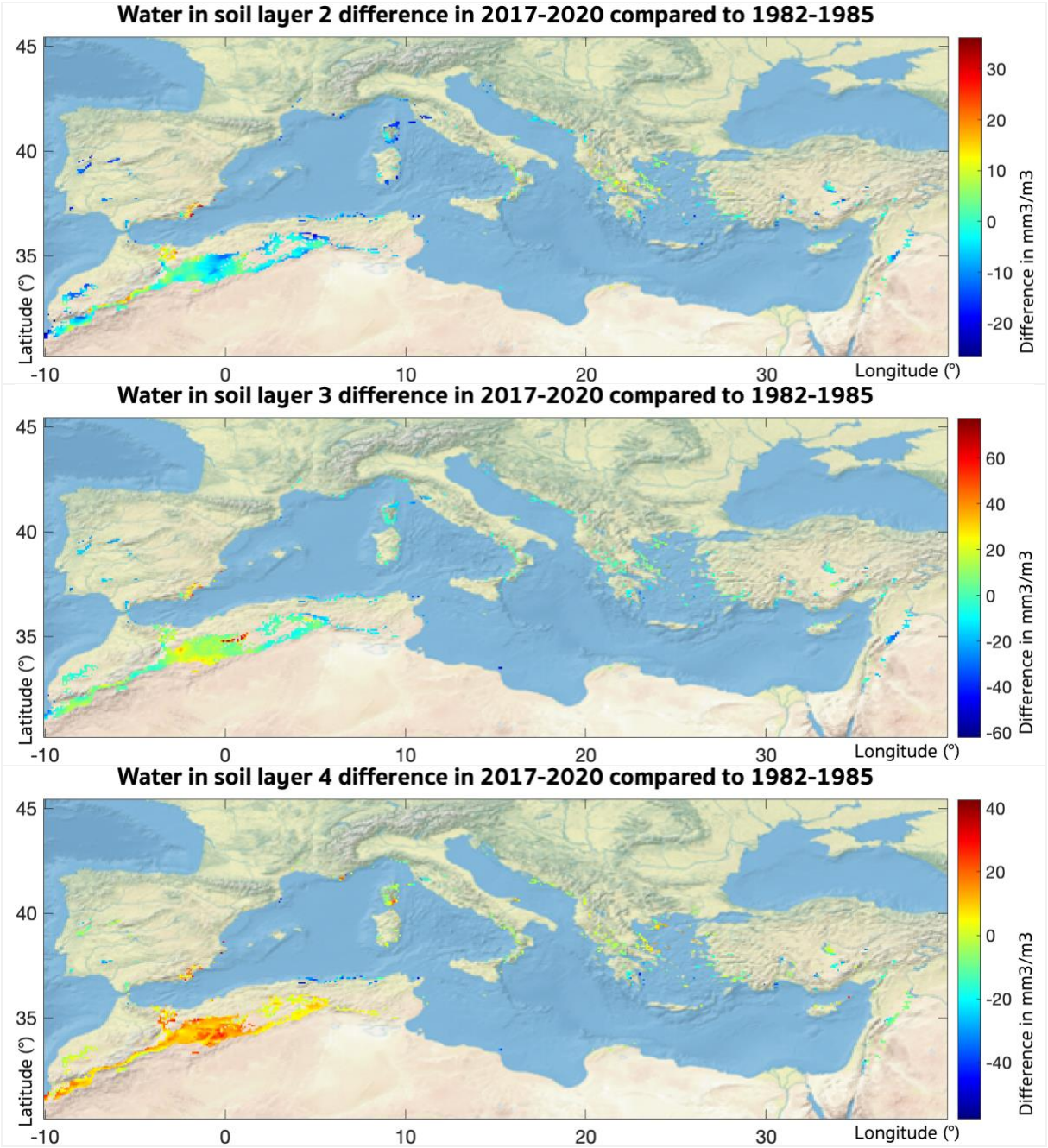

Figure 20. The difference of the different soil moisture variables between the start and end period. The difference is calculated with values indicating a daily value, averaged over the entire period.

4.4. REGREENING VERSUS DE-GREENING

The observed differing regional variable change over the studied 38 years between mostly the north and southwest, makes the more in-depth study of regreened and de-greened areas especially relevant. The region around the Atlas Mountains seems to have the largest NDVI decrease, whilst the region around the northern coastline of the Mediterranean Sea seems to have the largest NDVI increase (figure 12). To validate these rough figure observations, a selection of the 10% most strongly de-greened and regreened areas is needed. Figure 21 shows the locations of these areas, which are consistent with the observations made from figure 12.

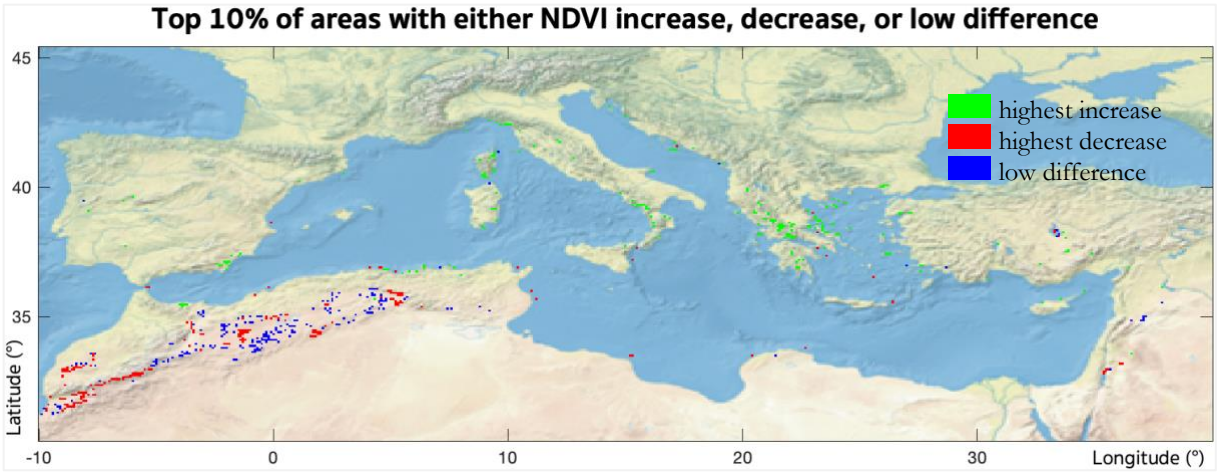

Figure 21. The selected top 10% NDVI difference areas. Green areas are the where the highest regreening took place, red the highest de-greening and blue the lowest difference (N/group= 209).

For regreened areas the mean NDVI increase was 0.1234, while for the de-greened areas the mean NDVI difference was -0.0479. Both changes were found to be significant when conducting paired T-tests ($p<0.001$). The different groups were also validated to have a significant mean difference from each other by means of a two-sample T-test ($p<0.001$). This was also true for two-sample T-tests between the de/regreened areas and the top 10% of areas where NDVI differences were found to be lowest ($p<0.001$). In table 3 the average differences of the variables are given for each group. All variables except total runoff have mean values that significantly differ for the two groups.

Variable	Regreened	De-greened	*p*
Average annual precipitation (mm)	65.0516	-13.4710	**
Average annual daily temperature (°C)	1.2509	1.0425	**
Average daily sensible heat flux (Joule/m2)	0.0135	0.0547	**
Average daily latent heat flux (Joule/m2)	0.4036	0.0441	**
Average daily vapor pressure deficit (kPa)	0.0703	0.1193	**
Average annual evapotranspiration:			
Total evaporation (mm)	58.9796	6.4370	**
Vegetation transpiration (mm)	6.3537	3.1424	*
Canopy evaporation (mm)	5.7229	-0.6310	**
Bare soil evaporation (mm)	32.1683	1.3814	**
Snow evaporation (mm)	-0.5260	-0.0243	**
Open water evaporation (mm)	15.2607	2.5677	**
Average annual runoff:			
Total runoff (mm)	-6.9140	2.1324	-
Soil surface runoff (mm)	13.3027	-0.3240	**
Subsurface runoff (mm)	-20.2180	-1.8128	**
Average daily soil moisture:			
Layer 1: 0-7 cm (mm3/m-3)	-0.0873	-4.9836	**
Layer 2: 7-28 cm (mm3/m-3)	0.8209	-2.2538	**
Layer 3: 28-100 cm (mm3/m-3)	-0.8574	2.4791	**
Layer 4: 100-289 cm (mm3/m-3)	-4.4798	5.1222	**

Table 3. Mean differences between the start and end period for the regreened and de-greened areas. The third column gives the level of significance of the difference between the means of the two groups, which was calculated with a two-sample T-test (*$p<0.05$, **$p<0.001$).

To investigate the relationship of NDVI to the observed variable differences in the two areas, for both groups NDVI regression analyses were conducted. The results of the Pearson regression coefficients are provided in table 4. Within the regreened group, the strongest correlation is found for VPD. Thus, the mean VPD increase of 0.0703 kPa for regreened areas is lower than the increase for the de-greened areas due to some inhibiting interaction with vegetation activity. Furthermore, precipitation, latent heat flux, surface runoff, and soil moisture in layers 1 and 2 gave significant moderate correlations in the regreened area. For the de-greened area, only canopy evaporation gave a significant correlation, which was negative. This is logical, as de-greening goes together with a canopy decrease.

Variable	Regreening	De-greening
Precipitation	0.2371**	-0.0139
Temperature	-0.1113	-0.1172
Sensible heat flux	-0.0870	0.0067
Latent heat flux	0.2033*	-0.0034
Vapor pressure deficit	-0.2428**	-0.1130
Evapotranspiration:		
Total evaporation	0.2031*	-0.0034
Vegetation transpiration	0.1135	-0.0679
Canopy evaporation	0.1074	-0.1487*
Bare soil evaporation	0.0957	0.0844
Snow evaporation	0.0528	-0.0634
Runoff:		
Total runoff	0.1366*	-0.1104
Surface runoff	0.1711*	-0.0098
Subsurface runoff	0.0875	-0.1200
Average annual soil moisture:		
Layer 1: 0-7 cm	0.1887*	-0.1104
Layer 2: 7-28 cm	0.1977*	0.0057
Layer 3: 28-100 cm	0.0998	0.1001
Layer 4: 100-289 cm	0.1054	0.0590

Table 4. Summary of the Pearson correlations (*p<0.05, **p<0.001) of the variables with the NDVI differences of the regreened and de-greened groups. From dark to light green the highlighting indicates significant values that had a rounded of absolute value of respectively 0.2 and 0.1.

4.5. CLIMATE CHANGE INVESTIGATION

The results of the analysis of variable behavior in the areas were NDVI change was low, are provided in table 5. A paired t-test between the NDVI of the start and end period of the selected grid cells validated that the change was insignificant (p>0.5). For all variables except all runoff variables and canopy evaporation, the means of the two periods differ significantly. Within the area, on average precipitation has decreased by 7.9 mm, while temperature increased with 1 °C.

When interpreting the abovementioned results, the values in table 5 need to be kept in mind.

Variable	1982-1985	2017-2020	Difference	*p*
Average annual precipitation (mm)	244.9840	237.1993	-7.7847	**
Average annual daily temperature (°C)	16.6003	17.6239	1.0236	**
Average daily sensible heat flux (Joule/m2)	3.6911	3.7226	0.0355	**
Average daily latent heat flux (Joule/m2)	1.6642	1.7252	0.061	**
Average daily vapor pressure deficit (kPa)	1.2063	1.3127	0.1064	**
Average annual evapotranspiration:				
Total evaporation (mm)	242.8335	251.7581	8.9246	**
Vegetation transpiration (mm)	18.8472	20.4060	1.5588	*
Canopy evaporation (mm)	11.2898	11.2579	-0.0319	-
Bare soil evaporation (mm)	18.9705	20.3785	1.408	**
Snow evaporation (mm)	0.4457	0.3414	-0.1043	**
Open water evaporation (mm)	193.2846	199.3789	6.0943	**
Average annual runoff:				
Total runoff (mm)	12.8412	11.8321	-1.0091	-
Soil surface runoff (mm)	5.7694	6.1333	0.3639	-
Subsurface runoff (mm)	7.0674	5.6884	-1.379	-
Average daily soil moisture:				
Layer 1: 0-7 cm (mm3/m-3)	74.0585	69.4050	-4.6535	**
Layer 2: 7-28 cm (mm3/m-3)	147.0441	144.8720	-2.1721	**
Layer 3: 28-100 cm (mm3/m-3)	155.3894	160.2927	4.9033	**
Layer 4: 100-289 cm (mm3/m-3)	131.8611	140.3410	8.4799	**

Table 5. Mean values of the start and end period of the group where no significant vegetation change was observed. The third column gives the difference between the two, where start period values were substracted from values of the end period. The fourth column gives the level of significance of the difference between the means of the two groups, which was calculated with a pared T-test (*$p<0.05$, **$p<0.001$).

5. DISCUSSION

5.1. CLIMATE-VEGETATION INTERACTIONS IN THE MEDITERRANEAN

Going from correlations to causal relationships can be challenging, especially when so many variables are interplay and when correlations are not extremely strong. However, there are some trends which can be observed within the observed study area. First of all, within the area the average temperature has significantly increased by 1 degree. It was hypothesized that a vegetation increase would induce temperature decrease by means of an increased latent heat flux. Surprisingly, in the study area this was not the case. Temperature significantly correlated in a positive relationship with NDVI, and in areas where regreening occurred the average increase was often larger than 1 degree. This finding cannot be explained by the energy balance between the sensible heat flux and latent, as for the first correlations were quite low, and for the latter a strong positive correlation with NDVI was found. Moreover, in summer the correlation of NDVI with temperature shows an even higher positive value. Thus, regreening within the Mediterranean does not seem adequate as a heatwave mitigation strategy when looking solely at its correlation with vegetation activity. An explanation for the observed correlation could be that dense vegetation has a lower albedo (Bonan, 2008), increasing the total solar energy that is absorbed. However, it is possible that other factors of a significant influence here. For example, the regions that showed the strongest regreening were located nearer coastal areas, as opposed to the de-greened regions. Such areas are often under more influence of strong winds and water streams. When these have warm temperatures, they can heat up the nearby regions, which would explain the higher temperatures observed there. It could even be the other way around, that higher temperatures in the coastal areas induced vegetation transpiration due to increased VPD. This means that the photosynthetic activity of plants increased, giving higher NDVI values.

For precipitation, the causality of the found correlation can also be debated. Here, the observed correlation was as positive, as hypothesized. Especially during fall and winter, which are the periods when on average most rain falls (figure 9), precipitation mostly increased in areas where regreening was observed. Within the same seasons, bare soil evaporation, canopy evaporation, VPD, and soil surface runoff show strongest correlations with NDVI. This correlation can be explained by the precipitation increase during these seasons. For the question of drought mitigation by vegetation, it is more interesting to see how soil moisture is affected during periods of high precipitation. It was hypothesized that an increase in vegetation would increase infiltration due to the increase of root depth and spread. For the highest soil layer, this seems to be the case. This is indicated by the moderately strong and positive correlations with NDVI during fall and winter.

However, this effect does not last until spring, when moderate negative correlations are present, and can thus not contribute to summer drought mitigation.

Furthermore, in the more deeper soil layers correlations for all seasons are quite strong and negative. This could be partly explained by the fact that an enhancement of vegetation activity goes together with vegetation transpiration and that the water used for this comes is suctioned from the deeper layers. Additionally, for most soil layers the negative correlations are often strongest in the spring season. Likewise, this can be explained by the increase in vegetation transpiration during that period, as it is the growing season in the area (figure 13). That VPD correlates strongest with NDVI in this season also follows from the explanation of increased transpiration activity. However, when considering these interactions, it seems clear that the higher precipitation that is present in regreened areas does not cascade into higher soil moisture levels in summer and potential drought mitigation. On the other hand, this observation makes it more probable that the causal relationship is mostly in the direction of increased vegetation to increased precipitation. When more rain falls in winter, this does not seem to cause more moisture availability in growing seasons, and thus does not stimulate vegetation growth. However, when interpreting the differences between the correlations of vegetation with strongly de-greened and regreened areas, the potential of regreening for drought mitigation seems higher. This can be deduced from the fact that only in the regreened areas, there was a significant positive correlation of the moisture in the highest soil layers with NDVI. If this increase in soil moisture is present during summer periods, it increased water availability for evapotranspiration, leading to a cooling effect.

5.2. RESEARCH LIMITATIONS

The results obtained by this study of the Mediterranean area are the outcome of various choices. Therefore, below the most important choices that could have affected the results are reflected upon. Firstly, the temporal scale that was selected for this study was quite small for detecting climatic changes, as global climate change goes very gradually. However, if a longer time period was selected, NDVI data availability would have been less reliable as before 1982 there were not many good observations and often models that include years before 1982 use estimations. Furthermore, the fact that not NDVI observations of all years between 1982 and 2020 were used, makes it impossible to establish if the observed regreening and de-greening was gradual or abrupt. The lack of this decreases interpretation possibilities of the results. More abrupt changes in vegetation probably interact differently with hydrology and meteorology. Additionally, using averages of only 4 years for the start and end period does not completely overcome the influences of El Nino Southern Oscillation (ENSO) and North Atlantic Oscillation (NAO) cycles.

Secondly, the study area that was selected had more than half of its grid cells within one connected region, around the Atlas Mountains. It was clear from the results that this region for many variables behaved differently than the areas located north of the Mediterranean Sea. Additionally, the areas in the north were often located near the coast, as opposed to the areas in the southwest. Therefore, the areas of the selected grid cells in the northern and southwestern regions could be under influence of different factors that interfere with the variables that were studied. This could have caused the insignificant correlations, and undermined visibility of relationships between the variables and NDVI.

Thirdly, the research does not give insights in how the variables interplay with each other. Correlations between the variables could provide a better understanding of their relationship to each other. Additionally factors of regions next to the study areas potentially interact with the local hydro-metrological variables of the selected grid cells. For example, understanding how evapotranspiration from nearby areas affected precipitation in the study areas can be of important value for a better understanding of vegetation-climate interactions within the area. Furthermore, for the regreened and de-greened groups, no analysis was performed of the seasonal behaviour of the variables. This makes the yearly correlations of NDVI with the variables difficult to interpret.

Moreover, using satellite-based datasets comes with some limitations. Methods used for processing the observations influences the eventual outcomes of these models. The choices made for calibration, the functions used for calculating not directly observable variables, the quality of measurements and instruments all influence the output data (Zeng et al., 2022). However, the ERA5-Land dataset is supposed to be conducted with the most up to date observations and state-of-the-art scientific knowledge. Therefore, it is one of the most reliable datasets available.

5.3. RESEARCH IMPLICATIONS AND RECOMMENDATIONS

From the results of this study, it is not possible to give policy recommendations on land-use which could help mitigate heatwaves and droughts. However, the results of the correlations in the strongly regreened area do hint at a mitigating effect of regreening on droughts. To gain a better understanding of how vegetation activity interacts with the local climate in the Mediterranean Basin, future research should address the limitations of this research. For example, it would be valuable to study the interplay of the different variables with each other. Additionally, as increased vegetation activity correlated with higher temperatures, research on the interplay of albedo here is necessary. Furthermore, excluding the Atlas Mountain range from the study area could lead to a better understanding of the effects of regreening on the local climate.

6. CONCLUSION

The Mediterranean are threatened by an increase in drought and heatwave intensity and duration. Since scientific literature suggests a cooling and wetting effect of vegetation, this study aimed to answer the question on how vegetation activity has interacted with the local climate within areas in the Mediterranean Basin. The satellite-based data analysis of NDVI and hydro-meteorological correlations show that within the Mediterranean basin, vegetation activity has a positive relationship with both temperature and precipitation. It is most likely that increased vegetation activity causes an increase in precipitation. This can be explained by the fact that the former goes hand in hand with transpiration increases, which decrease the VPD. As a result, cloud formation is enhanced, and precipitation likelihood increases. This mechanism is most dominantly present during fall and winter. However, overall, the precipitation increase does not lead to more soil moisture during summer months. On the other hand, for strongly regreened areas there seems to be a positive relationship between soil moisture and vegetation activity. Thus, the potential of regreening for drought mitigation is not clear and needs to be further investigated. Furthermore, the stronger temperature increase observed for regreened areas can most likely be explained by albedo decreases. Likewise, to validate this assumption, future research is necessary.

REFERENCES

Albano, P. G., Steger, J., Bošnjak, M., Dunne, B., Guifarro, Z., Turapova, E., ... & Zuschin, M. (2021). Native biodiversity collapse in the eastern Mediterranean. *Proceedings of the Royal Society B*, *288*(1942), 20202469.

And, C. D., & Rambal, S. (1995). Field study of leaf photosynthetic performance by a Mediterranean deciduous oak tree (Quercus pubescens) during a severe summer drought. *New Phytologist*, *131*(2), 159-167.

Allen, R. G., Pereira, L. S., Raes, D., & Smith, M. (1998). Crop evapotranspiration-Guidelines for computing crop water requirements-FAO Irrigation and drainage paper 56. *Fao, Rome*, *300*(9), D05109.

Anders, I., & Rockel, B. (2009). The influence of prescribed soil type distribution on the representation of present climate in a regional climate model. *Climate dynamics*, *33*(2), 177-186.

Anderson, D. B. (1936). Relative humidity or vapor pressure deficit. *Ecology*, *17*(2), 277-282.

Angert, A., Biraud, S., Bonfils, C., Henning, C. C., Buermann, W., Pinzon, J., ... & Fung, I. (2005). Drier summers cancel out the CO2 uptake enhancement induced by warmer springs. *Proceedings of the National Academy of Sciences*, *102*(31), 10823-10827.

Bangash, R. F., Passuello, A., Sanchez-Canales, M., Terrado, M., López, A., Elorza, F. J., ... & Schuhmacher, M. (2013). Ecosystem services in Mediterranean river basin: climate change impact on water provisioning and erosion control. *Science of the Total Environment*, *458*, 246-255.

Bastin, J. F., Clark, E., Elliott, T., Hart, S., van den Hoogen, J., Hordijk, I., ... & Crowther, T. W. (2019). Understanding climate change from a global analysis of city analogues. *PloS one*, *14*(7), e0217592.

Bhattacharya, S. (2003*). The 2003 Europe heat wave caused 35,000 deaths*. New Scientist, October 10th

Blumler, M. A. (2005). Three conflated definitions of Mediterranean climates. *Middle States Geographer*, *38*(1), 52-60.

Bonan, G. B. (2008). Forests and climate change: forcings, feedbacks, and the climate benefits of forests. *science*, *320*(5882), 1444-1449.

Bounoua, L., Collatz, G. J., Los, S. O., Sellers, P. J., Dazlich, D. A., Tucker, C. J., & Randall, D. A. (2000). Sensitivity of climate to changes in NDVI. *Journal of Climate*, *13*(13), 2277-2292.

Brown, M. E., Pinzón, J. E., Didan, K., Morisette, J. T., & Tucker, C. J. (2006). Evaluation of the consistency of long-term NDVI time series derived from AVHRR, SPOT-vegetation, SeaWiFS, MODIS, and Landsat ETM+ sensors. *IEEE Transactions on geoscience and remote sensing*, *44*(7), 1787-1793.

Chávez, R. O., Clevers, J. G. P. W., Decuyper, M., De Bruin, S., & Herold, M. (2016). 50 years of water extraction in the Pampa del Tamarugal basin: Can Prosopis tamarugo trees survive in the hyper-arid Atacama Desert (Northern Chile)? *Journal of Arid Environments*, *124*, 292-303.

Climate Data Record Program, 2018. *Climate Algorithm Theoretical Basis Document (C-ATBD).* AVHRR Land Bundle - Surface Reflectance and Normalized Difference Vegetation Index. CDR Program Document Number: CDRP-ATBD-0459.

Coenders-Gerrits, A. M. J., Van der Ent, R. J., Bogaard, T. A., Wang-Erlandsson, L., Hrachowitz, M., & Savenije, H. H. G. (2014). Uncertainties in transpiration estimates. *Nature*, *506*(7487), E1-E2.

Dallman, P. R. (1998). *Plant life in the world's Mediterranean climates: California, Chile, South Africa, Australia, and the Mediterranean basin*. Univ of California Press.

Drumond, A., Nieto, R., Hernandez, E., & Gimeno, L. (2011). A Lagrangian analysis of the variation in moisture sources related to drier and wetter conditions in regions around the Mediterranean Basin. *Natural Hazards and Earth System Sciences*, *11*(8), 2307-2320.

Dutrieux, L. P., Verbesselt, J., Kooistra, L., & Herold, M. (2015). Monitoring forest cover loss using multiple data streams, a case study of a tropical dry forest in Bolivia. *ISPRS Journal of Photogrammetry and Remote Sensing*, *107*, 112-125.

Esler, K. J., Jacobsen, A. L., & Pratt, R. B. (2018). *The biology of Mediterranean-type ecosystems*. Oxford University Press.

Forzieri, G., Cescatti, A., e Silva, F. B., & Feyen, L. (2017). Increasing risk over time of weather-related hazards to the European population: a data-driven prognostic study. *The Lancet Planetary Health*, *1*(5), e200-e208.

Franch, B., Vermote, E. F., Roger, J. C., Murphy, E., Becker-Reshef, I., Justice, C., ... & Devadiga, S. (2017). A 30+ year AVHRR land surface reflectance climate data record and its application to wheat yield monitoring. *Remote Sensing*, *9*(3), 296.

Giorgi, F. (2006). Climate change hot-spots. *Geophysical research letters*, *33*(8).

Gitelson, A. A., & Merzlyak, M. N. (1998). Remote sensing of chlorophyll concentration in higher plant leaves. *Advances in Space Research*, *22*(5), 689-692.

Gitelson, A. A., Merzlyak, M. N., & Lichtenthaler, H. K. (1996). Detection of red edge position and chlorophyll content by reflectance measurements near 700 nm. *Journal of plant physiology*, *148*(3-4), 501-508.

González-Hidalgo, J. C., Peña-Monné, J. L., & de Luis, M. (2007). A review of daily soil erosion in Western Mediterranean areas. *Catena*, *71*(2), 193-199.

Gouveia, C. M., Trigo, R. M., Beguería, S., & Vicente-Serrano, S. M. (2017). Drought impacts on vegetation activity in the Mediterranean region: An assessment using remote sensing data and multi-scale drought indicators. *Global and Planetary Change*, *151*, 15-27.

Guan, X., Huang, J., Guo, N., Bi, J., & Wang, G. (2009). Variability of soil moisture and its relationship with surface albedo and soil thermal parameters over the Loess Plateau. *Advances in Atmospheric Sciences*, *26*(4), 692-700.

Guillod, B. P., Orlowsky, B., Miralles, D. G., Teuling, A. J., & Seneviratne, S. I. (2015). Reconciling spatial and temporal soil moisture effects on afternoon rainfall. *Nature communications*, *6*(1), 1-6.

Hély, C., & Lézine, A. M. (2014). Holocene changes in African vegetation: tradeoff between climate and water availability. *Climate of the Past, 10*(2), 681-686.
IPCC, Intergovernmental Panel on Climate Change (2021). *Climate Change 2021: The physical science basis*. Summary for policymakers.

Hillel, D. (1998). *Environmental soil physics: Fundamentals, applications, and environmental considerations*. Elsevier.

Hirschi, M., Seneviratne, S. I., Alexandrov, V., Boberg, F., Boroneant, C., Christensen, O. B., ... & Stepanek, P. (2011). Observational evidence for soil-moisture impact on hot extremes in southeastern Europe. *Nature Geoscience*, *4*(1), 17-21.

Holben, B. N. (1986). Characteristics of maximum-value composite images from temporal AVHRR data. *International journal of remote sensing*, *7*(11), 1417-1434.

Jin, H., & Eklundh, L. (2014). A physically based vegetation index for improved monitoring of plant phenology. *Remote Sensing of Environment, 152*, 512-525.

Kuglitsch, F. G., Toreti, A., Xoplaki, E., Della-Marta, P. M., Zerefos, C. S., Türkeş, M., & Luterbacher, J. (2010). Heat wave changes in the eastern Mediterranean since 1960. *Geophysical Research Letters*, *37*(4).

Lamarche, C., Santoro, M., Bontemps, S., d'Andrimont, R., Radoux, J., Giustarini, L., ... & Arino, O. (2017). Compilation and validation of SAR and optical data products for a complete and global map of inland/ocean water tailored to the climate modeling community. *Remote Sensing*, *9*(1), 36.

Larrasoaña, J. C., Roberts, A. P., & Rohling, E. J. (2013). Dynamics of green Sahara periods and their role in hominin evolution. *PloS one, 8*(10), e76514.

Lawrence, D. M., Thornton, P. E., Oleson, K. W., & Bonan, G. B. (2007). The partitioning of evapotranspiration into transpiration, soil evaporation, and canopy evaporation in a GCM: Impacts on land–atmosphere interaction. *Journal of Hydrometeorology*, *8*(4), 862-880.

Liu, H., Gong, P., Wang, J., Clinton, N., Bai, Y., & Liang, S. (2020). Annual dynamics of global land cover and its long-term changes from 1982 to 2015. *Earth System Science Data*, *12*(2), 1217-1243.

Longobardi, A., & Villani, P. (2010). Trend analysis of annual and seasonal rainfall time series in the Mediterranean area. *International journal of Climatology*, *30*(10), 1538-1546.

Lorenz, R., Davin, E. L., Lawrence, D. M., Stöckli, R., & Seneviratne, S. I. (2013). How important is vegetation phenology for European climate and heat waves?. *Journal of Climate*, *26*(24), 10077-10100.

Los, S. O., Collatz, G. J., Bounoua, L., Sellers, P. J., & Tucker, C. J. (2001). Global interannual variations in sea surface temperature and land surface vegetation, air temperature, and precipitation. *Journal of Climate*, *14*(7), 1535-1549.

Maiorano, L., Falcucci, A., Zimmermann, N. E., Psomas, A., Pottier, J., Baisero, D., ... & Boitani, L. (2011). The future of terrestrial mammals in the Mediterranean basin under climate change. *Philosophical Transactions of the Royal Society B: Biological Sciences*, *366*(1578), 2681-2692.

Mathbout, S., Lopez-Bustins, J. A., Royé, D., Martin-Vide, J., Bech, J., & Rodrigo, F. S. (2018). Observed changes in daily precipitation extremes at annual timescale over the eastern Mediterranean during 1961–2012. *Pure and Applied Geophysics*, *175*(11), 3875-3890.

Meier, R., Schwaab, J., Seneviratne, S. I., Sprenger, M., Lewis, E., & Davin, E. L. (2021). Empirical estimate of forestation-induced precipitation changes in Europe. *Nature geoscience*, *14*(7), 473-478.

Meneses-Tovar, C. L. (2011). NDVI as indicator of degradation. *Unasylva*, *62*(238), 39-46.

Miralles, D.G., Gentine, P., Seneviratne, S.I. & Teuling, A.J. (2019). Land-atmosphere feedbacks during droughts and heatwaves: state of the science and current challenges. Annals of the New York Academy of Sciences 1436, 19-35.

Miralles, D. G., Teuling, A. J., Van Heerwaarden, C. C., & Vilà-Guerau de Arellano, J. (2014). Mega-heatwave temperatures due to combined soil desiccation and atmospheric heat accumulation. *Nature geoscience*, *7*(5), 345-349.

Mueller, B., & Seneviratne, S. I. (2012). Hot days induced by precipitation deficits at the global scale. *Proceedings of the national academy of sciences*, *109*(31), 12398-12403.

Moore, F. C., & Lobell, D. B. (2015). The fingerprint of climate trends on European crop yields. *Proceedings of the National Academy of sciences*, *112*(9), 2670-2675.

Muñoz Sabater, J., (2019): ERA5-Land monthly averaged data from 1981 to present. *Copernicus Climate Change Service (C3S) Climate Data Store (CDS).* (Accessed on 16-01-2022), 10.24381/cds.68d2bb3

Myneni, R. B., Hall, F. G., Sellers, P. J., & Marshak, A. L. (1995). The interpretation of spectral vegetation indexes. *IEEE Transactions on Geoscience and Remote Sensing*, *33*(2), 481-486.

O'Connor, J. C., Dekker, S. C., Staal, A., Tuinenburg, O. A., Rebel, K. T., & Santos, M. J. (2021). Forests buffer against variations in precipitation. *Global change biology, 27*(19), 4686-4696.

Oki, T., Kanae, S., 2006. Global hydrological cycles and world water resources. Science 313, 1068–1072.

Pastor-Guzman, J., Atkinson, P. M., Dash, J., & Rioja-Nieto, R. (2015). Spatiotemporal variation in mangrove chlorophyll concentration using Landsat 8. *Remote sensing*, *7*(11), 14530-14558.

Prentice, I. C., Cramer, W., Harrison, S. P., Leemans, R., Monserud, R. A., & Solomon, A. M. (1992). Special paper: a global biome model based on plant physiology and dominance, soil properties and climate. *Journal of biogeography*, 117-134.

Quesada, B., Vautard, R., Yiou, P., Hirschi, M., & Seneviratne, S. I. (2012). Asymmetric European summer heat predictability from wet and dry southern winters and springs. *Nature Climate Change*, *2*(10), 736-741.

Rahman, H., Pinty, B., & Verstraete, M. M. (1993). Coupled surface-atmosphere reflectance (CSAR) model: 2. Semiempirical surface model usable with NOAA advanced very high resolution radiometer data. *Journal of Geophysical Research: Atmospheres*, *98*(D11), 20791-20801.

Ray, D. K., West, P. C., Clark, M., Gerber, J. S., Prishchepov, A. V., & Chatterjee, S. (2019). Climate change has likely already affected global food production. *PloS one*, *14*(5), e0217148.

Rietkerk, M., Dekker, S. C., De Ruiter, P. C., & van de Koppel, J. (2004). Self-organized patchiness and catastrophic shifts in ecosystems. *Science*, *305*(5692), 1926-1929.

Samaniego, L., Thober, S., Kumar, R., Wanders, N., Rakovec, O., Pan, M., ... & Marx, A. (2018). Anthropogenic warming exacerbates European soil moisture droughts. *Nature Climate Change, 8*(5), 421-426.

San-Miguel-Ayanz, J., Moreno, J. M., & Camia, A. (2013). Analysis of large fires in European Mediterranean landscapes: lessons learned and perspectives. *Forest Ecology and Management*, *294*, 11-22.

Savenije, H. H. (2004). The importance of interception and why we should delete the term evapotranspiration from our vocabulary. *Hydrological processes*, *18*(8), 1507-1511.

Schenk, H. J., & Jackson, R. B. (2002). Rooting depths, lateral root spreads and below-ground/above-ground allometries of plants in water-limited ecosystems. *Journal of Ecology*, 480-494.

Seneviratne, S.I., Corti, T., Davin, E.L., Hirschi, M., Jaeger, E.B., Lehner, I., Orlowsky, B. & Teuling, A.J. (2010). Investigating soil moisture-climate interactions in a changing climate: a review. Earth-Science Reviews 99, 125-161.

Semenza, J. C., Tran, A., Espinosa, L., Sudre, B., Domanovic, D., & Paz, S. (2016). Climate change projections of West Nile virus infections in Europe: implications for blood safety practices. *Environmental Health*, *15*(1), 125-136.

Serra, P., Pons, X., & Saurí, D. (2008). Land-cover and land-use change in a Mediterranean landscape: a spatial analysis of driving forces integrating biophysical and human factors. *Applied Geography*, *28*(3), 189-209.

Skalák, P., Farda, A., Zahradníček, P., Trnka, M., Hlásny, T., & Štěpánek, P. (2018). Projected shift of Köppen–Geiger zones in the central Europe: A first insight into the implications for ecosystems and the society. *International Journal of Climatology, 38(*9), 3595-3606.

Sousa, P. M., Trigo, R. M., Pereira, M. G., Bedia, J., & Gutiérrez, J. M. (2015). Different approaches to model future burnt area in the Iberian Peninsula. *Agricultural and Forest Meteorology*, *202*, 11-25.

Stefanon, M., D'Andrea, F., & Drobinski, P. (2012). Heatwave classification over Europe and the Mediterranean region. *Environmental Research Letters*, *7*(1), 014023.

Stephens, G. L., Li, J., Wild, M., Clayson, C. A., Loeb, N., Kato, S., ... & Andrews, T. (2012). An update on Earth's energy balance in light of the latest global observations. *Nature Geoscience*, *5*(10), 691-696.

Sugathan, N., Biju, V., & Renuka, G. (2014). Influence of soil moisture content on surface albedo and soil thermal parameters at a tropical station. *Journal of earth system science*, *123*(5), 1115-1128.

Tarpley, J. D., Schneider, S. R., & Money, R. L. (1984). Global vegetation indices from the NOAA-7 meteorological satellite. *Journal of Climate and Applied Meteorology*, 491-494.

Taylor, C. M., de Jeu, R. A., Guichard, F., Harris, P. P., & Dorigo, W. A. (2012). Afternoon rain more likely over drier soils. *Nature*, *489*(7416), 423-426.

Terrado, M., Acuña, V., Ennaanay, D., Tallis, H., & Sabater, S. (2014). Impact of climate extremes on hydrological ecosystem services in a heavily humanized Mediterranean basin. *Ecological indicators*, *37*, 199-209.

Teuling, A. J., Seneviratne, S. I., Stöckli, R., Reichstein, M., Moors, E., Ciais, P., ... & Wohlfahrt, G. (2010). Contrasting response of European forest and grassland energy exchange to heatwaves. *Nature geoscience*, *3*(10), 722-727.

Teuling, A. J. (2018). A hot future for European droughts. *Nature Climate Change*, *8*(5), 364-365.

Tran, A., Sudre, B., Paz, S., Rossi, M., Desbrosse, A., Chevalier, V., & Semenza, J. C. (2014). Environmental predictors of West Nile fever risk in Europe. *International journal of health geographics*, *13*(1), 1-11.

Trenberth, K. E., Fasullo, J. T., & Kiehl, J. (2009). Earth's global energy budget. *Bulletin of the American Meteorological Society*, *90*(3), 311-324.

Tsanis, I. K., Koutroulis, A. G., Daliakopoulos, I. N., & Jacob, D. (2011). Severe climate-induced water shortage and extremes in Crete. *Climatic Change*, *106*(4), 667-677.

Tucker, C. J. (1979). Red and photographic infrared linear combinations for monitoring vegetation. *Remote sensing of Environment*, *8*(2), 127-150.

Turco, M., Jerez, S., Augusto, S., Tarín-Carrasco, P., Ratola, N., Jiménez-Guerrero, P., & Trigo, R. M. (2019). Climate drivers of the 2017 devastating fires in Portugal. *Scientific reports*, *9*(1), 1-8.

Turco, M., Llasat, M. C., von Hardenberg, J., & Provenzale, A. (2014). Climate change impacts on wildfires in a Mediterranean environment. *Climatic Change*, *125*(3), 369-380.

Turco, M., Rosa-Cánovas, J. J., Bedia, J., Jerez, S., Montávez, J. P., Llasat, M. C., & Provenzale, A. (2018). Exacerbated fires in Mediterranean Europe due to anthropogenic warming projected with non-stationary climate-fire models. *Nature communications*, *9*(1), 1-9.

Valdes-Abellan, J., Pardo, M. A., & Tenza-Abril, A. J. (2017). Observed precipitation trend changes in the western Mediterranean region. *International Journal of Climatology*, *37*, 1285-1296.

Vautard, R., Yiou, P., D'andrea, F., De Noblet, N., Viovy, N., Cassou, C., ... & Fan, Y. (2007). Summertime European heat and drought waves induced by wintertime Mediterranean rainfall deficit. *Geophysical Research Letters*, *34*(7).

Vermote, E. NOAA CDR Program. (2019). NOAA Climate Data Record (CDR) of AVHRR Normalized Difference Vegetation Index (NDVI), Version 5. NOAA National Centers for Environmental Information. https://doi.org/10.7289/V5ZG6QH9.

Vicente-Serrano, S. M., Camarero, J. J., Olano, J. M., Martín-Hernández, N., Peña-Gallardo, M., Tomás-Burguera, M., ... & El Kenawy, A. (2016). Diverse relationships between forest growth and the Normalized Difference Vegetation Index at a global scale. *Remote Sensing of Environment*, *187*, 14-29.

Vicente-Serrano, S. M., Lopez-Moreno, J. I., Beguería, S., Lorenzo-Lacruz, J., Sanchez-Lorenzo, A., García-Ruiz, J. M., ... & Espejo, F. (2014). Evidence of increasing drought severity caused by temperature rise in southern Europe. *Environmental Research Letters*, *9*(4), 044001.

Wang, K., & Dickinson, R. E. (2012). A review of global terrestrial evapotranspiration: Observation, modeling, climatology, and climatic variability. *Reviews of Geophysics*, *50*(2).

Wei, J., & Dirmeyer, P. A. (2012). Dissecting soil moisture-precipitation coupling. *Geophysical Research Letters*, *39*(19).

Wei, Z., Yoshimura, K., Wang, L., Miralles, D. G., Jasechko, S., & Lee, X. (2017). Revisiting the contribution of transpiration to global terrestrial evapotranspiration. *Geophysical Research Letters*, *44*(6), 2792-2801.

te Wierik, S. A., Cammeraat, E. L., Gupta, J., & Artzy-Randrup, Y. A. (2021). Reviewing the Impact of Land Use and Land-Use Change on Moisture Recycling and Precipitation Patterns. *Water Resources Research*, *57*(7), e2020WR029234.

Yuan, W., Zheng, Y., Piao, S., Ciais, P., Lombardozzi, D., Wang, Y., ... & Yang, S. (2019). Increased atmospheric vapor pressure deficit reduces global vegetation growth. *Science advances*, *5*(8), eaax1396.

Zaitchik, B. F., Macalady, A. K., Bonneau, L. R., & Smith, R. B. (2006). Europe's 2003 heat wave: a satellite view of impacts and land–atmosphere feedbacks. *International Journal of Climatology: A Journal of the Royal Meteorological Society*, *26*(6), 743-769.

Zampieri, M., D'andrea, F., Vautard, R., Ciais, P., de Noblet-Ducoudré, N., & Yiou, P. (2009). Hot European summers and the role of soil moisture in the propagation of Mediterranean drought. *Journal of Climate*, *22*(18), 4747-4758.

Zeng, Y., Hao, D., Huete, A., Dechant, B., Berry, J., Chen, J. M., ... & Chen, M. (2022). Optical vegetation indices for monitoring terrestrial ecosystems globally. *Nature Reviews Earth & Environment*, 1-17.

Zhang, H., Chang, J., Zhang, L., Wang, Y., Li, Y., & Wang, X. (2018). NDVI dynamic changes and their relationship with meteorological factors and soil moisture. *Environmental Earth Sciences*, *77*(16), 1-11.

Zhu, X., & Liu, D. (2015). Improving forest aboveground biomass estimation using seasonal Landsat NDVI time-series. *ISPRS Journal of Photogrammetry and Remote Sensing*, *102*, 222-231.

Zittis, G., Hadjinicolaou, P., Fnais, M., & Lelieveld, J. (2016). Projected changes in heat wave characteristics in the eastern Mediterranean and the Middle East. *Regional environmental change*, *16*(7), 1863-1876.

APPENDIX I: VALIDATION OF METHODS

COMPUTATION OF MEDITERANEAN CLIMATE MASK

For the computation of the mask that indicated areas with a Mediterranean climate, the Köppen-Geiger climate classifications Csa and Csb were used. However, as depicted in figure A, a large area east of the Mediterranean Basin also fell within this classification. This part was cut off from the mask that was used in this study. Literature suggested that this eastern area has another biome, and often within literature this area is not considered to fall within the Mediterranean Basin.

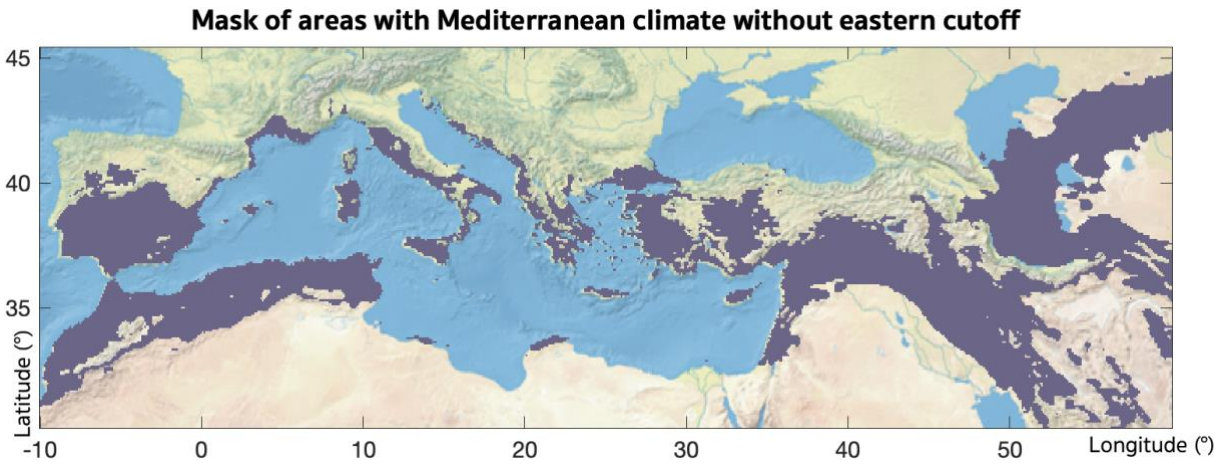

Figure A. Purple regions indicate the selected grid cells where a Mediteranean climate is present according to Köppen-Geiger climate classification.

COMPUTATION OF CROPLAND MASK

Figure B depicts the two cropland maps that were conducted from large resolution land cover maps. Upon rescaling to 0.1, the logical values of the grid cells were averaged, creating percentages of the amount of cropland in each grid cell. It is clear from the figure that the map of 1982 had a lower resolution, leading to less variation in percentages upon rescaling. In the map of 2020 often near white grid cells are present, because rescaling caused a percentage above 0 even if only 1/36 of the original cells had agriculture.

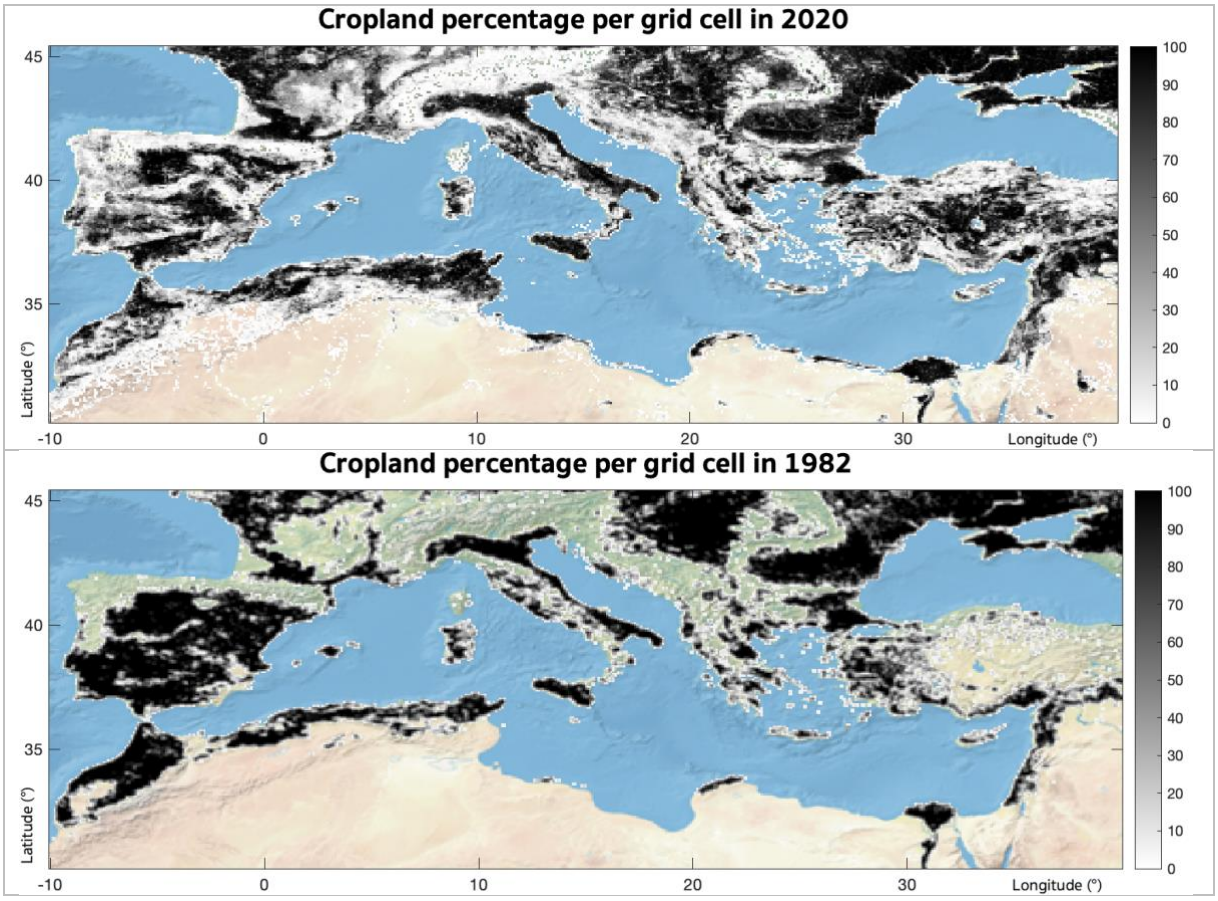

Figure B. Computed maps indicating cropland percentages per grid cell for 2020 and 1982.

CROPLAND PERCENTAGE SELECTION

Within the selected areas with a Mediterranean climate, a dominating region with selected grid cells for 0% agriculture is located around the Atlas Mountains. To overcome that only this region is used for this study, the cropland percentage was increased from 0%. The trade-off is that when the percentage is too high, the study area will be under higher influence of agricultural irrigation, whilst when it is too low the Atlas Mountains region is dominant. Therefore, by observing the maps and making rough calculations of the selected cells in the Atlas Mountain region, the mask with cropland below 15% was selected. Here, the Atlas Mountain region still covers a bit over half of the grid cell. However, increasing the percentage did not make this ratio much smaller, whilst 20% of cropland within a grid cell might substantially influence the hydro-meteorological variables that were studied. Figure C shows the areas selected for the different cropland percentages.

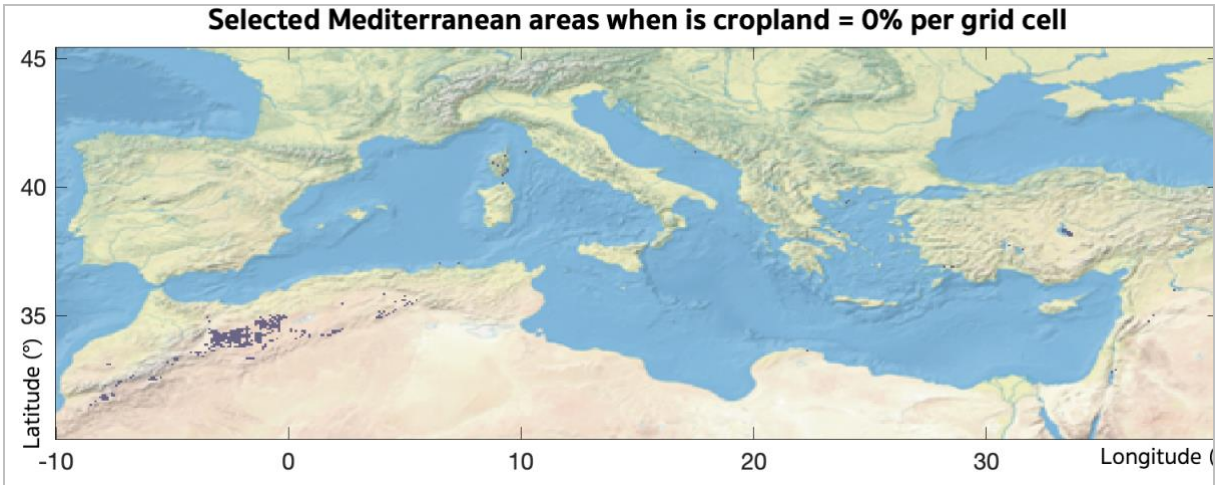

N= 349, area of Atlas Mountains N ≈ 302

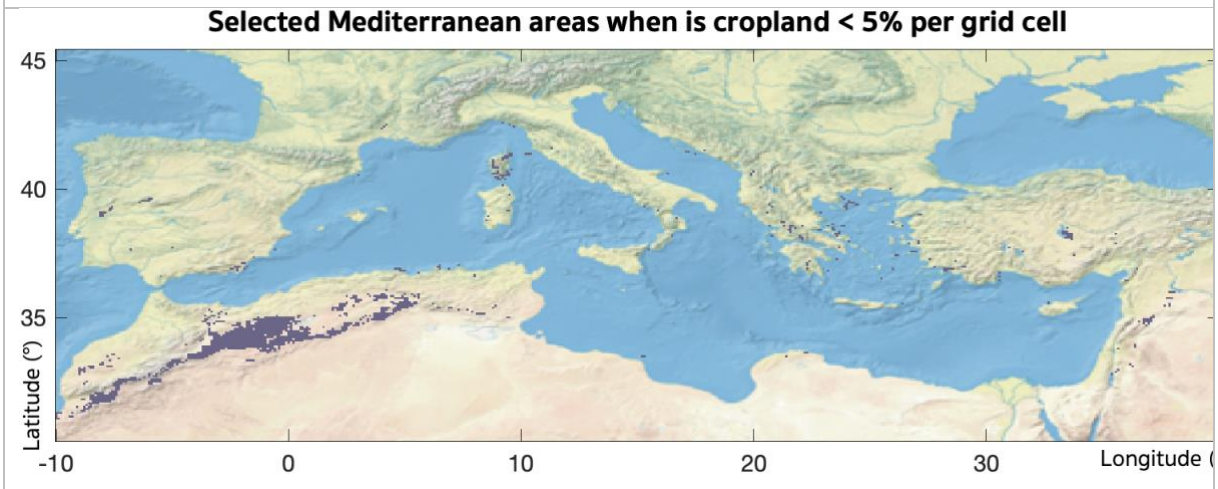

N= 1250, area of Atlas Mountains N ≈ 902

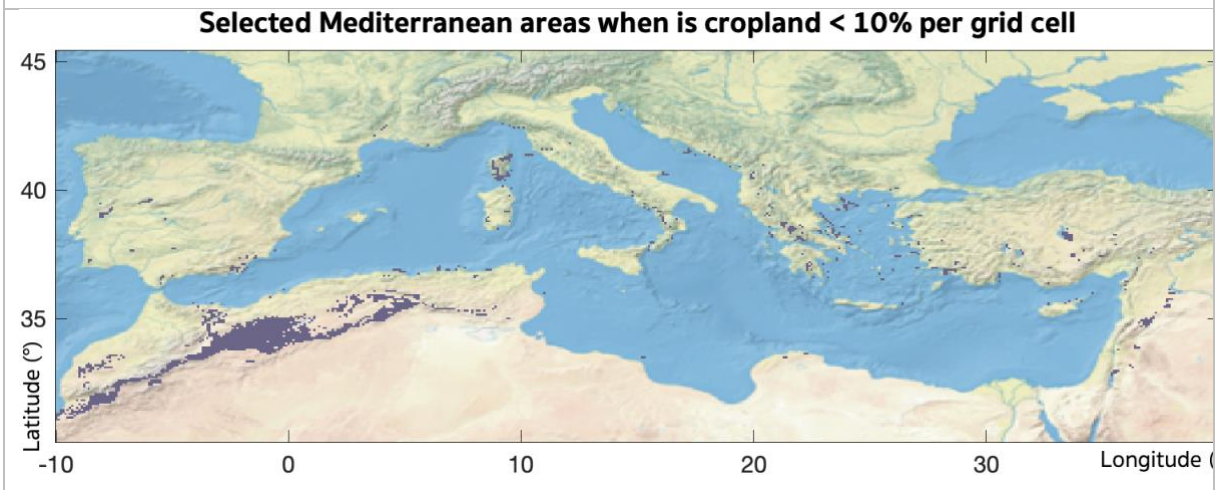

N= 1681, area of Atlas Mountains N ≈ 1099

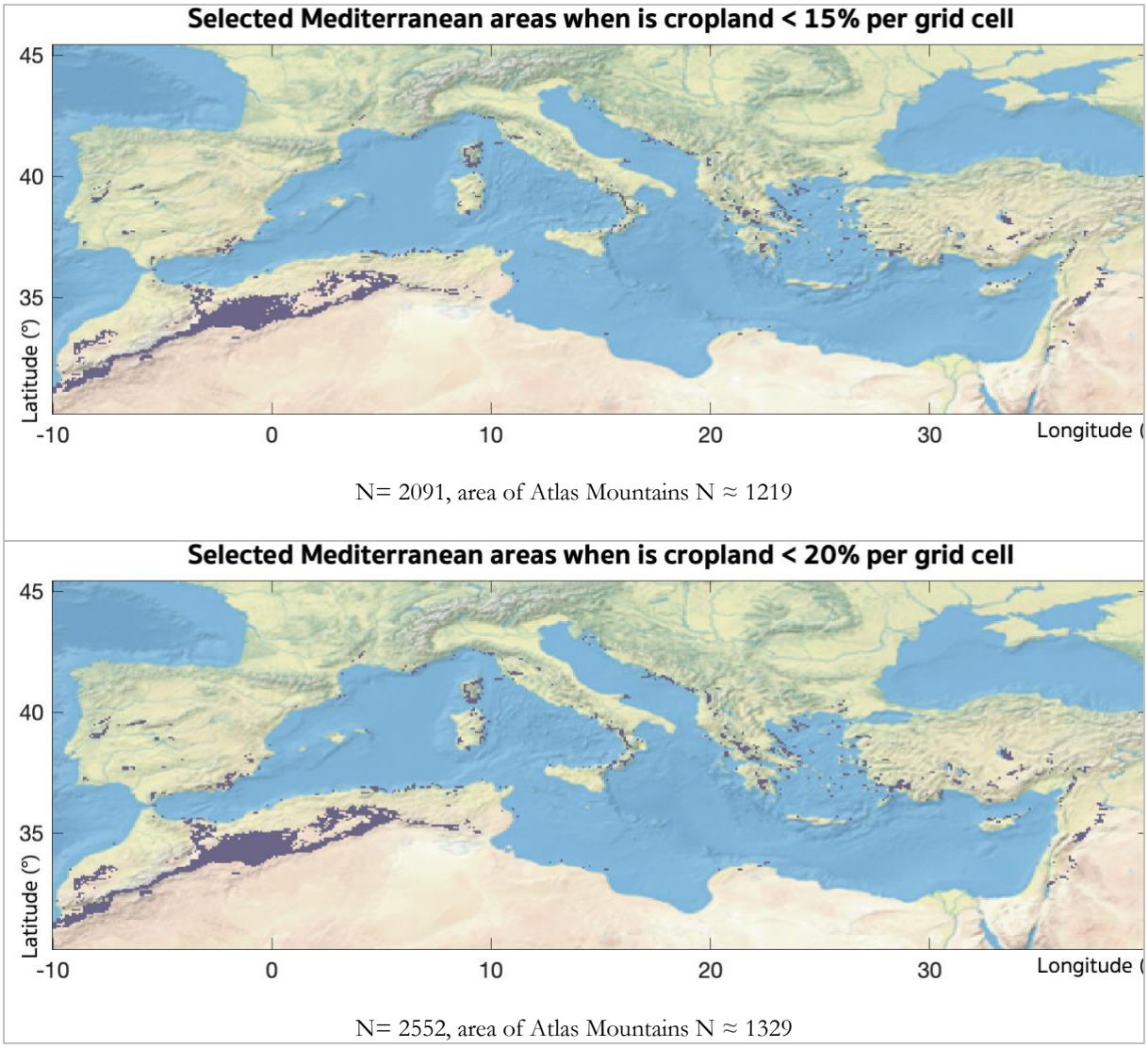

Figure C. Purple regions indicate the selected grid cells where the percentage of cropland is below a certain threshold (from up to down: 0, 5, 10, 15, 20, 25). Additionally, below each map the total amount of selected grid cells is given, and a rough calculation of the cells that are located in the Atlas Mountain region.

PATTERN OF AVERAGE NDVI PER MONTH

Figure D shows images that were made when upon initial exploration of the NDVI data. It was observed that for the years 2019 and 2020, for most parts of the winter days (October-January) the satellite observations were of very poor quality. Often more than half of the grid cells had NaN values, or otherwise very low values. Probably many observations were performed during times of the day with a large solar zenith angle or had a lot of cloud cover. Additionally, it seemed like something was flying in front of the satellite radiometer. However, as during summer months observations were normal, the MVC method that was used in this study still led to obtaining the accurate maximum NDVI values throughout the year for each grid cell.

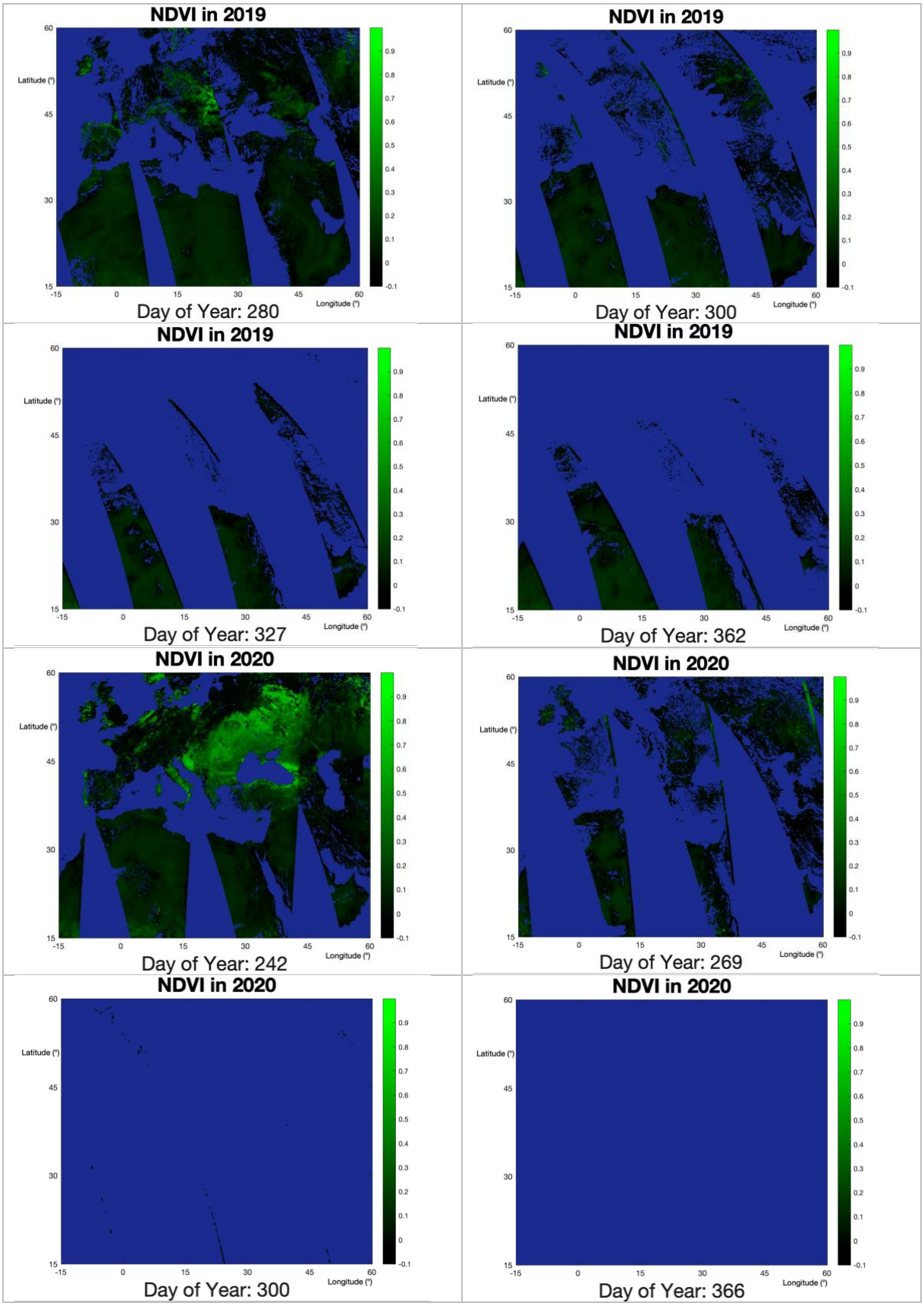

Figure D. Images conducted with the daily satellite NDVI observations for some days in 2019 and 2020 to illustrate the poor quality of the measurements during the winter period of these years. Blue pixels were shown when grid cells had a NaN value.

Additionally, due to this bad quality for some periods, it was not possible to calculate reliable seasonal NDVI values per grid cell. However, to still gain some insight into NDVI behavior throughout the year in the Mediterranean area, figure E was created. It shows the mean NDVI values of all grid cells per month, with each grid cell expressing the mean of its 5 maximum values. It is also clear from this figure how in 2019 and 2020 the pattern greatly deviates from the other years in the winter period.

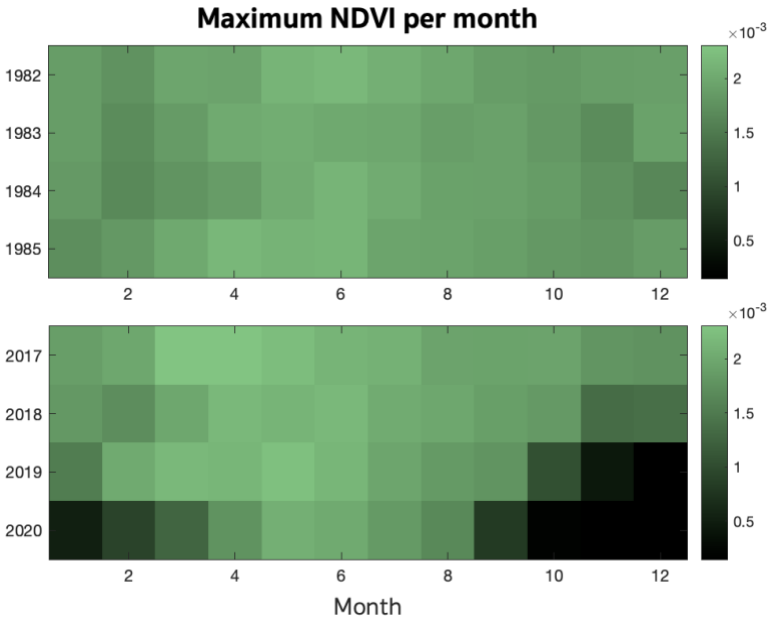

Figure E. The NDVI values were calculated by taking the mean value of all grid cells of the selected areas. For each grid cell the maximum 5 NDVI values measured over the whole month were taken. For the years 2019 and 2020 in some winter months the data quality was very low, with very low overall measurements, leading to the low NDVI measured in these months.

As the years 2019 and 2020 did not show a reliable NDVI pattern, these years were not included for the creation of the mean NDVI pattern depicted in figure 13. Figure F depicts how the mean NDVI pattern for the end period when 2019 and 2020 are not included.

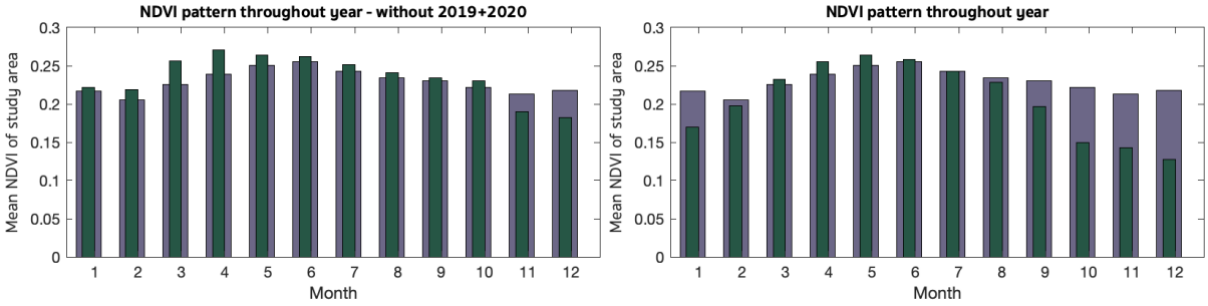

Figure F. Mean of maximum NDVI values of each grid cell for the start and end period. In the left figure, the years 2019 and 2020 are not included in the calculation of the end period. Purple bars indicate the start period, green bars the end period.

APPENDIX II: ADDITIONAL RESULTS

MEAN MONTHLY VARIATION OF VARIABLES

Figure G depicts the seasonal pattern of all variables, except precipitation and temperature since these were already provided within the results section.

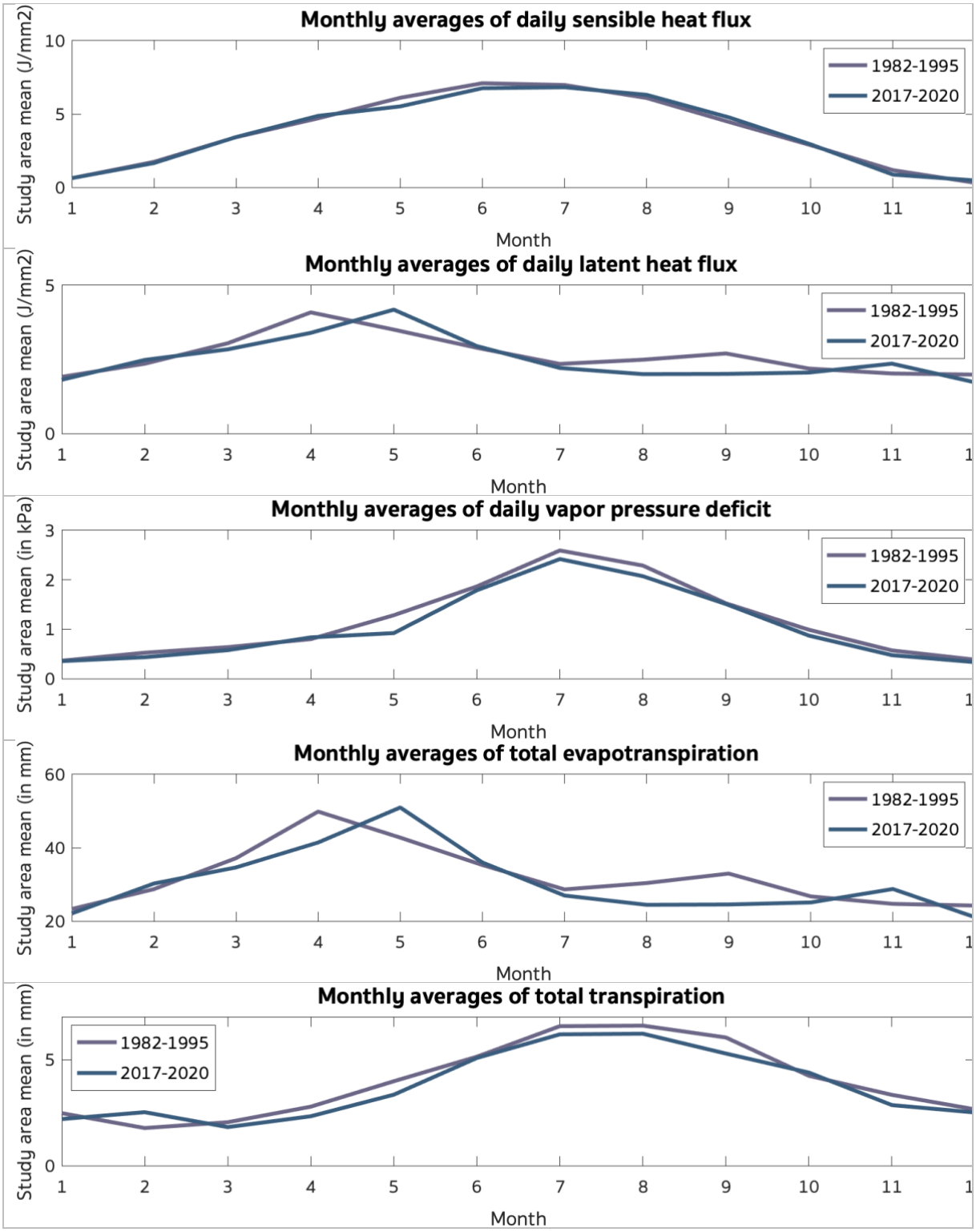

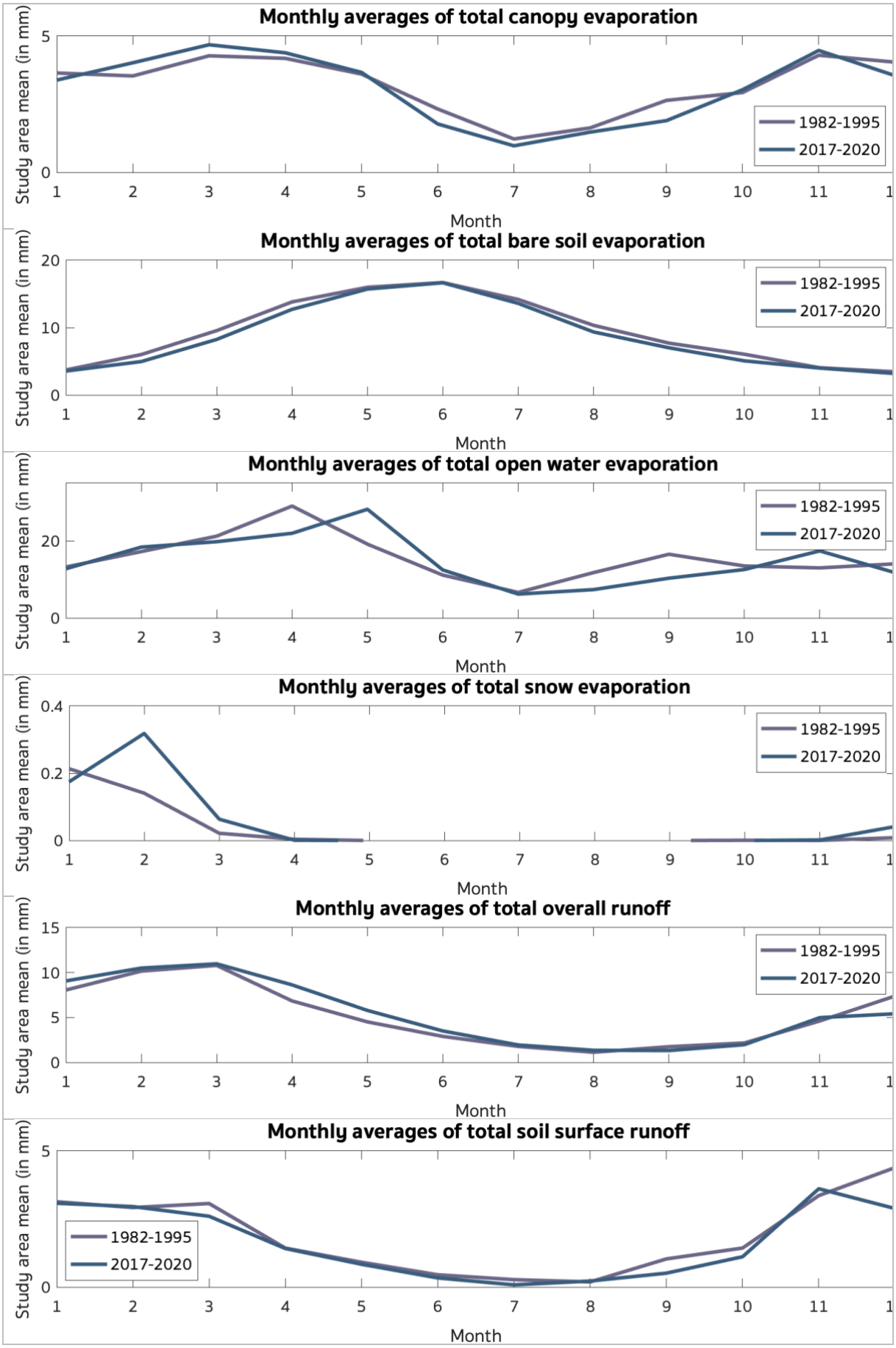
Monthly averages of total canopy evaporation
Study area mean (in mm)
Month
1982-1995
2017-2020
Monthly averages of total bare soil evaporation
Monthly averages of total open water evaporation
Monthly averages of total snow evaporation
Monthly averages of total overall runoff
Monthly averages of total soil surface runoff

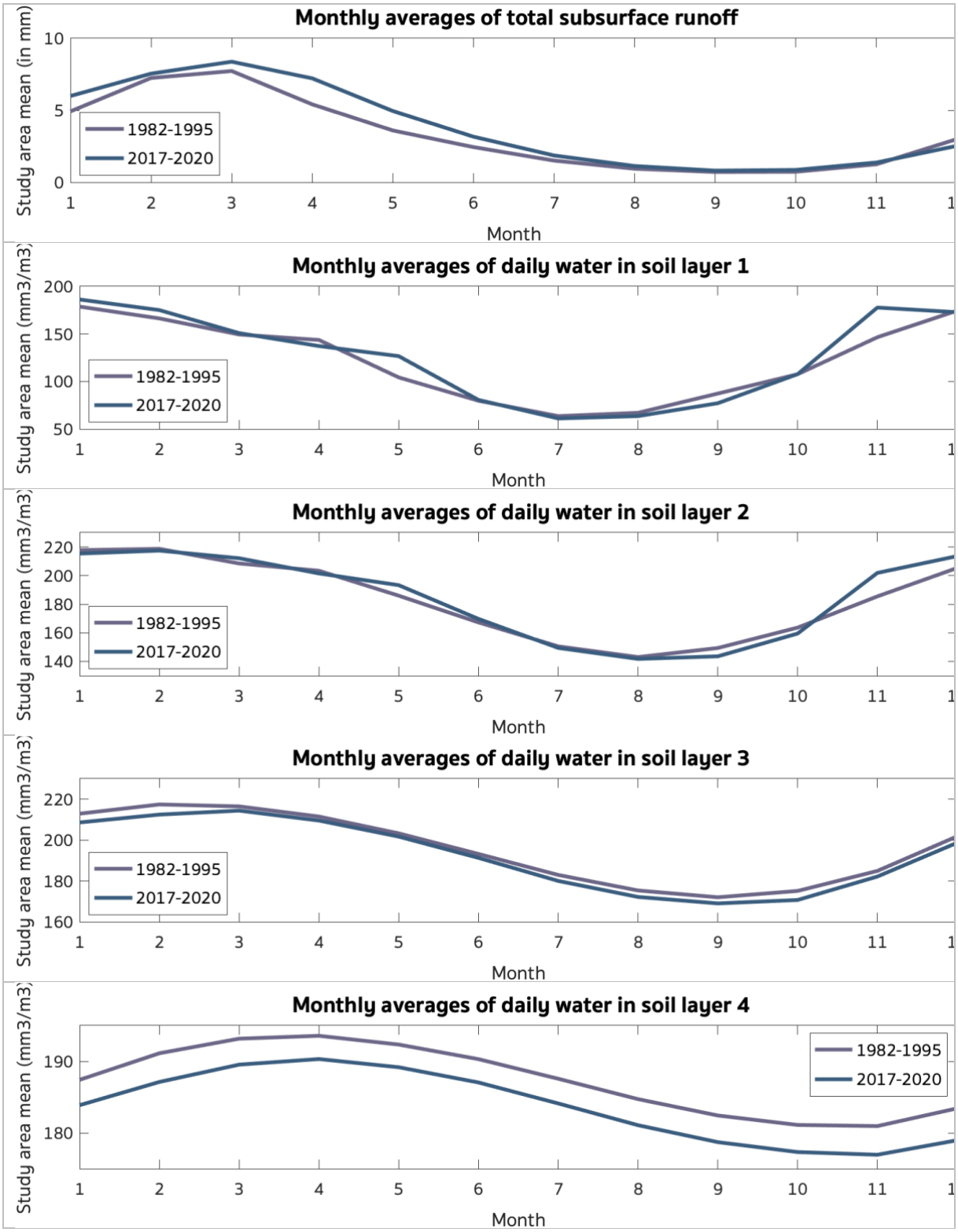

Figure G. The monthly mean values per time period. As is specified within their title, some figures show monthly accumulated values ('total') whilst the other show daily mean values.

ABSOLUTE NDVI VALUES IN 1982-1985

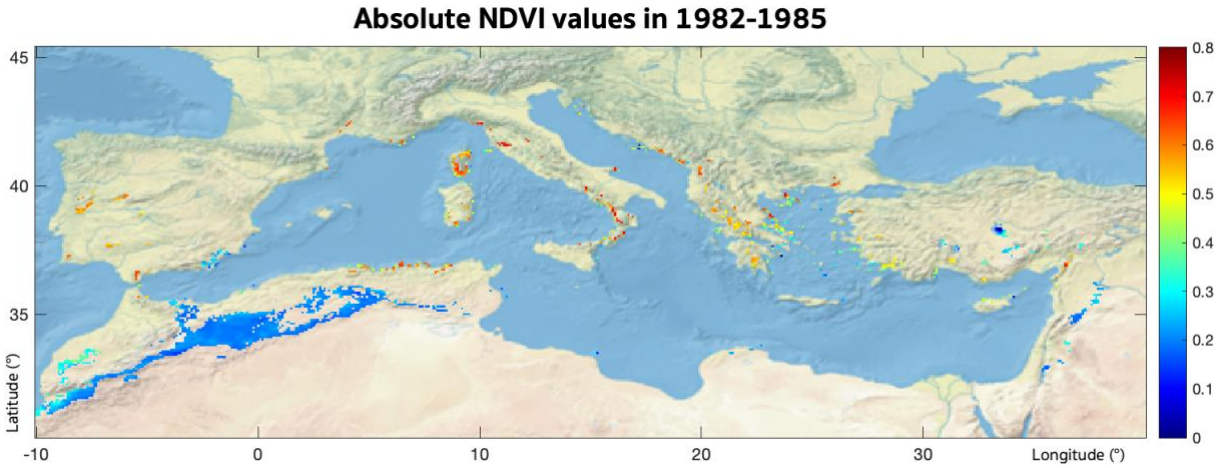

Figure H. Absolute mean NDVI values in 1982-1985 for the selected cells.

CORRELATION PLOTS INCLUDING ALL GRID CELLS

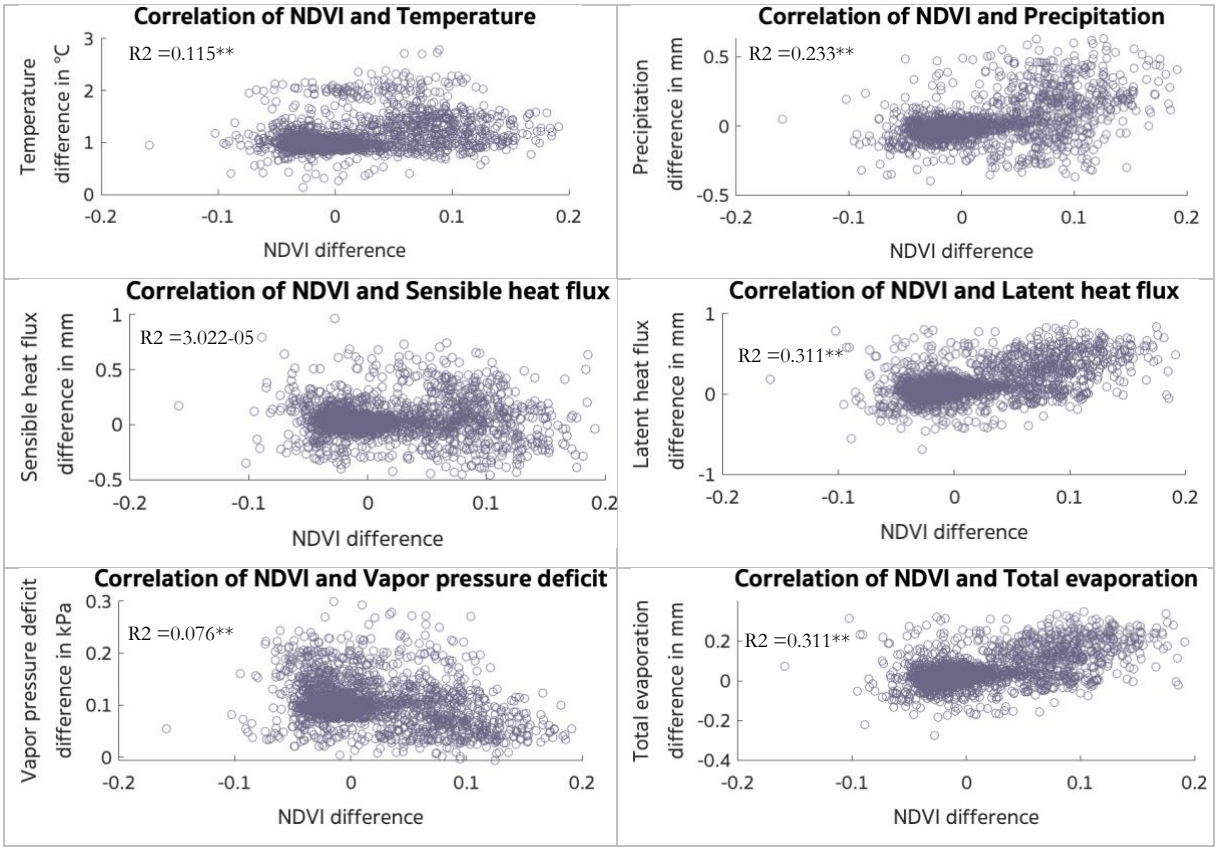

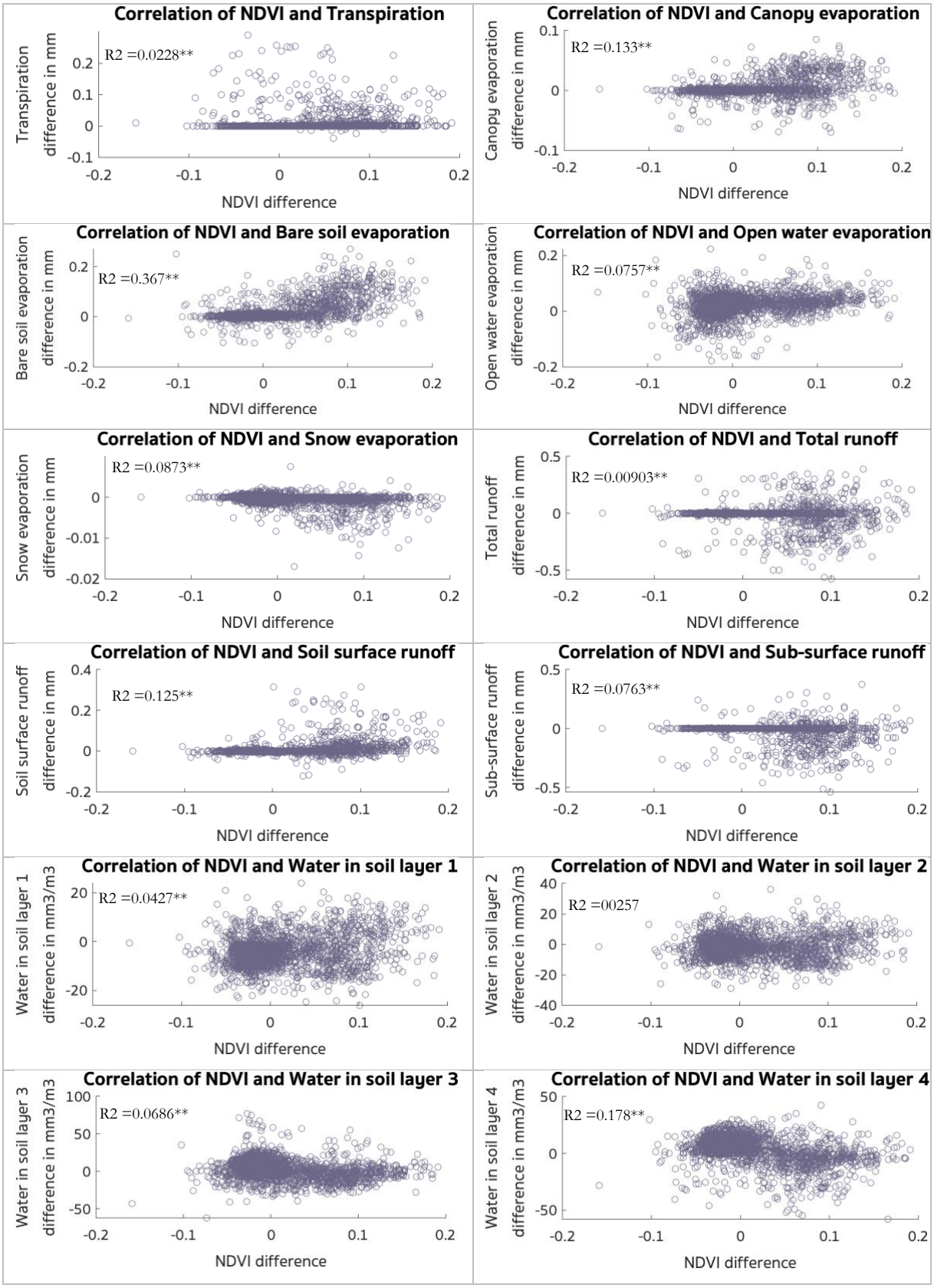

Figure I. Scatter plots depicting the correlations of NDVI difference with variable difference. All variable differences were calculated with daily values, and not with values that accumulated the entire year. For each plot corresponding the R-squared value is provided ($p<0.05$, $^{**}p<0.001$).

APPENDIX III: MATLAB CODE

```
%% NDVI highest value selection per year
% parameters:
year = 2020 % must be done for years 1982-1984 and 2017-2020
startnamefiles = 'AVHRR-Land_v005-preliminary_AVH13C1_NOAA-19_' %name of files that is same for all of the year, must be copied
manually from filename

% path selection:
folder = ['/Users/eva/Documents/Studie/Sustainable Development MS/Thesis/Matlab/NDVI/'+string(year)];
cd(folder)

% 1. NDVI data download
   %impossible to do completely by code
   %but file names can be copied from website to Ecxel
   %then import Excel file as cell array
   %name of this array is here Map1

parfor a = 1:length(Map1)
   file = Map1(a);
   URL = ['https://www.ncei.noaa.gov/data/avhrr-land-normalized-difference-vegetation-index/access/'+string(year)+'/'+file];
websave(file, URL);
end

% 2. NDVI layered matrix development
files= dir('*.nc');
filenames = string(vertcat(files.name));

NDVIlayered = zeros(1502,901,1);
for k = 1:length(filenames)
   NDVI = ncread(filenames(k), 'NDVI');
   NDVImed = NDVI(3300:4801, 600:1500); % rough  Mediterranean area selection
  NDVIlayered = cat(3,NDVIlayered,[NDVImed]);
end
NDVIlayered(:,:,1) = []; %remove zeros matrix from layers

clearvars -except NDVIlayered
evalc(['NDVIlayered'+string(year)+' = '+NDVIlayered])
save(['NDVIlayered'+string(year)], ['NDVIlayered'+string(year)], '-v7.3');

% 3. NDVI mean of 5 maximum values per year, per cell
meanmaxall=mean(maxk(NDVIlayered, 5, 3),3);
save(['meanmaxall'+string(year)],['meanmaxall'+string(year)]);

%% Constuction of map with NDVI differences between start and end period
% 1. Loading all  matrices of max NDVI per year, and saving in same folder:
years = [1982; 1983; 1984; 1985; 2017; 2018; 2019; 2020];
newfolder = ['/Users/eva/Documents/Studie/Sustainable Development MS/Thesis/Matlab/NDVI/Total of NDVI MED and LC']
for y = 1:8
   folder = ['/Users/eva/Documents/Studie/Sustainable Development MS/Thesis/Matlab/NDVI/'+string(years(y))];
   cd(folder);
   load(['meanmaxall'+string(years(y))]);
   cd(newfolder)
   save(['meanmaxall'+string(years(y))],['meanmaxall'+string(years(y))]);
end

% 2. Taking the mean of startperiod and end period
%start:
layered= cat(3, meanmaxall1982, meanmaxall1983, meanmaxall1984, meanmaxall1985);
meanmaximastart = mean(layered, 3, 'omitnan');
%end:
layered= cat(3, meanmaxall2017, meanmaxall2018, meanmaxall2019, meanmaxall2020);
meanmaximaend = mean(layered, 3, 'omitnan');
% calculating differences:
difference = meanmaximaend- meanmaximastart;
save('difference', 'difference')

% 2. Scaling difference map to ERA5 resolution
for i = 1:751;
for j = 1:450;
   map = difference;
deze_data = map(2*(i-1)+1:2*i,2*(j-1)+1:2*j);
deze_data = deze_data(:);
differencescaled(i,j) = mean(deze_data, 'omitnan');
end
end
save('differencescaled','differencescaled')
```

```
%% Mask for cropland filter
% 1. For 1982:
cd '/Users/eva/Documents/Studie/Sustainable Development MS/Thesis/Matlab/Landcover map/GLASS-GLC'
lc1982 = imread('GLASS-GLC_7classes_1982.tif');
crops1982 = (lc1982==10); %10 is agriculture flag (readme file states this)
% for coordinates:
I = geotiffinfo('GLASS-GLC_7classes_1982.tif');
[x,y]=pixcenters(I);
lats_dataset = (reshape(repelem(y, 8016), 8016,[])');
lons_dataset = reshape(repelem(x, 3229), 3229, []);
% mediteranean preselected area was lat = 15-60 & long = -15-60, so I tried
% to scale to these coordinates:
lats_dataset1 = lats_dataset(557:1559, 3674:5345); % coordinates here are 14.9794 - 60.0299
lons_dataset1 = lons_dataset(557:1559,3674:5345); % coordinates here are -15.0243 - 60.0299
% --> so coordinates have a very small difference, lie a very small bit
% outside the boudaries

dataset = crops1982(557:1559,3674:5345);
lats =  15.00:0.1:60.00;
lons = -15.00:0.1:60.00;
for i = 1:451
for j = 1:751
idx = lats_dataset1 >= lats(i)-0.1 & lats_dataset1 < lats(i)+0.1 & lons_dataset1 >= lons(j)-0.1 & lons_dataset1 < lons(j)+0.1;
data_current_grid = dataset(idx);
crops1982_scaled(j,i) = mean(data_current_grid);
end
end
crops_1982scaled = flipud(crops1982_scaled);
save('crops_1982scaled', 'crops_1982scaled')

% 2. For 2020:
cd '/Users/eva/Documents/Studie/Sustainable Development MS/Thesis/Matlab/Landcover map/Copernicus2016-2020'
status2020= ncread('C3S-LC-L4-LCCS-Map-300m-P1Y-2020-v2.1.1.nc', 'lccs_class');
crops2020mask = (status2020==10|status2020==11|status2020==12|status2020==20|status2020==30); % these flags stand for all the flags
with a type of cropland
% first scaling to 0.05 resolution
for i = 1:7200
for j = 1:3600
deze_data = crops2020mask(18*(i-1)+1:18*i,18*(j-1)+1:18*j);
deze_data = deze_data(:);
crops2020scaled005(i,j) = mean(deze_data, 'omitnan');
end
end
% then select the right area:
cropsscaled2020med = crops2020scaled005(3300:4801, 600:1500);
% further scaling to 0.1 resolution
for i = 1:751;
for j = 1:450;
    map = cropsscaled2020med;
deze_data = map(2*(i-1)+1:2*i,2*(j-1)+1:2*j);
deze_data = deze_data(:);
crops2020scaled01(i,j) = mean(deze_data, 'omitnan');
end
end
save('crops2020scaled01','crops2020scaled01')

% 3. Combining both masks, choosing different cropland percentages:
cropsmask0 = (crops2020scaled01==0)' .* (crops_1982scaled(1:450, :)==0);
cropsmask5 = (crops2020scaled01<=0.05)' .* (crops_1982scaled(1:450, :)<=0.05);
cropsmask10 = (crops2020scaled01<=0.1)' .* (crops_1982scaled(1:450, :)<=0.1);
cropsmask15 = (crops2020scaled01<=0.15)' .* (crops_1982scaled(1:450, :)<=0.15);
cropsmask20 = (crops2020scaled01<=0.2)' .* (crops_1982scaled(1:450, :)<=0.2);

%% Mask for Meditterranean climate
% 1. Own calculation:
% requirements Csa/b classification (units in Celsius and mm!) :
% 1. (Thot>10+ & 0<Tcold<18)
% 2. (Psdry < 40 & Psdry< Pwwet/3)
% 3. (Thot≥22 OR Tmon10≥4)
cd '/Users/eva/Documents/Studie/Sustainable Development MS/Thesis/Matlab/ERA5'
totalprec = ncread('Era52.nc', 'tp');
temp= ncread('Era52.nc','t2m');
% calculate mean values per month in 39 year period (1982-2020)
z= [1:12:468];
jan_prec=mean(totalprec(:,:,z), [3], 'omitnan');
feb_prec=mean(totalprec(:,:,z+1), [3], 'omitnan');
mar_prec=mean(totalprec(:,:,z+2), [3], 'omitnan');
```

```
apr_prec=mean(totalprec(:,:,z+3), [3], 'omitnan');
may_prec=mean(totalprec(:,:,z+4), [3], 'omitnan');
jun_prec=mean(totalprec(:,:,z+5), [3], 'omitnan');
jul_prec=mean(totalprec(:,:,z+6), [3], 'omitnan');
aug_prec=mean(totalprec(:,:,z+7), [3], 'omitnan');
sep_prec=mean(totalprec(:,:,z+8), [3], 'omitnan');
oct_prec=mean(totalprec(:,:,z+9), [3], 'omitnan');
nov_prec=mean(totalprec(:,:,z+10), [3], 'omitnan');
dec_prec=mean(totalprec(:,:,z+11), [3], 'omitnan');
vector_meanprec = cat(3, jan_prec, feb_prec, mar_prec, apr_prec, may_prec, jun_prec, jul_prec, aug_prec, sep_prec, oct_prec, nov_prec,
dec_prec);

jan_temp=mean(temp(:,:,z), [3], 'omitnan');
feb_temp=mean(temp(:,:,z+1), [3], 'omitnan');
mar_temp=mean(temp(:,:,z+2), [3], 'omitnan');
apr_temp=mean(temp(:,:,z+3), [3], 'omitnan');
may_temp=mean(temp(:,:,z+4), [3], 'omitnan');
jun_temp=mean(temp(:,:,z+5), [3], 'omitnan');
jul_temp=mean(temp(:,:,z+6), [3], 'omitnan');
aug_temp=mean(temp(:,:,z+7), [3], 'omitnan');
sep_temp=mean(temp(:,:,z+8), [3], 'omitnan');
oct_temp=mean(temp(:,:,z+9), [3], 'omitnan');
nov_temp=mean(temp(:,:,z+10), [3], 'omitnan');
dec_temp=mean(temp(:,:,z+11), [3], 'omitnan');
vector_meantemp = cat(3, jan_temp, feb_temp, mar_temp, apr_temp,
may_temp,jun_temp,jul_temp,aug_temp,sep_temp,oct_temp,nov_temp,dec_temp);

% calculate Thot for each coordinate:
Thot = max(vector_meantemp, [], 3, 'omitnan');
% calculate where the this value is above 10 deg. Celsius:
temp1 = Thot>(10+273.15);
%caldulate Tcold for each coordinate:
Tcold = min(vector_meantemp, [], 3, 'omitnan');
% calutlate 0<Tcold<18
temp2 = 273.15<Tcold<(18+273.15);
% total calculation:
mask1 = Thot>10+273.15 & 273.15<Tcold<(18+273.15);

% calculate Psdry summer:
Psdry = min(vector_meanprec(:,:,4:9), [], 3, 'omitnan');
% calculate Pwwet winter:
winter = [1:3,10:12];
Pwwet = max(vector_meanprec(:,:,(winter)), [], 3, 'omitnan');
% calculate total mask 2
mask2 = (Psdry < 0.04) & (Psdry< (Pwwet/3));

% calculate Tmon (amount of months were temp is above 10)
Tmon10 = vector_meantemp>(10+273.15);
% total mask 3
mask3 = (Thot>=(22+273.15)) | ((sum(Tmon10,3, 'omitnan'))>=4);

% exculde arid regions (B classifiation)
MAP = mean(vector_meanprec(:,:,:), 3, 'omitnan');
MAPwinter = sum(vector_meanprec(:,:,(winter)), 3, 'omitnan');
MAPsummer = sum(vector_meanprec(:,:,4:9), 3, 'omitnan');
MAPtotal = sum(vector_meanprec, 3, 'omitnan');
MAT = mean(vector_meantemp(:,:,:), 3, 'omitnan');
if (MAPwinter ./ MAPtotal)>=0.7
    Pthreshold = 2 .*(MAT - 273.15)
elseif (MAPsummer ./ MAPtotal)>=0.7
   Pthreshold = 2 .*(MAT- 273.15) + 28
else Pthreshold = 2 .*(MAT- 273.15) + 14
end
exclusionB = (MAP * 1000000)<(10 .* Pthreshold);

%exclude Cw regions:
Pwdry = min(vector_meanprec(:,:,(winter)), [], 3, 'omitnan');
Pswet = max(vector_meanprec(:,:,4:9), [], 3, 'omitnan');
exclusionCw = Pwdry <Pswet/10;
%exclude D (Thot>10 & Tcold≤0)
excludeD = (Thot>10) & (Tcold<=0); %gives zero values, as expected
%exclude E (Thot <10)
excludeE = Thot <10; %gives zero values, as expected
% total mask:
maskmedclimate = mask1 .* mask2 .* mask3 .* (exclusionB==0).* (exclusionCw==0);

% 2. Other map: Adjustment of premade Mediterranean mask:
```

```
medit = shaperead('Mediterranean_basin.shp');
X1 = medit(1).X;
Y1 = medit(1).Y;
dataLen1 = length(X1);

X2 = medit(2).X;
Y2 = medit(2).Y;
dataLen2 = length(X2);

gridlons_01deg = -179.90:0.1:179.90;
gridlats_01deg = 89.90:-0.1:-89.90;

medit_mask01 = inpolygon(repmat(gridlons_01deg,length(gridlats_01deg),1),repmat(gridlats_01deg,1,length(gridlons_01deg)),X1(:),Y1(:)) + ...
    inpolygon(repmat(gridlons_01deg,length(gridlats_01deg),1),repmat(gridlats_01deg,1,length(gridlons_01deg)),X2(:),Y2(:));

medit_mask01zoomed = medit_mask01(300:750, 1650:2400) % same grid cells as ERA5 dataset

save('medit_mask01zoomed.mat', 'medit_mask01zoomed')

% 3. Cutting of east boudary of own mask with pre-made mask:
newmaskmed = maskmedclimate';
for y = 1:451
    allx = medit_mask01zoomed(y,:);
[I,J] = find(allx==1);
   x = max(J);
    newmaskmed(y,(x+1):751) = 0;
end
save('newmaskmed', 'newmaskmed')

% calculate the areas that fall within Mediterranean climate and have the chosen crops percentage:
evalc(['cropsmask = cropsmask'+string(crop_per)]);
usefulareas = cropsmask15 .* meditclimatemask(1:450,:);

% calculate NDVI differences for the selected areas:
NDVIdiff_usefulareas = usefulareas .* differencescaled';

%% Load ERA5 variables
cd '/Users/eva/Documents/Studie/Sustainable Development MS/Thesis/Matlab/ERA5'
twomdewtemp = ncread('Era5indicators.nc', 'd2m'); %in Kelvin
twomtemp = ncread('Era5indicators.nc', 't2m'); % in Kelvin
evatopcanopy = ncread('Era5indicators.nc', 'evatc'); % in m of water equivalent
evavegtransp = ncread('Era5indicators.nc', 'evavt');% in m of water equivalent
potevap = ncread('Era5indicators.nc', 'pev'); % in m.
run_off = ncread('Era5indicators.nc', 'ro'); % in m.
surfacelatheatflux= ncread('Era5indicators.nc', 'slhf'); % in Joule per m*-2 but make it negative as it is reversed!
surfnetsolarrad = ncread('Era5indicators.nc', 'ssr'); % in Joule per m*-2
surfnetthermalrad = ncread('Era5indicators.nc', 'str');  % in Joule per m*-2
surfsensheatflux = ncread('Era5indicators.nc', 'sshf');% in Joule per m*-2 but make it negative as it is reversed!
evaporation = ncread('Era5indicators.nc', 'e'); % in m of water equivalent, but is negative so must be reversed!
totalprec = ncread('Era5indicators.nc', 'tp'); % in m.
volsoilwater1 = ncread('Era5indicators.nc', 'swvl1'); % in m3 per m-3
volsoilwater2 = ncread('Era5indicators.nc', 'swvl2'); % in m3 per m-3
volsoilwater3 = ncread('Era5indicators.nc', 'swvl3'); % in m3 per m-3
volsoilwater4 = ncread('Era5indicators.nc', 'swvl4'); % in m3 per m-3
baresoileva = ncread('Era5indicators.nc', 'evabs'); % in m of water equivalent
evaopenwater = ncread('Era5indicators.nc', 'evaow'); % in m of water equivalent
snoweva = ncread('Era5indicators.nc', 'es'); % i m of water equivalent
subsurfacerunoff = ncread('Era5indicators.nc', 'ssro'); % in m
surfacerunoff = ncread('Era5indicators.nc', 'sro'); % in m
cd '/Users/eva/Documents/Studie/Sustainable Development MS/Thesis/Matlab/NDVI/Total of NDVI MED and LC'

% adjust the variable units and calculate VPD
temp_dewpoint = twomdewtemp-272.15; % conversion to Celsius
temperature = twomtemp-272.15; % conversion to Celsius
transpiration = evavegtransp * -1000; % conversion to mm of water equivalent
runoff = run_off * 1000; % conversion to mm
latentheat = surfacelatheatflux/-1000000; % conversion to Joule per mm2, and make flux positive
sensibleheat = surfsensheatflux/-1000000; % conversion to Joule per mm2, and make flux positive
totalevaporation = evaporation * -1000; % conversion to mm of water equivalent, and make flux positive
precipitation = totalprec * 1000; % conversion to mm
waterlayer1 = volsoilwater1 * 1000; % conversion to mm3 per m3
waterlayer2 = volsoilwater2 * 1000; % conversion to mm3 per m3
waterlayer3 = volsoilwater3 * 1000; % conversion to mm3 per m3
waterlayer4 = volsoilwater4 * 1000; % conversion to mm3 per m3
VPD = ((0.6108*(2.7183.^((17.27*temperature)./(temperature+237.3)))) - (0.6108*(2.7183.^((17.27*temp_dewpoint)./(temp_dewpoint+237.3)))))
;  % in kPa
canopyevaporation = evatopcanopy * -1000; % conversion to mm of water equivalent
```

```
baresoileva = baresoileva *-1000; % conversion flux and to mm of water equivalent
evaopenwater = evaopenwater *-1000; % conversion flux and to mm of water equivalent
snoweva = snoweva *-1000; % conversion flux and to mm of water equivalent
subsurfacerunoff = subsurfacerunoff * 1000; % in mm
surfacerunoff = surfacerunoff * 1000; % in mm

%% ERA5 variable into layered matrices with monthly means of start and end period
% parameters:
variable = [insert variable];
name = '[insert name variable]';
unit = '[insert unit of variable]';

% build layered matrices with monthly averages
% - start period:
z= [1:12:48];
start_jan=mean(variable(:,:,z), [3], 'omitnan');
start_feb=mean(variable(:,:,z+1), [3], 'omitnan');
start_mar=mean(variable(:,:,z+2), [3], 'omitnan');
start_apr=mean(variable(:,:,z+3), [3], 'omitnan');
start_may=mean(variable(:,:,z+4), [3], 'omitnan');
start_jun=mean(variable(:,:,z+5), [3], 'omitnan');
start_jul=mean(variable(:,:,z+6), [3], 'omitnan');
start_aug=mean(variable(:,:,z+7), [3], 'omitnan');
start_sep=mean(variable(:,:,z+8), [3], 'omitnan');
start_oct=mean(variable(:,:,z+9), [3], 'omitnan');
start_nov=mean(variable(:,:,z+10), [3], 'omitnan');
start_dec=mean(variable(:,:,z+11), [3], 'omitnan');
vector_start = cat(3, start_jan, start_feb, start_mar, start_apr, start_may, start_jun, start_jul, start_aug, start_sep, start_oct, start_nov, start_dec);

% - end period:
f = [49:12:96];
end_jan=mean(variable(:,:,f), [3], 'omitnan');
end_feb=mean(variable(:,:,f+1), [3], 'omitnan');
end_mar=mean(variable(:,:,f+2), [3], 'omitnan');
end_apr=mean(variable(:,:,f+3), [3], 'omitnan');
end_may=mean(variable(:,:,f+4), [3], 'omitnan');
end_jun=mean(variable(:,:,f+5), [3], 'omitnan');
end_jul=mean(variable(:,:,f+6), [3], 'omitnan');
end_aug=mean(variable(:,:,f+7), [3], 'omitnan');
end_sep=mean(variable(:,:,f+8), [3], 'omitnan');
end_oct=mean(variable(:,:,f+9), [3], 'omitnan');
end_nov=mean(variable(:,:,f+10), [3], 'omitnan');
end_dec=mean(variable(:,:,f+11), [3], 'omitnan');
vector_end= cat(3, end_jan, end_feb, end_mar, end_apr, end_may, end_jun, end_jul, end_aug, end_sep, end_oct, end_nov, end_dec);

% Indicator matrix only for selected areas:
useful_vector_start =usefulareas' .* vector_start(:, 1:450,:);
useful_vector_end = usefulareas' .* vector_end(:, 1:450,:);

% Initial investigation of variable:
% 1. Matrices with yearly means, for both periods:
mean_start = mean(useful_vector_start, [3], 'omitnan') ;
mean_end = mean(useful_vector_end, [3], 'omitnan') ;

% - Mean, max and, min of whole area, for both periods:
formean_useful_start = mean_start';
formean_useful_start(usefulareas==0) =[];
formean_useful_end = mean_end';
formean_useful_end(usefulareas==0) =[];

% - Mean of whole area per month, for both periods:
mean_months_start = mean(mean(useful_vector_start, 'omitnan'), 'omitnan');
mean_months_start(:,1)=[]
mean_months_end = mean(mean(useful_vector_end, 'omitnan'), 'omitnan');
mean_months_end(:,1)=[]

for n = 1:12
   month_start = useful_vector_start(:,:,n)';
   month_start(usefulareas==0) = [];
   mean_month_start = mean(month_start, 'omitnan');
   month_end = useful_vector_end(:,:,n)';
   month_end(usefulareas==0) = [];
   mean_month_end = mean(month_end, 'omitnan');
   mean_months_start(n) = mean_month_start;
   mean_months_end(n) = mean_month_end;
end
```

```
% Difference between the two periods:
% 1. per month:
diff_mean_month = useful_vector_end - useful_vector_start; % layered matrix with differences for all 12 months
mean_diff_mean_month= mean(mean(diff_mean_month, 'omitnan'), 'omitnan'); mean_diff_mean_month(:,1)=[];
plot(mean_diff_mean_month)

% 2. over whole year:
diff_mean_year = mean_end - mean_start; % one map of difference between periods

% 3. Correlation variable with NDVI
%--for the whole year:
%- remove unselected grid values, make vectors:
vector_NDVIdiff_usefulareas = NDVIdiff_usefulareas;
vector_NDVIdiff_usefulareas(usefulareas==0) = [];
vector_useful_diff = diff_mean_year';
vector_useful_diff(usefulareas==0) = [];

[RHO,PVAL] = corr(vector_NDVIdiff_usefulareas', (vector_useful_diff'), 'Type', 'Spearman', 'rows', 'complete')

%--per season
season1 = [3:5]; % spring
season2 = [6:8]; % summer
season3 = [9:12]; % fall
season4 = [1:2,12]; % winter
diff_season1 = mean(diff_mean_month(:,:,season1), 3, 'omitnan')';
diff_season2 = mean(diff_mean_month(:,:,season2), 3, 'omitnan')';
diff_season3 = mean(diff_mean_month(:,:,season3), 3, 'omitnan')';
diff_season4 = mean(diff_mean_month(:,:,season4), 3, 'omitnan')';
diff_season1(usefulareas==0) = [];
diff_season2(usefulareas==0) = [];
diff_season3(usefulareas==0) = [];
diff_season4(usefulareas==0) = [];
[rho_season1,PVALs1] = corr(vector_NDVIdiff_usefulareas', diff_season1', 'Type', 'Spearman', 'rows', 'complete');
[rho_season2,PVALs2] = corr(vector_NDVIdiff_usefulareas', (diff_season2'), 'Type', 'Spearman', 'rows', 'complete');
[rho_season3,PVALs3] = corr(vector_NDVIdiff_usefulareas', (diff_season3'), 'Type', 'Spearman', 'rows', 'complete');
[rho_season4,PVALs4] = corr(vector_NDVIdiff_usefulareas', (diff_season4'), 'Type', 'Spearman', 'rows', 'complete');
% results in table
table = ["season1", "season2", "season3", "season4"; rho_season1, rho_season2, rho_season3, rho_season4; PVALs1, PVALs2, PVALs3,
PVALs4]

%% Further variable investigation: comparison different NDVI groups
%calculate higest 10 percent of NDVI differences (regreening/degreening)
max10percincrease = (NDVIdiff_usefulareas>=prctile(vector_NDVIdiff_usefulareas(:),90));
max10percdecrease = (NDVIdiff_usefulareas<=prctile(vector_NDVIdiff_usefulareas(:),10));
amount_group = sum(sum(max10percincrease));
%amount of values for the 2 NDVI differences is 209 (10% of usefulareas)

% NDVI difference of areas:
NDVI_10perincr = max10percincrease .* differencescaled';
NDVI_10perdecr = max10percdecrease .* differencescaled';
% Variable of areas:
variable_10percincr = max10percincrease .* mean_year(:, 1:450)';
variable_10percdecr =max10percdecrease.* mean_year(:, 1:450)';
%vector of matrices:
NDVI_10perincr_vector = NDVI_10perincr;
NDVI_10perincr_vector(max10percincrease==0)=[];
NDVI_10perdecr_vector = NDVI_10perdecr;
NDVI_10perdecr_vector(max10percdecrease==0)=[];
indicator_5percincr_vector = indicator_10percincr;
indicator_5percincr_vector(max10percincrease==0)=[];
regression analysis:
regression_increase = fitlm(NDVI_10perincr_vector, indicator_10percincr_vector)
regression_decrease = fitlm(NDVI_10perincr_vector, indicator_10percdecr_vector)
[r,PVAL] = corr(NDVI_10perincr_vector(:), indicator_10percincr_vector(:), 'Type', 'Pearson', 'rows', 'complete')
[r,PVAL] = corr(NDVI_10perincr_vector(:), indicator_10percdecr_vector(:), 'Type', 'Pearson', 'rows', 'complete')
% T-test:
[H,P]= ttest2(NDVI_10perincr_vector, NDVI_10perdecrvector)

%% Climate change analysis:
lowNDVIdiff = (differencescaled<0.00623 & differencescaled> -0.00623); % also gives 209 grid cells
lowNDVIdiff_usefulareas = lowNDVIdiff' .* usefulareas;
NDVI_lowdiff = lowNDVIdiff_usefulareas .* differencescaled';

variable_lowdiffstart = lowNDVIdiff_usefulareas.* mean_start(:, 1:450)';
variable_lowdiffend = lowNDVIdiff_usefulareas.* mean_end(:, 1:450)';
variable_lowdiffstart(lowNDVIdiff_usefulareas==0)=[];
variable_lowdiffend(lowNDVIdiff_usefulareas==0)=[];
```

```
meanlowstart = mean(indicator_lowdiffstart)
meanlowend = mean(indicator_lowdiffend)
% T-test:
[Hlow,P]= ttest(indicator_lowdiffstart,indicator_lowdiffend)

%% Additional: background map used for visualization figures
% Source: Natural Earth (Open Source): https://www.naturalearthdata.com/downloads/10m-natural-earth-1/10m-natural-earth-1-with-shaded-relief-water-and-drainages/
elevation = imread('NE1_LR_LC_SR_W_DR.tif');
[A,R,cmap] = readgeoraster('NE1_LR_LC_SR_W_DR.tif');
C = imresize(A, 0.25); % zelfde maat als ERA5, maar nu nog juiste coordinaten..
% for coordinates:
I = geotiffinfo('NE1_LR_LC_SR_W_DR.tif'); [x,y]=pixcenters(I);

lats =  -89.9:0.0888:89.9;
for i = 1:2025
fornewy = (y >= lats(i)-0.1 & y < lats(i)+0.1);
    data_current_grid = y(fornewy);
    newy(i) = mean(data_current_grid);
end
newyflip = flip(newy);

lons = -179.8: 0.0888 :179.8;
for j = 1:4050
    fornewx = x >= lons(j)-0.1 & x < lons(j)+0.1;
    data_current_gridx = x(fornewx);
    newx(j) = mean(data_current_gridx);
end
%for frame
rightarea = C(350:843, 1857:2702, :); elevationmap = imresize(rightarea,[450 751]);
save('elevationmap', 'elevationmap')
```